SCATTERING FROM VARIABLE RESISTIVE AND IMPEDANCE SHEETS

by

Kamal Sarabandi

Radiation Laboratory

Department of Electrical Engineering and Computer Science

The University of Michigan

March 13, 1989

SCATTERING FROM VARIABLE RESISTIVE AND IMPEDANCE SHEETS

by

Kamal Sarabandi

Radiation Laboratory

Department of Electrical Engineering and Computer Science

The University of Michigan

March 13, 1989

Abstract

Scattering from variable planar resistive and impedance sheets with one dimensional variations is studied in this report. An approximate solution is obtained using a perturbation technique in the Fourier domain. It is shown that the solution for a variable resistive sheet with resistivity $R(x)$ is identical to the solution for an impedance surface with impedance $\eta(x)$ by replacing $R(x)$ with $\eta(x)/2$. The solution for the induced current on the sheet in terms of the resistivity (impedance) function is given in a recursive form. The closed form nature of the solution enables us to study the statistical behavior of the scattered field when the perturbation function is a random process.

The solutions based on the perturbation technique are compared with those obtained by other methods such as the moment method for periodic resistive and impedance sheets (Appendix A), numerical solution of the integral equation for scattering from a dielectric object above a resistive sheet (Appendix B), and GTD for the problem of impedance insert.

Contents

List of Figures

List of Tables

1 Introduction

In view of the difficulties associated with obtaining exact solutions of Maxwell's equations under given initial and boundary conditions, approximate solutions are often sought instead. A common approximation technique is perturbation theory which is useful primarily when the problem under consideration closely resembles one whose exact solution is known. Perturbational methods have been successfully used for many problems such as cavity and waveguide problems [e.g. Stephen et al 1967, Eftimiu and Huddleston 1983], scattering from stratified media [Bates and Wall 1976], and scattering from rough metallic surfaces [Rice 1951].

In this paper we will employ a perturbation method to solve the scattering problem of variable resistive and impedance sheets. Study of this problem is motivated by number of important applications. For example, a thin dielectric slab whose thickness and dielectric constant are non-uniform provides a model for a vegetation leaf, and can be approximated by a resistive sheet with variable resistivity. The variable resistivity $R(x)$ is an explicit function of the thickness and material properties of the slab. Another variable resistive sheet of concern is a periodic resistive sheet, with application to spatial filters and polarizers. Characterization of the scattering behavior of a variable impedance sheet is also a matter of increasing concern since dielectric coated perfect conductors can be modeled by a surface impedance, and a variation of the material property of a terrain surface can be represented by a variable impedance surface.

The approximate solution is obtained using a perturbation technique in the

Fourier domain. The solution for the induced current on the sheet in terms of the resistivity function is given in a recursive form. The closed form nature of the solution enables us to study the statistical behavior of the scattered field when the resistivity function is a random process. The solution for the current on an impedance sheet with impedance $\eta(x)$ is identical with that of the resistive sheet and can be obtained by replacing $R(x)$ with $\eta(x)/2$.

The solution to any desired order for a periodic perturbation is obtained analytically and the results are compared with an exact solution obtained using a moment method which is developed in Appendix A. The technique is also used to characterize the scattering behavior of a thin dielectric slab with a hump and the solution is compared to that obtained using the moment method in conjunction with the exact image theory for resistive sheets developed in Appendix B. To demonstrate the ability of this perturbation technique to handle sharp variations in the spatial domain, the problem of scattering from an impedance insert is considered and compared with a uniform GTD solution [Herman and Volakis 1988].

2 Derivation of Integral Equation for Resistive Sheet

The resistive sheet is simply an electric current sheet modelling a thin dielectric layer capable of supporting electric currents. The electric current on the sheet is proportional to the tangential electric field and the proportionality constant is

denoted by a complex resistivity R given by

$$R = \frac{iZ_0}{k_0\tau(\epsilon - 1)} \tag{1}$$

Here, Z_0 and k_0 are the characteristic impedance and propagation constant, respectively, of free space. Also τ and $\epsilon = \epsilon' + i\epsilon''$ are the thickness and the dielectric constant of the dielectric layer, respectively, and for convenience a time factor $e^{-i\omega t}$ has been assumed and suppressed.

The electromagnetic boundary conditions that govern the fields on the resistive sheet are given by [Senior et al 1987]

$$[\hat{\mathbf{n}} \times \mathbf{E}]_-^+ = 0 \tag{2}$$

$$\hat{\mathbf{n}} \times (\hat{\mathbf{n}} \times \mathbf{E}) = -R\mathbf{J} \tag{3}$$

$$\mathbf{J} = [\hat{\mathbf{n}} \times \mathbf{H}]_-^+ \tag{4}$$

where $\hat{\mathbf{n}}$ is the unit vector normal to the top (+) side of the sheet, $\mathbf{J}$ is the induced current on the sheet, and $[\quad]_-^+$ denotes the discontinuity across the sheet.

Consider a planar resistive sheet occupying the xy plane and having a resistivity which is only a function of x. Suppose a plane wave is incident on the sheet at an angle ϕ_0 measured from the normal. The geometry of the problem is depicted in Fig. 1. For the E polarization case where the electric field is perpendicular to the plane of incidence, we assume

$$\mathbf{E}^i = \hat{\mathbf{y}} e^{ik_0(\sin\phi_0 x - \cos\phi_0 z)} \tag{5}$$

$$\mathbf{H}^i = Y_0(\cos\phi_0 \hat{\mathbf{x}} + \sin\phi_0 \hat{\mathbf{z}}) e^{ik_0(\sin\phi_0 x - \cos\phi_0 z)}. \tag{6}$$

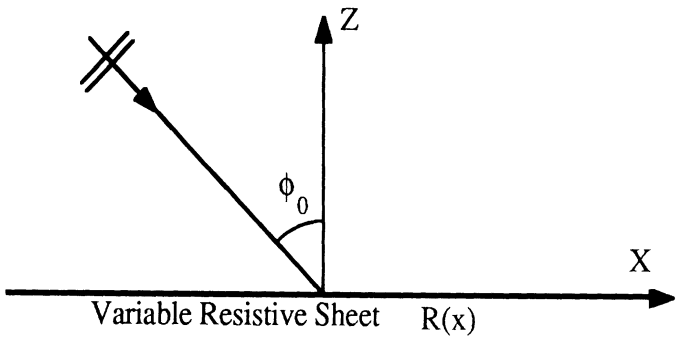

Figure 1: Geometry of the scattering problem for a variable resistive sheet.

The scattered field due to the induced current is

$$\mathbf{E}^s(\vec{\rho}) = -i\omega\mu_0 \int_s \mathbf{J}(\vec{\rho'}) \cdot \overline{\overline{\Gamma}}(\vec{\rho}, \vec{\rho'}) \mathrm{d}s' \tag{7}$$

where $\overline{\overline{\Gamma}}(\vec{\rho}, \vec{\rho'})$ is the two-dimensional dyadic Green's function and is given by

$$\overline{\overline{\Gamma}}(\vec{\rho}, \vec{\rho'}) = -\frac{i}{4}[\overline{\overline{I}} + \frac{\nabla\nabla}{k_0^2}] H_0^{(1)}(k_0 \mid \vec{\rho} - \vec{\rho'} \mid) \tag{8}$$

Here, $H_0^{(1)}$ is the Hankel function of first kind and zeroth-order. The induced current in this case has only a y component, and from (7) the scattered field is found to be

$$\mathbf{E}^s(\vec{\rho}) = -\hat{\mathbf{y}} \frac{k_0 Z_0}{4} \int_{-\infty}^{+\infty} J_y(x') H_0^{(1)}(k_0 \mid \vec{\rho} - \vec{\rho'} \mid) \mathrm{d}x' \tag{9}$$

The induced current and the total electric field given by

$$\mathbf{E}^t = \mathbf{E}^i + \mathbf{E}^s \tag{10}$$

must satisfy the boundary condition given by (3). Noting that $\hat{\mathbf{n}} = \hat{\mathbf{z}}$ and substituting for $\mathbf{E}^i$ and $\mathbf{E}^s$ from (5) and (9) the following integral equation for the

induced current can be obtained:

$$R(x)J_y(x) = e^{ik_0 \sin\phi_0 x} - \frac{k_0 Z_0}{4}\int_{-\infty}^{+\infty} J_y(x')H_0^{(1)}(k_0 \mid x - x' \mid)\mathrm{d}x' \qquad (11)$$

For the H-polarization case in which the magnetic field vector is perpendicular to the plane of incidence, we have

$$\mathbf{E}^i = -(\cos\phi_0\hat{\mathbf{x}} + \sin\phi_0\hat{\mathbf{z}})e^{ik_0(\sin\phi_0 x - \cos\phi_0 z)} \qquad (12)$$

$$\mathbf{H}^i = \hat{\mathbf{y}}Y_0 e^{ik_0(\sin\phi_0 x - \cos\phi_0 z)}. \qquad (13)$$

In this case the induced current has only a x component and from (7) the scattered electric field components are

$$E_x^s(x,z) = -\frac{k_0 Z_0}{4}\int_{-\infty}^{+\infty} J_x(x')(1 + \frac{1}{k_0^2}\frac{\partial^2}{\partial x^2})H_0^{(1)}(k_0\sqrt{(x-x')^2 + z^2})\mathrm{d}x' \qquad (14)$$

$$E_z^s(x,z) = -\frac{Z_0}{4k_0}\int_{-\infty}^{+\infty} J_x(x')\frac{\partial^2}{\partial x \partial z}H_0^{(1)}(k_0\sqrt{(x-x')^2 + z^2})\mathrm{d}x' \qquad (15)$$

The scattered magnetic field is in the y direction and can be obtained from

$$H_y^s(x,z) = -\frac{1}{4i}\int_{-\infty}^{+\infty} J_x(x')\frac{\partial}{\partial z}H_0^{(1)}(k_0\sqrt{(x-x')^2 + z^2})\mathrm{d}x' \qquad (16)$$

By obtaining the total field at the surface of the sheet and applying the boundary condition (3) the following integral equation for the induced current in the H polarization case can be derived:

$$R(x)J_x(x) = -\cos\phi_0 e^{ik_0 \sin\phi_0 x} - \frac{k_0 Z_0}{4}\int_{-\infty}^{+\infty} J_x(x')(1 + \frac{1}{k_0^2}\frac{\partial^2}{\partial x^2})H_0^{(1)}(k_0 \mid x - x' \mid)\mathrm{d}x'. \qquad (17)$$

3 Derivation of Integral Equation for Impedance Sheet

Consider an impedance surface occupying the xy plane. Suppose the impedance is a function only of the variable x and is denoted by $\eta(x)$. Further assume that this surface is illuminated by a plane wave at an angle ϕ_0 as depicted in Fig. 1. The boundary condition on the surface is

$$\hat{\mathbf{n}} \times (\hat{\mathbf{n}} \times \mathbf{E}) = -\eta(x)\hat{\mathbf{n}} \times \mathbf{H} \tag{18}$$

The field scattered from this surface can be obtained by replacing the total tangential magnetic field on the surface by an electric current over a perfect magnetic conductor using the field equivalence principle [Harrington 1961]. The equivalent electric current is

$$\mathbf{J} = \hat{\mathbf{n}} \times \mathbf{H}. \tag{19}$$

and by invoking image theory, the magnetic wall can be removed by doubling the electric current.

The incident electric and magnetic field in the E polarization case are given by (5) and (6) respectively. In this case the total tangential magnetic field on the surface is in the x direction which implies that the electric current is in the y direction. The scattered electric field can be obtained from expression (9) and is

$$E_y^s(x,z) = -\frac{k_0 Z_0}{2} \int_{-\infty}^{+\infty} J_y(x') H_0^{(1)}(k_0\sqrt{(x-x')^2+z^2})\mathrm{d}x'. \tag{20}$$

The total electric field on the surface is composed of the incident field, the field

reflected from the magnetic wall, and the scattered field. From (18) and (19) we have

$$[E_y^i + E_y^r + E_y^s]_{z=0} = \eta(x) J_y(x) \tag{21}$$

which leads to the following integral equation for the electric current:

$$\frac{\eta(x)}{2} J_y(x) = e^{ik_0 \sin\phi_0 x} - \frac{k_0 Z_0}{4} \int_{-\infty}^{+\infty} J_y(x') H_0^{(1)}(k_0 \mid x - x' \mid) \mathrm{d}x'. \tag{22}$$

When the incident field is H-polarized the total tangential magnetic field is in the y direction which implies that the equivalent electric current flows in the x direction. The scattered electric field can be obtained from (14) and (15) by doubling the electric current. Also, from the boundary condition (17), we have

$$[E_x^i + E_x^r + E_x^s]_{z=0} = \eta(x) J_x(x). \tag{23}$$

Upon substituting the appropriate quantities from equations (12) and (14) into the above equation the following integral equation for the electric current can be obtained:

$$\frac{\eta(x)}{2} J_x(x) = -\cos\phi_0 e^{ik_0 \sin\phi_0 x} - \frac{k_0 Z_0}{4} \int_{-\infty}^{+\infty} J_x(x')(1 + \frac{1}{k_0^2} \frac{\partial^2}{\partial x^2}) H_0^{(1)}(k_0 \mid x - x' \mid) \mathrm{d}x'. \tag{24}$$

The scattered magnetic field in this case is

$$H_y^s(x, z) = -\frac{1}{2i} \int_{-\infty}^{+\infty} J_x(x') \frac{\partial}{\partial z} H_0^{(1)}(k_0 \sqrt{(x - x')^2 + z^2}) \mathrm{d}x'. \tag{25}$$

Note that the integral equations obtained for the impedance sheet are identical to those obtained for the resistive sheet if $R(x)$ is replaced by $\eta(x)/2$. Therefore all the analysis that will be carried out for the resistive sheet can be applied to the corresponding impedance sheet.

4 Perturbation Solution

The integral equations for the induced current on the resistive sheet are Fredholm integral equations of the second type, and for an arbitrary resistivity function $R(x)$ there is no known technique for finding their exact solution. Here we obtain an approximate iterative solution to these integral equations using a perturbation technique and Fourier transform. For the sake of simplicity let us represent the integral equations (11) and (17) by the following equation:

$$R(x)J(x) = ae^{ik_0 \sin\phi_0 x} - \frac{k_0 Z_0}{4}(J * g)(x) \tag{26}$$

where $g(x)$ is the kernel of the integral equation and $(J * g)(x)$ denotes the convolution integral. The kernel function $g(x)$ and constant a are

$$g(x) = \begin{cases} H_0^{(1)}(k_0 \mid x \mid) & \text{E-polarization} \\ (1 + \frac{1}{k_0^2}\frac{\partial^2}{\partial x^2})H_0^{(1)}(k_0 \mid x \mid) & \text{H-polarization} \end{cases} \tag{27}$$

$$a = \begin{cases} 1 & \text{E-polarization} \\ -\cos\phi_0 & \text{H-polarization} \end{cases} \tag{28}$$

By taking the Fourier transform of (26), the integral equation in the Fourier domain becomes

$$\frac{1}{2\pi}(\tilde{R} * \tilde{J})(\alpha) = 2\pi a\delta(\alpha - k_0 \sin\phi_0) - \frac{k_0 Z_0}{4}\tilde{J}(\alpha)\tilde{g}(\alpha) \tag{29}$$

where the Fourier transform of functions are denoted by a tilda and δ is the Dirac delta function. The Fourier transform of the kernel function for E- and

H-polarization cases respectively are given by

$$\tilde{g}(\alpha) = \frac{2}{\sqrt{k_0^2 - \alpha^2}} \tag{30}$$

$$\tilde{g}(\alpha) = \frac{2}{k_0^2}\sqrt{k_0^2 - \alpha^2} \tag{31}$$

where the branch of square root is defined such that $\sqrt{-1} = i$. When the resistivity of the sheet is constant, an exact solution to the integral equation (26) can be obtained, and if $R(x) = R_0$, then

$$\tilde{R}(\alpha) = 2\pi R_0 \delta(\alpha). \tag{32}$$

The transform of the current can be obtained from (29) and is given by

$$\tilde{J}_0(\alpha) = \frac{a[2\pi\delta(\alpha - k_0 \sin\phi_0)]}{R_0 + \frac{k_0 Z_0}{4}\tilde{g}(\alpha)}, \tag{33}$$

and the induced current in the spatial domain for E and H polarization respectively are

$$\mathbf{J}_0^e(x) = \hat{\mathbf{y}}\frac{2Y_0 \cos\phi_0}{1 + 2R_0 Y_0 \cos\phi_0} e^{ik_0 \sin\phi_0 x}, \tag{34}$$

$$\mathbf{J}_0^h(x) = \hat{\mathbf{x}}\frac{-2Y_0 \cos\phi_0}{2R_0 Y_0 + \cos\phi_0} e^{ik_0 \sin\phi_0 x}. \tag{35}$$

which are identical to the result obtained from a plane wave reflection coefficient calculation [Senior et al 1987].

If the resistivity has a small variation as a function of position, let

$$R(x) = R_0(1 + \Delta r(x)) \tag{36}$$

where $r(x)$ is the perturbation function assuming $\mid r(x) \mid \leq 1$ and Δ is a complex constant ($\mid \Delta \mid < 1$). The induced current on the sheet is assumed to be

$$J(x) = \sum_{n=0}^{+\infty} J_n(x)\Delta^n, \tag{37}$$

where $J_n(x)$ denotes the n^{th} component of the induced current. Obviously, if $\Delta = 0$ then $J(x) = J_0(x)$. From (36) and (37)

$$\tilde{R}(\alpha) = 2\pi R_0 \delta(\alpha) + R_0 \tilde{r}(\alpha)\Delta \tag{38}$$

$$\tilde{J}(\alpha) = \sum_{n=0}^{+\infty} \tilde{J}_n(\alpha)\Delta^n, \tag{39}$$

and when substituted into (29), the terms given by (33) can be cancelled, and the remaining terms can be written as

$$\sum_{n=1}^{+\infty} \{R_0[\tilde{J}_n(\alpha) + \frac{1}{2\pi}\tilde{r}(\alpha) * \tilde{J}_{n-1}(\alpha)] + \frac{k_0 Z_0}{4}\tilde{g}(\alpha)\tilde{J}_n(\alpha)\}\Delta^n = 0 \tag{40}$$

Since this must hold for any value of Δ, all of the coefficients must be zero. Thus for E polarization

$$\tilde{J}_n^e(\alpha) = -2Y_0 R_0 \cdot \frac{\sqrt{1 - \frac{\alpha^2}{k_0^2}}}{1 + 2Y_0 R_0 \sqrt{1 - \frac{\alpha^2}{k_0^2}}} \cdot \frac{1}{2\pi}(\tilde{r} * \tilde{J}_{n-1}^e)(\alpha), \tag{41}$$

and for H polarization we have

$$\tilde{J}_n^h(\alpha) = -2Y_0 R_0 \cdot \frac{1}{2Y_0 R_0 + \sqrt{1 - \frac{\alpha^2}{k_0^2}}} \cdot \frac{1}{2\pi}(\tilde{r} * \tilde{J}_{n-1}^h)(\alpha). \tag{42}$$

The above recursive relations along with the expressions for $\tilde{J}_0(\alpha)$ given in (34) and (35) can be used to derive the induced currents to any desired order of approximation. The first-order solution can be obtained very easily and the transforms

of the first component of the induced current for E and H polarizations are

$$\tilde{J}_1^e(\alpha) = \frac{-4Y_0^2 R_0 \cos\phi_0}{1 + 2Y_0 R_0 \cos\phi_0} \cdot \frac{\sqrt{1 - \frac{\alpha^2}{k_0^2}}}{1 + 2Y_0 R_0 \sqrt{1 - \frac{\alpha^2}{k_0^2}}} \tilde{r}(\alpha - k_0 \sin\phi_0) \tag{43}$$

$$\tilde{J}_1^h(\alpha) = \frac{4Y_0^2 R_0 \cos\phi_0}{\cos\phi_0 + 2Y_0 R_0} \cdot \frac{1}{2Y_0 R_0 + \sqrt{1 - \frac{\alpha^2}{k_0^2}}} \tilde{r}(\alpha - k_0 \sin\phi_0) \tag{44}$$

The complexity of obtaining high-order solutions depends on the perturbation function $r(x)$.

5 Periodic Resistivity

A simple case where it is possible to determine the n$^{\text{th}}$ components of the induced currents is a periodic resistivity with period L. In this case we can write

$$r(x) = \sum_{m=-\infty}^{+\infty} c_m e^{i\frac{2\pi m}{L}x}, \tag{45}$$

and the Fourier transform of the perturbation function is

$$\tilde{r}(\alpha) = 2\pi \sum_{m=-\infty}^{+\infty} c_m \delta(\alpha - \frac{2\pi m}{L}). \tag{46}$$

For the E polarization case the transform of the n$^{\text{th}}$ component of the induced current can be obtained from (41) and (46) and is

$$\tilde{J}_n^e(\alpha) = -2Y_0 R_0 \cdot \frac{1}{2Y_0 R_0 + \sqrt{1 - \frac{\alpha^2}{k_0^2}}} \cdot \sum_{m=-\infty}^{+\infty} c_m \tilde{J}_{n-1}^e(\alpha - \frac{2\pi m}{L}) \tag{47}$$

By employing the expression (33) for $\tilde{J}_0(\alpha)$and after some algebraic manipulation, a closed form for $\tilde{J}_n(\alpha)$ can be obtained:

$$\begin{aligned}\tilde{J}_n^e(\alpha) = & \frac{-2Y_0R_0\cos\phi_0(-2Y_0R_0)^n}{1+2Y_0R_0\cos\phi_0} \\ & \cdot\sum_{m_n=-\infty}^{+\infty}\cdots\sum_{m_1=-\infty}^{+\infty}[\prod_{i=1}^{n}\frac{\sqrt{1-(\sin\phi_0+\frac{\lambda}{L}\sum_{j=1}^{i}m_j)^2}}{(1+2Y_0R_0\sqrt{1-(\sin\phi_0+\frac{\lambda}{L}\sum_{j=1}^{i}m_j)^2}}] \\ & \cdot c_{m_n}\cdots c_{m_1}2\pi\delta[\alpha-k_0\sin\phi_0-\tfrac{2\pi}{L}(\textstyle\sum_{\ell=1}^{n}m_\ell)]\end{aligned} \tag{48}$$

and in the spatial domain

$$\begin{aligned}J_n^e(x) = & \frac{2Y_0R_0\cos\phi_0(-2Y_0R_0)^n}{1+2Y_0R_0\cos\phi_0} \\ & \cdot\sum_{m_n=-\infty}^{+\infty}\cdots\sum_{m_1=-\infty}^{+\infty}[\prod_{i=1}^{n}\frac{\sqrt{1-(\sin\phi_0+\frac{\lambda}{L}\sum_{j=1}^{i}m_j)^2}}{(1+2Y_0R_0\sqrt{1-(\sin\phi_0+\frac{\lambda}{L}\sum_{j=1}^{i}m_j)^2}}] \\ & \cdot c_{m_n}\cdots c_{m_1}e^{i(k_0\sin\phi_0+\frac{2\pi}{L}\sum_{\ell=1}^{n}m_\ell)x}\end{aligned} \tag{49}$$

A problem associated with the perturbation techniques is that when there is a sharp variation in the perturbation function there could be a sharp variation in the solution which is not to the order of perturbation. Therefore in an n^{th} – order solution it is not guaranteed that the solution is of $O(\Delta^{n+1})$ for all values of the variable in the domain of the integral equation. To check the validity of our assumption we consider two limiting cases: 1) when the perturbation function has sharp variations in the spatial domain and 2) when the perturbation function has sharp variations in the Fourier domain. The first case will be studied in Section 7 and to study the latter case we consider a constant function $(r(x) = 1)$ for the perturbation function. Note that the perturbation technique was applied to the integral equation (29), and in this case the perturbation function $\tilde{r}(\alpha) = 2\pi\delta(\alpha)$ has the sharpest variation possible. When $r(x) = 1$ the resistivity is constant and

from equation (34) it follows directly that

$$J_0^e(x) = \frac{2Y_0 \cos\phi_0}{1 + 2Y_0R_0(1+\Delta)\cos\phi_0} e^{ik_0 \sin\phi_0 x}. \tag{50}$$

The solution based on the perturbation technique can be obtained from equation (49) with $L = \infty$ and

$$c_m = \begin{cases} 1 & m = 0 \\ 0 & \text{otherwise} \end{cases}; \tag{51}$$

thus

$$J_n^e(x) = \frac{2Y_0 \cos\phi_0(-2Y_0R_0)^n}{(1 + 2Y_0R_0\cos\phi_0)^{n+1}} e^{ik_0 \sin\phi_0 x}, \tag{52}$$

and

$$J^e(x) = \sum_{n=0}^{+\infty} \frac{2Y_0 \cos\phi_0(-2Y_0R_0)^n}{(1 + 2Y_0R_0\cos\phi_0)^{n+1}} e^{ik_0 \sin\phi_0 x} \Delta^n. \tag{53}$$

This series is absolutely convergent and represents the Taylor series expansion of equation (50), implying that the perturbation solution can be made as close as we wish to the exact solution.

For H polarization the analysis is similar and the expression for the component of the induced current in the Fourier and spatial domains respectively are given by:

$$\begin{aligned} \tilde{J}_n^h(\alpha) = \; & \frac{-2Y_0R_0\cos\phi_0(-2Y_0R_0)^n}{2Y_0R_0+\cos\phi_0} \\ & \cdot \sum_{m_n=-\infty}^{+\infty} \cdots \sum_{m_1=-\infty}^{+\infty} \prod_{i=1}^{n} \frac{1}{(2Y_0R_0+\sqrt{1-(\sin\phi_0+\frac{\lambda}{L}\sum_{j=1}^{i} m_j)^2}} \\ & c_{m_n} \cdots c_{m_1} 2\pi\delta[\alpha - k_0\sin\phi_0 - \tfrac{2\pi}{L}(\textstyle\sum_{\ell=1}^{n} m_\ell)] \end{aligned} \tag{54}$$

$$J_n^h(x) = \frac{-2Y_0R_0\cos\phi_0(-2Y_0R_0)^n}{2Y_0R_0+\cos\phi_0}$$
$$\cdot\sum_{m_n=-\infty}^{+\infty}\cdots\sum_{m_1=-\infty}^{+\infty}\prod_{i=1}^{n}\frac{1}{(2Y_0R_0+\sqrt{1-(\sin\phi_0+\frac{\lambda}{L}\sum_{j=1}^{i}m_j)^2}} \tag{55}$$
$$\cdot c_{m_n}\cdots c_{m_1}e^{i(k_0\sin\phi_0+\frac{2\pi}{L}\sum_{\ell=1}^{n}m_\ell)x}.$$

In Appendix A a numerical solution for a periodic resistive sheet is given. The solution is based on the moment method, and in Section 8 the results are compared with the above perturbation solution.

The closed form expression for the induced current enables us to study the case when the perturbation is a periodic random process. In this case the perturbation function may still be represented as a Fourier series but with the Fourier coefficients ($c_m's$) as random variables. It can be shown from (A.14) that the average value of the diffracted field is directly proportional to the average value of the induced current. To obtain the average value of the current, assume that the periodic process has zero mean, which implies that the Fourier coefficients have zero mean ($\langle c_m\rangle = 0$), and further assume that the Fourier coefficients are mutually independent. These assumptions imply that the process is wide sense stationary, and from (49) and (55) the following expressions for the mean value of the components of the induced current can be obtained:

$$\langle J_n^e(x)\rangle = \frac{2Y_0R_0\cos\phi_0(-2Y_0R_0)^n}{1+2Y_0R_0\cos\phi_0}$$
$$\cdot\sum_{m=-\infty}^{+\infty}\prod_{i=1}^{n}\left[\frac{\sqrt{1-(\sin\phi_0+\frac{i\lambda m}{L})^2}}{(1+2Y_0R_0\sqrt{1-(\sin\phi_0+\frac{i\lambda m}{L})^2}}\right]\langle c_m^n\rangle e^{i(k_0\sin\phi_0+\frac{2\pi nm}{L})x} \tag{56}$$

$$\langle J_n^h(x)\rangle = \frac{-2Y_0R_0\cos\phi_0(-2Y_0R_0)^n}{2Y_0R_0+\cos\phi_0}$$
$$\cdot\sum_{m=-\infty}^{+\infty}\prod_{i=1}^{n}\left[\frac{1}{(2Y_0R_0+\sqrt{1-(\sin\phi_0+\frac{i\lambda m}{L})^2}}\right]\langle c_m^n\rangle e^{i(k_0\sin\phi_0+\frac{2\pi nm}{L})x}. \tag{57}$$

6 Scattering Model for a Variable Thickness Dielectric Slab

Consider a dielectric slab whose thickness is a function of x (see Fig. 2). Let the thickness be

$$T(x) = \tau_0(1 + \frac{w^2}{x^2 + w^2} \cdot \Delta) \tag{58}$$

where w is a measure of the width and Δ is the height of the dielectric hump with a possibly different dielectric constant. This thickness function resembles the variation in thickness of a vegetation leaf and in this case w and Δ are random variables. If the dielectric slab is electrically thin, it can be represented by two

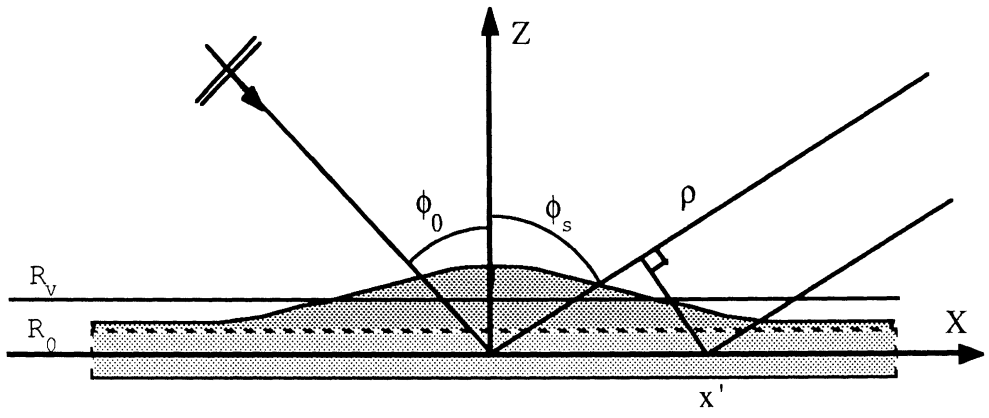

Figure 2: Geometry of a dielectric slab with a hump.

parallel resistive sheets one with a constant thickness τ_0 and the other one with a variable thickness

$$\tau(x) = \frac{w^2}{x^2 + w^2}\Delta\tau_0 \tag{59}$$

where we assume here that $\Delta \ll 1$. Resistivity of the underlying and the top sheets are respectively denoted by R_0 and R_v which can be obtained from equation (1). These parallel sheets can be replaced by an equivalent sheet whose resistivity is equal to that of the two parallel resistors R_0 and R_v, i.e.

$$R(x) = \frac{R_0 R_v}{R_0 + R_v}. \tag{60}$$

By substituting the expressions for R_0 and R_v in the above equation and then approximating the resultant expression to the first order of Δ it can be shown

$$R(x) = R_0 \frac{\tau_0}{\tau_0 + \tau(x)} = R_0 \frac{1}{1 + \frac{w^2 \Delta}{x^2 + w^2}} \simeq R_0 (1 - \frac{w^2}{x^2 + w^2} \Delta) \tag{61}$$

The perturbation function then takes the form

$$r(x) = \frac{-w^2}{x^2 + w^2}. \tag{62}$$

and the transform of this is

$$\tilde{r}(\alpha) = -\pi w e^{-w|\alpha|} \tag{63}$$

The Fourier transforms of the first components of the induced current for E and H polarization can be obtained from (43) and (44) respectively, and are

$$\tilde{J}_1^e(\alpha) = \frac{4Y_0^2 R_0 \cos\phi_0}{1 + 2Y_0 R_0 \cos\phi_0} \cdot \frac{\sqrt{1 - \frac{\alpha^2}{k_0^2}}}{1 + 2Y_0 R_0 \sqrt{1 - \frac{\alpha^2}{k_0^2}}} \cdot (\pi w e^{-w|\alpha - k_0 \sin\phi_0|}) \tag{64}$$

$$\tilde{J}_1^h(\alpha) = \frac{-4Y_0^2 R_0 \cos\phi_0}{\cos\phi_0 + 2Y_0 R_0} \cdot \frac{1}{2Y_0 R_0 + \sqrt{1 - \frac{\alpha^2}{k_0^2}}} \cdot (\pi w e^{-w|\alpha - k_0 \sin\phi_0|}). \tag{65}$$

The scattered field due to the zeroth-order induced current consists of reflected and transmitted plane waves in the specular and forward directions, while the first

component of the induced current gives rise to a cylindrical wave which will be denoted by the superscript s. In the far zone

$$\sqrt{(x-x')^2+z^2} \simeq \rho - x' \sin\phi_s \tag{66}$$

where ρ and ϕ_s denote the distance and direction of observation point, and

$$H_0^{(1)}(k_0\sqrt{(x-x')^2+z^2}) \simeq \sqrt{\frac{2}{\pi k_0 \rho}} e^{i(k_0\rho-\frac{\pi}{4})} e^{-ik_0 \sin\phi_s x'}, \tag{67}$$

$$\frac{1}{k_0^2}\frac{\partial^2}{\partial x^2} H_0^{(1)}(k_0\sqrt{(x-x')^2+z^2}) \simeq \sqrt{\frac{2}{\pi k_0 \rho}} e^{i(k_0\rho-\frac{\pi}{4})} \cos^2\phi_s e^{-ik_0 \sin\phi_s x'}, \tag{68}$$

$$\frac{1}{k_0^2}\frac{\partial^2}{\partial x \partial z} H_0^{(1)}(k_0\sqrt{(x-x')^2+z^2}) \simeq -\sqrt{\frac{2}{\pi k_0 \rho}} e^{i(k_0\rho-\frac{\pi}{4})} \cos\phi_s \sin\phi_s e^{-ik_0 \sin\phi_s x'}. \tag{69}$$

It is now easy to obtain the far field amplitude $\mathbf{P}(\phi_0, \phi_s)$ defined by

$$\mathbf{E}^s \simeq \sqrt{\frac{2}{\pi k_0 \rho}} e^{i(k_0\rho-\frac{\pi}{4})} \mathbf{P}(\phi_0, \phi_s). \tag{70}$$

in terms of which the bistatic echo width is

$$\sigma(\phi_0, \phi_s) = \frac{2\lambda}{\pi} \mid \mathbf{P}(\phi_0, \phi_s) \mid^2 . \tag{71}$$

In the E polarization case the scattered field is in the y direction and

$$\mathbf{P}_e(\phi_0, \phi_s) = \hat{\mathbf{y}} \frac{-k_0 Z_0}{4} \int_{-\infty}^{+\infty} J_1^e(x') e^{-ik_0 \sin\phi_s x'} \mathrm{d}x' = \hat{\mathbf{y}} \frac{-k_0 Z_0}{4} \tilde{J}_1^e(k_0 \sin\phi_s). \tag{72}$$

For H polarization substitution of (68) and (69) into (14) and (15) shows that the scattered field has only a $\hat{\phi}$ component, and the far field amplitude is

$$\mathbf{P}_h(\phi_0, \phi_s) = \hat{\phi} \cos\phi_s \frac{k_0 Z_0}{4} \int_{-\infty}^{+\infty} J_1^h(x') e^{-ik_0 \sin\phi_s x'} \mathrm{d}x' = \hat{\phi} \frac{k_0 Z_0}{4} \cos\phi_s \tilde{J}_1^h(k_0 \sin\phi_s). \tag{73}$$

Hence, from (64) and (65),

$$\mathbf{P}_e(\phi_0,\phi_s)=\hat{\mathbf{y}}\frac{-k_0Y_0R_0\cos\phi_0}{1+2Y_0R_0\cos\phi_0}\cdot\frac{\cos\phi_s}{1+2Y_0R_0\cos\phi_s}\cdot(\pi w\Delta e^{-k_0w|\sin\phi_s-\sin\phi_0|}), \quad (74)$$

$$\mathbf{P}_h(\phi_0,\phi_s)=\hat{\phi}\frac{-k_0Y_0R_0\cos\phi_0}{\cos\phi_0+2Y_0R_0}\cdot\frac{\cos\phi_s}{2Y_0R_0+\cos\phi_s}\cdot(\pi w\Delta e^{-k_0w|\sin\phi_s-\sin\phi_0|}). \quad (75)$$

If w and Δ are independent random variables such that w is Gaussian with mean and standard deviation w_0 and s respectively, its probability density function is

$$f_W(w)=\frac{1}{\sqrt{2\pi}s}e^{-(\frac{w-w_0}{s})^2}. \quad (76)$$

Assume also that the second moment of the random variable Δ is known. The mean value of the bistatic scattering width may now be calculated from (71) and (72) by noting that

$$\langle w^2e^{-2k_0w|\sin\phi_s-\sin\phi_0|}\rangle=(s^2+w_0^2)e^{(k_0^2s^2|\sin\phi_s-\sin\phi_0|^2-2k_0w_0|\sin\phi_s-\sin\phi_0|)}, \quad (77)$$

with the result that

$$\langle\sigma_e(\phi_0,\phi_s)\rangle=2\pi\lambda\mid\frac{-k_0Y_0R_0\cos\phi_0}{1+2Y_0R_0\cos\phi_0}\cdot\frac{\cos\phi_s}{1+2Y_0R_0\cos\phi_s}\mid^2\langle\Delta^2\rangle\langle w^2e^{-2k_0w|\sin\phi_s-\sin\phi_0|}\rangle, \quad (78)$$

$$\langle\sigma_h(\phi_0,\phi_s)\rangle=2\pi\lambda\mid\frac{-k_0Y_0R_0\cos\phi_0}{\cos\phi_0+2Y_0R_0}\cdot\frac{\cos\phi_s}{2Y_0R_0+\cos\phi_s}\mid^2\langle\Delta^2\rangle\langle w^2e^{-2k_0w|\sin\phi_s-\sin\phi_0|}\rangle. \quad (79)$$

The above is a first-order solution, and for a higher order solution, analytical results may not be achievable. When the height of the dielectric hump above the resistive sheet is not much smaller than the wavelength, the above solution fails to work for two reasons: 1) the solution is a first-order one in Δ, and 2) the dielectric

hump cannot be modeled as a single resistive sheet. In such cases we have to resort to numerical techniques to get the solution. In Appendix B the Green's function for a planar resistive sheet is obtained and used to derive an integral equation for the induced polarization current. A moment method technique is then employed to obtain the solution for a dielectric structure of arbitrary cross section above the resistive sheet. Results based on the perturbation technique and the moment method are compared in Section 8.

7 Scattering from Impedance Insert

Another application of the perturbation technique is the scattering of a plane wave from the impedance insert whose geometry is shown in Fig. 3. The impedance

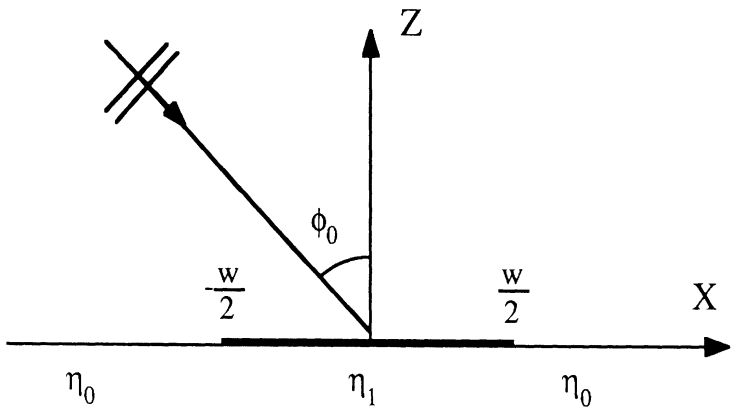

Figure 3: Geometry of an impedance insert.

of this surface can be represented as

$$\eta(x) = \eta_0(1 + \Delta \prod(\frac{x}{w}))$$

where $\prod(x)$ is the gate function defined by

$$\prod(x) = \begin{cases} 1 & \mid x \mid \leq \frac{1}{2} \\ 0 & \text{otherwise} \end{cases},$$

w is the width of the insert, and as before, Δ is a constant with $\mid \Delta \mid < 1$. The transform of the first components of the induced current for E and H polarization respectively can be obtained from (43) and (44) by replacing R_0 by $\eta_0/2$ as follows:

$$\tilde{J}_1^e(\alpha) = \frac{-2Y_0^2\eta_0 \cos\phi_0}{1 + Y_0\eta_0 \cos\phi_0} \cdot \frac{\sqrt{1 - \frac{\alpha^2}{k_0^2}}}{1 + Y_0\eta_0\sqrt{1 - \frac{\alpha^2}{k_0^2}}} w \frac{\sin(w(\alpha - k_0 \sin\phi_0)/2)}{w(\alpha - k_0 \sin\phi_0)/2} \tag{80}$$

$$\tilde{J}_1^h(\alpha) = \frac{2Y_0^2\eta_0 \cos\phi_0}{\cos\phi_0 + Y_0\eta_0} \cdot \frac{1}{Y_0\eta_0 + \sqrt{1 - \frac{\alpha^2}{k_0^2}}} w \frac{\sin(w(\alpha - k_0 \sin\phi_0)/2)}{w(\alpha - k_0 \sin\phi_0)/2} \tag{81}$$

Unfortunately, analytical expressions for the higher order components of the induced current cannot be obtained for this case but they can be found numerically. To observe the behavior of the current in the spatial domain, expressions (80) and (81) were transformed numerically and the results are shown in Figs. 4 and 5. They show the expected behavior of the currents at the edges.

The far field amplitudes can be found by doubling the expressions given by (72) and (73). Thus

$$\mathbf{P}_e(\phi_0, \phi_s) = \hat{\mathbf{y}} \frac{-k_0 Y_0 \eta_0 \cos\phi_0}{1 + Y_0\eta_0 \cos\phi_0} \cdot \frac{\cos\phi_s}{1 + Y_0\eta_0 \cos\phi_s} \cdot w\Delta \frac{\sin(wk_0(\sin\phi_s - \sin\phi_0)/2)}{wk_0(\sin\phi_s - \sin\phi_0)/2}, \tag{82}$$

$$\mathbf{P}_h(\phi_0, \phi_s) = \hat{\phi} \frac{-k_0 Y_0 \eta_0 \cos\phi_0}{\cos\phi_0 + Y_0\eta_0} \cdot \frac{\cos\phi_s}{Y_0\eta_0 + \cos\phi_s} \cdot w\Delta \frac{\sin(wk_0(\sin\phi_s - \sin\phi_0)/2)}{wk_0(\sin\phi_s - \sin\phi_0)/2}. \tag{83}$$

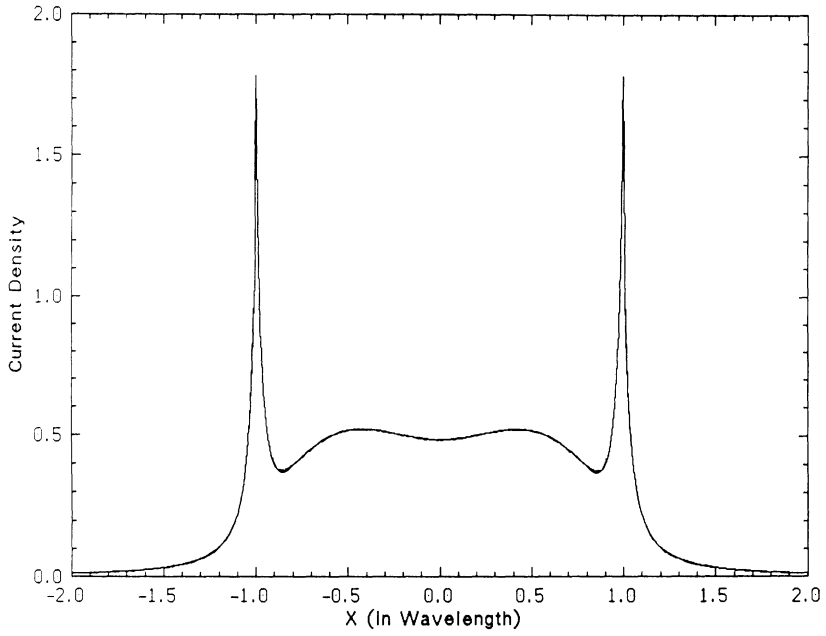

Figure 4: Distribution of the first component of induced current on an impedance insert for E polarization.

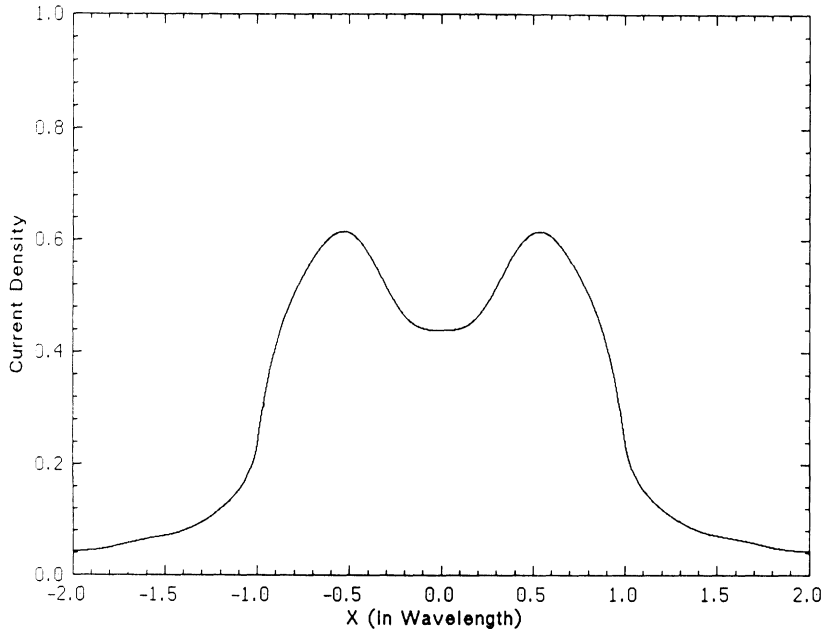

Figure 5: Distribution of the first component of induced current on an impedance insert for H polarization.

The results of this technique are compared with a uniform GTD solution [Herman and Volakis, 1988] that accounts for up to third order diffracted fields in the next Section.

8 Numerical Results

Computations based on the results derived in Sections 4-7 will now be presented and, where possible, compared with data obtained by other methods. First let us consider the periodic resistive sheet. Figures 6 and 7 show the amplitude and phase of the induced current on a resistive sheet with sinusoidal variation of period $L = 2\lambda$ and $\Delta = 0.7$ for E polarization. In these plots the first through fourth order solutions are presented using the expression (49), and compared with the data obtained by the moment method as given in Appendix A. It is seen that by increasing the order of solution we can get as close as we wish to the exact solution, and that the fourth order solution provides excellent agreement with the moment method data. We note here that the required order is directly proportional to Δ and L/λ. Similar results are shown in Figs. 8 and 9 for H polarization. The normalized field amplitudes of the propagating modes (Bragg modes) defined in Appendix A are given in Table 1 for a sinusoidal resistivity with $L = 3\lambda$, $\Delta = 0.7$, and $R_0 = 0 + i100$ at angle $\phi_0 = 30$ degrees. Since the resistivity is pure imaginary, there is no power loss and the total power carried by all of the modes is equal to the incident power. Table 2 gives the normalized field amplitude for a lossy resistive sheet $R_0 = 180 + i270$. In this case 31% and 29% of the incident power is dissipated

in the resistive sheet for E and H polarization respectively. Note that apart from the case $n = 0$, $E_n^- = E_n^+$ and $H_n^- = -H_n+$, where $E_n^\pm$ and $H_n^\pm$ are the field amplitudes of n^{th} mode in the upper (+) and lower (-) half-spaces for E and H polarizations respectively. When $n = 0$ the incident field should be added to the zeroth mode in the lower half-space, i.e. $E_0^- = E_0^+ + E^i$ and $H_0^- = -H_0^+ + H^i$.

We now turn to the problem of a variable thickness dielectric slab. The results of the perturbation technique presented in Section 6 are compared with the numerical solution based on exact image theory for a resistive sheet in conjunction with the moment method (see Appendix B). In all of the test cases the dielectric slab is assumed to be homogeneous with $\epsilon = 36 + i17$, $\tau_0 = \lambda/100$, $\Delta = 0.3$, and $\lambda = 3$ cm. These parameters correspond to $R_0 = 180 + i270$, $\alpha = 112 - i230$ and $\beta = 75 + i154$. Figures 10-20 show the bistatic echo width and the phase of the far field amplitude of a dielectric hump over the resistive sheet for $w = \lambda/15$ and $w = \lambda/25$ and two incidence angle $\phi_0 = 0$, $\phi_0 = 45$ for both polarizations. In each figure the results based on the perturbation technique are compared with the numerical results. The agreement is good in spite of the fact that the perturbation solution is only a first order one. For larger dielectric structures the perturbation technique cannot be used and the moment method is the only available method of solution. For example, the central vein of a vegetation leaf can be modelled as a square dielectric cylinder above a resistive sheet. Figure 21 shows the bistatic echo width of a square cylinder with dimensions $\lambda/10 \times \lambda/10$ in free space, above perfect conductor, and above a resistive sheet, at normal incidence with $f = 10$

GHz, $\epsilon = 36 + i17$, and $R_0 = 180 + i270$ for E polarization. The phase of the far field amplitude is shown in Fig. 22. Similar plots for H polarization are presented in Figs. 23 and 24. Figures 25 and 26 show the backscattered echo width and phase of the far field amplitude of the same structure with the same parameters for E and H polarizations. It can be deduced that a vein and a variation in the thickness of a leaf do not have a significant effect near the specular direction, but in other directions they are substantial contributors to the scattered field.

Figures 27-32 compare the results of the perturbation method and the GTD technique for the impedance insert problem where there are sharp variations in perturbation function in the spatial domain. The figures show the normalized bistatic echo width (σ/λ) of an impedance insert having $w = 2\lambda$ and $\eta_0 = 40 - i40$ using the two methods. The agreement is excellent (for $\Delta = 0.5$ the error is only 0.3 dB) in spite of the sharp changes in the perturbation function in the spatial domain.

9 Conclusions

Problems of scattering from variable resistive and impedance sheets have been studied using a perturbation technique in the Fourier domain. A recursive form for the n^{th} component of the induced current on the resistive sheet was derived that, in principle, allows evaluation of the current to the desired order of perturbation. Having analytical expression for the induced current in Fourier domain culminates in having an analytical form for the far field amplitude. The solution for the

induced current on an impedance sheet is identical to that of a resistive sheet whose resistivity is twice the impedance of the surface impedance.

The validity of the technique was checked in two limiting cases where the variation in perturbation function is sharp in either the spatial or the Fourier domain. It was shown that the perturbation method is capable of handling both. The first order expression for the induced current was obtained analytically for an arbitrary perturbation, but the ability to obtain analytical expressions for the higher orders depends on the perturbation function. For a periodic resistivity a closed form solution for any arbitrary order of perturbation was obtained. The results based on the perturbation method were compared with an exact solution based on the moment method as explained in Appendix A. The analytical results were also checked against a GTD solution for the impedance insert problem and the moment method for the problem of a dielectric hump over a resistive sheet as given in Appendix B. Excellent agreement between the analytical and other methods was observed. It was found that the required order of perturbation is proportional to the perturbation constant Δ and the width of perturbation in spatial domain, i.e. L for a periodic perturbation and w for the impedance insert and dielectric hump problems.

Acknowledgement

The author would like to thank Prof. T.B.A. Senior and Prof. F.T. Ulaby for their helpful comments and reviewing of this work.

This work was supported by NASA under contract NAG-5-480.

References

[1] Bates, R.H.T., D.J.N. Wall, Chandrasekhar transformation improve convergence of computation of scattering from linearly stratified media, *IEEE Trans. Antennas Propag.*, 24, 251-251, 1976.

[2] Eftimiu, C., P.L. Huddleston, Natural frequencies and modes of finite open circular cylinders, *IEEE Trans. Antennas Propag.*, 31, 910-917, 1983.

[3] Harrington, R.F., *Time-Harmonic Electromagnetic Fields*, New York: McGraw-Hill, 1961, p. 317.

[4] Herman, M.I., and J.L. Volakis, High frequency scattering from polygonal impedance cylinders and strips, *IEEE Trans. Antennas Propag.*, 36, 679-688.

[5] Rice, S.O., Reflection of electromagnetic waves from slightly rough surfaces, *Commun. Pure Appl. Math.*, 4, 361-378, 1951.

[6] Richmond, J.H., Scattering by a dielectric cylinder of arbitrary cross section shape, *IEEE Trans. Antennas Propag.*, 13, 334-341, 1965.

[7] Senior, T.B.A., K. Sarabandi, and F.T. Ulaby, Measuring and modeling the backscattering cross section of a leaf, *Radio Sci.*, 22, 1109-1116, 1987.

[8] Stephen, L.R., P. Diament, and S.P. Schlesinger, Perturbation analysis of axially nonuniform electromagnetic structures using nonlinear phase progression, *IEEE Trans. Antennas Propag.*, 15, 422-430, 1967.

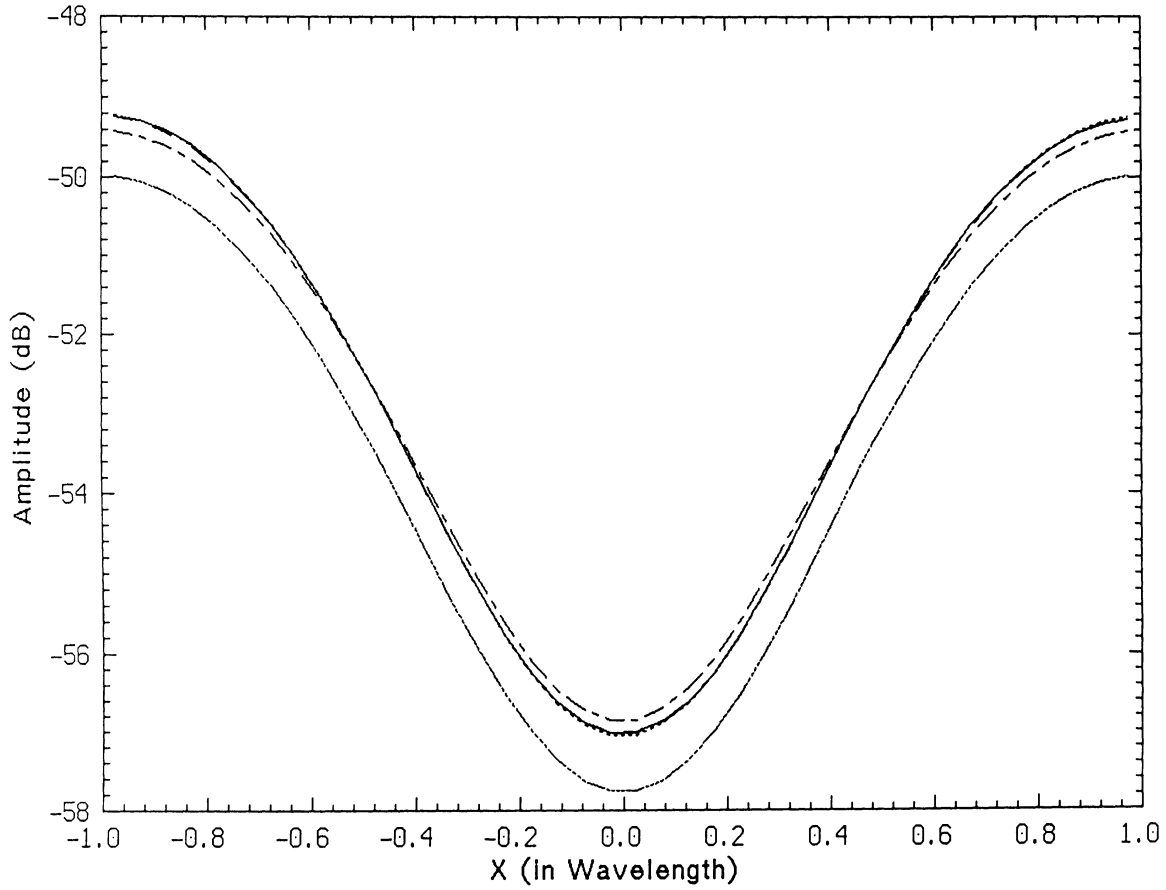

Figure 6: The amplitude of the induced current on a periodic resistive sheet with resistivity $R(x) = (180 + i270)(1 + 0.7\cos\frac{2\pi x}{L})$, $L = 2\lambda$ at normal incidence for E polarization: (——) moment method, (- - - - -) fourth order solution, (— —) third order solution, (— - —) second order solution, (— - - - —) first order solution.

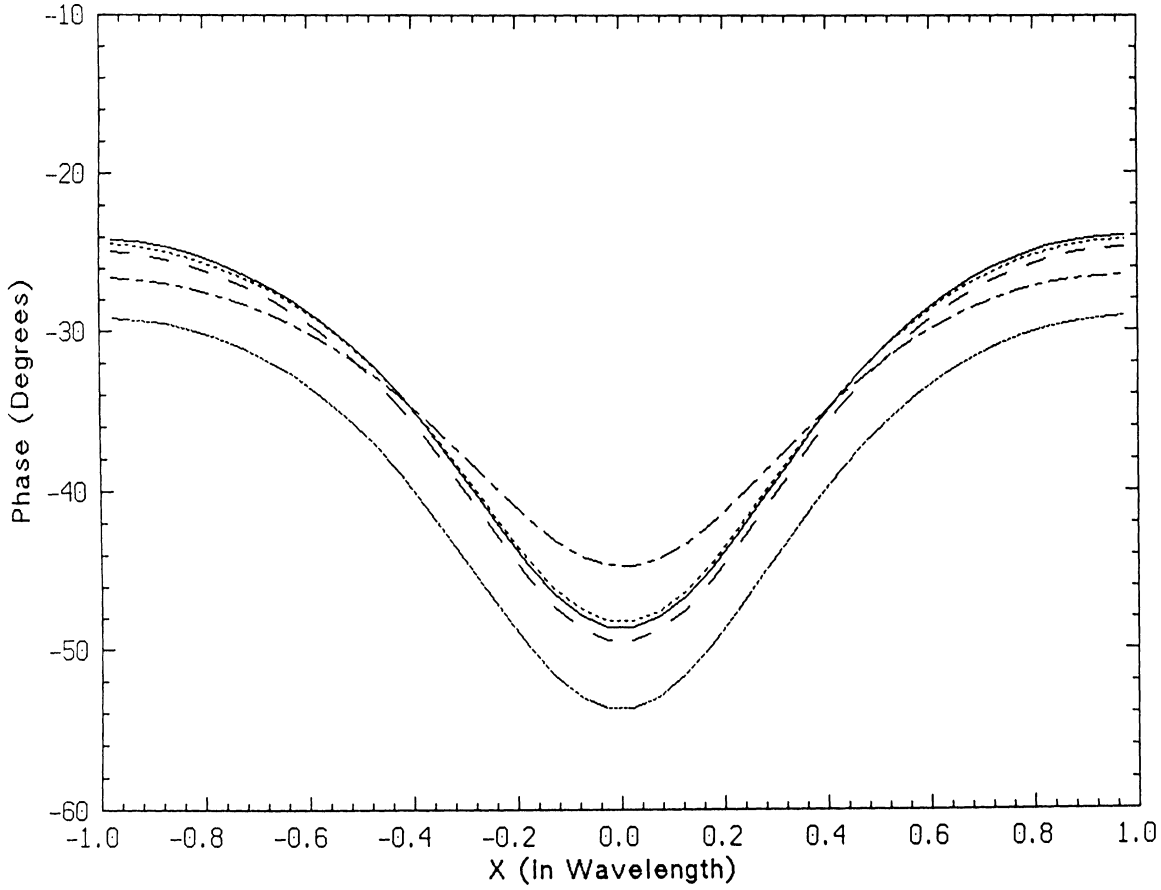

Figure 7: The phase of the induced current on a periodic resistive sheet with resistivity $R(x) = (180 + i270)(1 + 0.7\cos\frac{2\pi x}{L})$, $L = 2\lambda$ at normal incidence for E polarization: (——) moment method, (- - - - -) fourth order solution, (— —) third order solution, (— - —) second order solution, (— - - - —) first order solution.

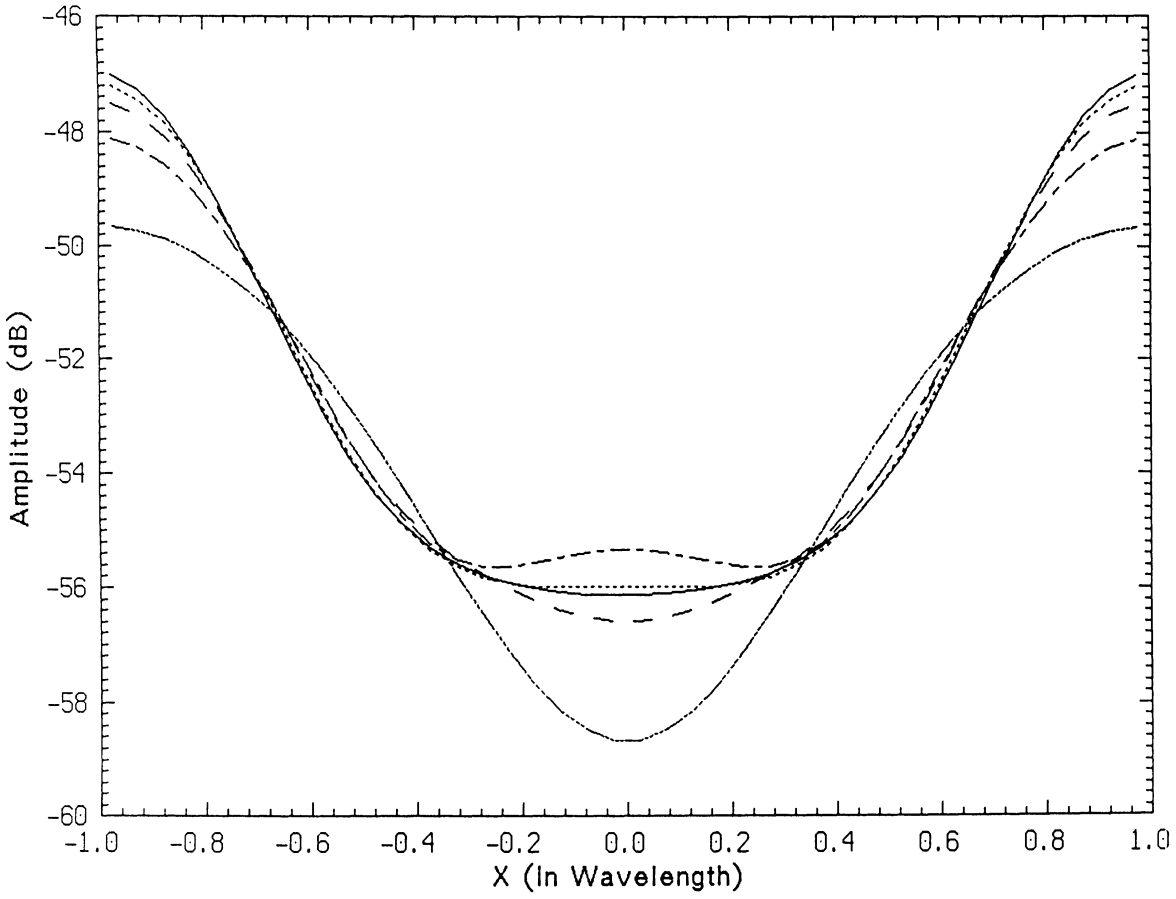

Figure 8: The amplitude of the induced current on a periodic resistive sheet with resistivity $R(x) = (180 + i270)(1 + 0.7\cos\frac{2\pi x}{L})$, $L = 2\lambda$ at normal incidence for H polarization: (——) moment method, (- - - -) fourth order solution, (— —) third order solution, (— - —) second order solution, (— - - - —) first order solution.

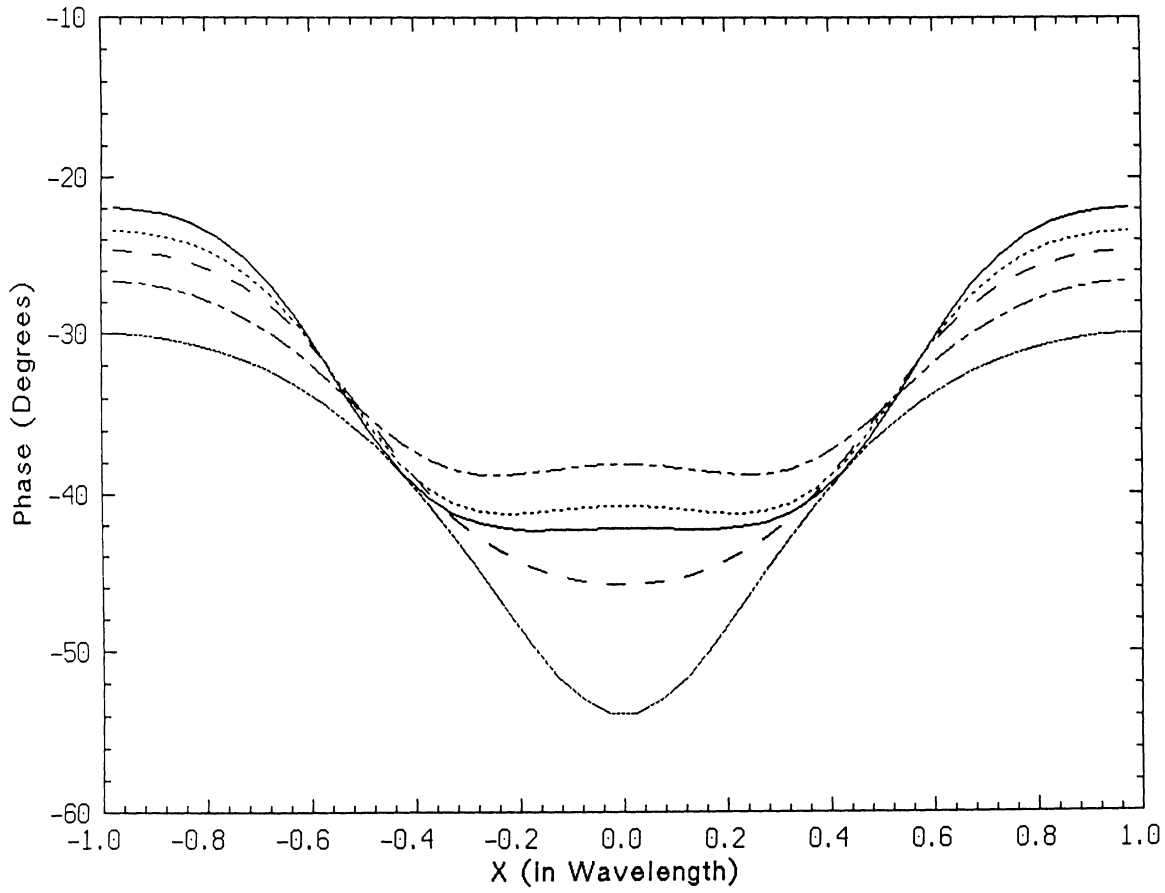

Figure 9: The phase of the induced current on a periodic resistive sheet with resistivity $R(x) = (180 + i270)(1 + 0.7\cos\frac{2\pi x}{L})$, $L = 2\lambda$ at normal incidence for H polarization: (——) moment method, (- - - - -) fourth order solution, (— —) third order solution, (— - —) second order solution, (— - - - —) first order solution.

n	E-polarization		H-polarization	
	E_n^+/E^i	E_n^-/E^i	H_n^+/H^i	H_n^-/H^i
-4	0.001∠62.37	0.001∠62.37	0.001∠-150.10	0.001∠29.90
-3	0.003∠169.70	0.003∠169.70	0.004∠-18.57	0.004∠161.43
-2	0.020∠-76.15	0.020∠-76.15	0.022∠99.93	0.022∠-80.07
-1	0.124∠40.43	0.124∠40.43	0.136∠-143.68	0.136∠36.32
0	0.887∠156.86	0.394∠62.13	0.831∠-27.13	0.460∠55.50
1	0.136∠49.53	0.136∠49.53	0.210∠-158.67	0.210∠21.33

Table 1: Normalized field amplitude of the propagating modes in the upper (+) and lower (-) half-spaces for a periodic resistive sheet $R(x) = R_0(1 + 0.7\cos\frac{2\pi x}{L})$ with $R_0 = 0 + i100$ and $L = 3\lambda$ at $\phi_0 = 30$ degree.

n	E-polarization		H-polarization	
	E_n^+/E^i	E_n^-/E^i	H_n^+/H^i	H_n^-/H^i
-4	0.002∠-105.65	0.002∠-105.65	0.003∠47.66	0.003∠-132.34
-3	0.008∠40.63	0.008∠40.63	0.008∠-145.58	0.008∠34.42
-2	0.028∠-163.62	0.026∠-163.62	0.030∠13.43	0.030∠-166.57
-1	0.110∠-6.41	0.110∠-6.41	0.112∠170.56	0.112∠-9.44
0	0.484∠150.69	0.625∠22.29	0.425∠-32.24	0.679∠19.49
1	0.141∠4.41	0.141∠4.41	0.135∠161.00	0.135∠-19.00

Table 2: Normalized field amplitude of the propagating modes in the upper (+) and lower (-) half-spaces for a periodic resistive sheet $R(x) = R_0(1 + 0.7\cos\frac{2\pi x}{L})$ with $R_0 = 180 + i270$ and $L = 3\lambda$ at $\phi_0 = 30$ degree.

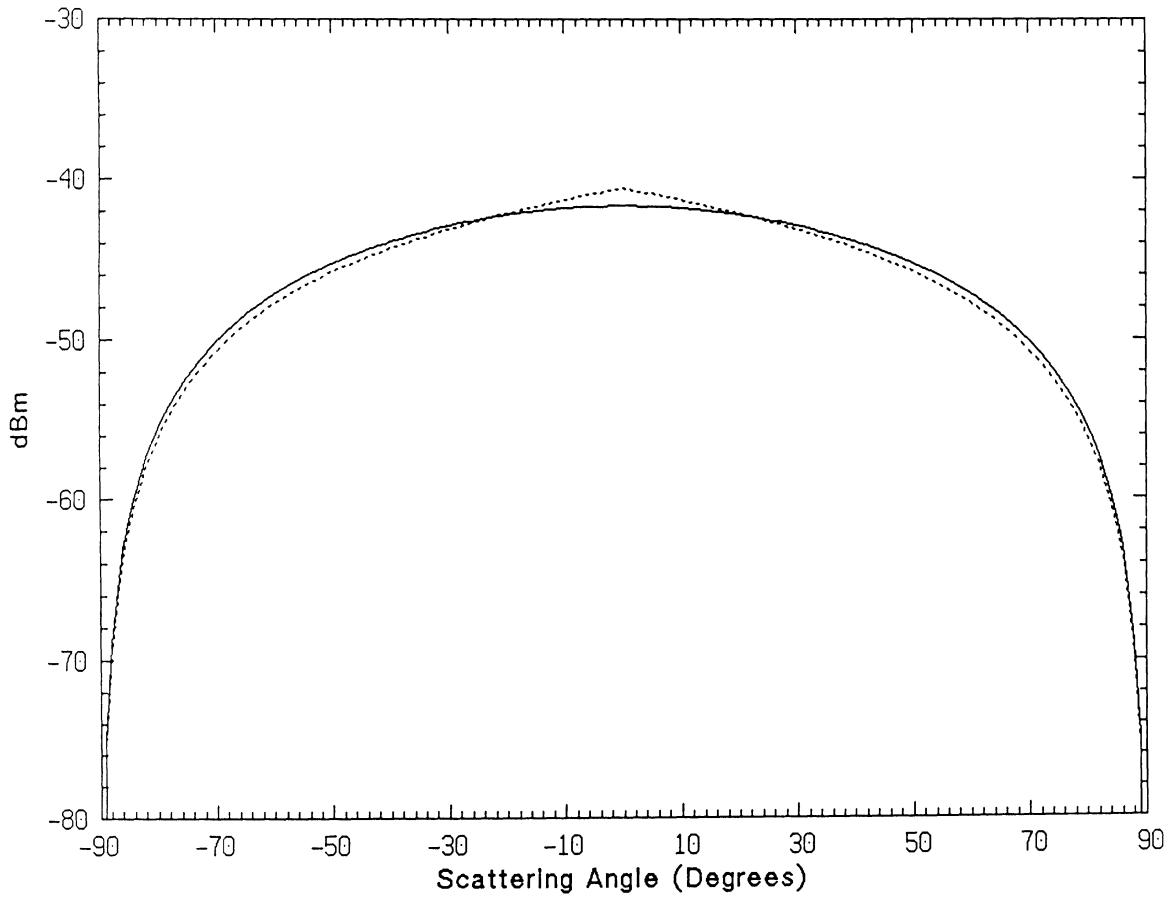

Figure 10: Bistatic echo width of a dielectric hump with $\epsilon = 36 + i17$, $\Delta = 0.3$, and $w = \lambda/15$ over a resistive sheet with $R_0 = 180 + i270$ ($\alpha = 112 - i230$) at $f = 10$ GHz and $\phi_0 = 0$ degrees for E polarization: (——) numerical technique, (- - - -) perturbation technique.

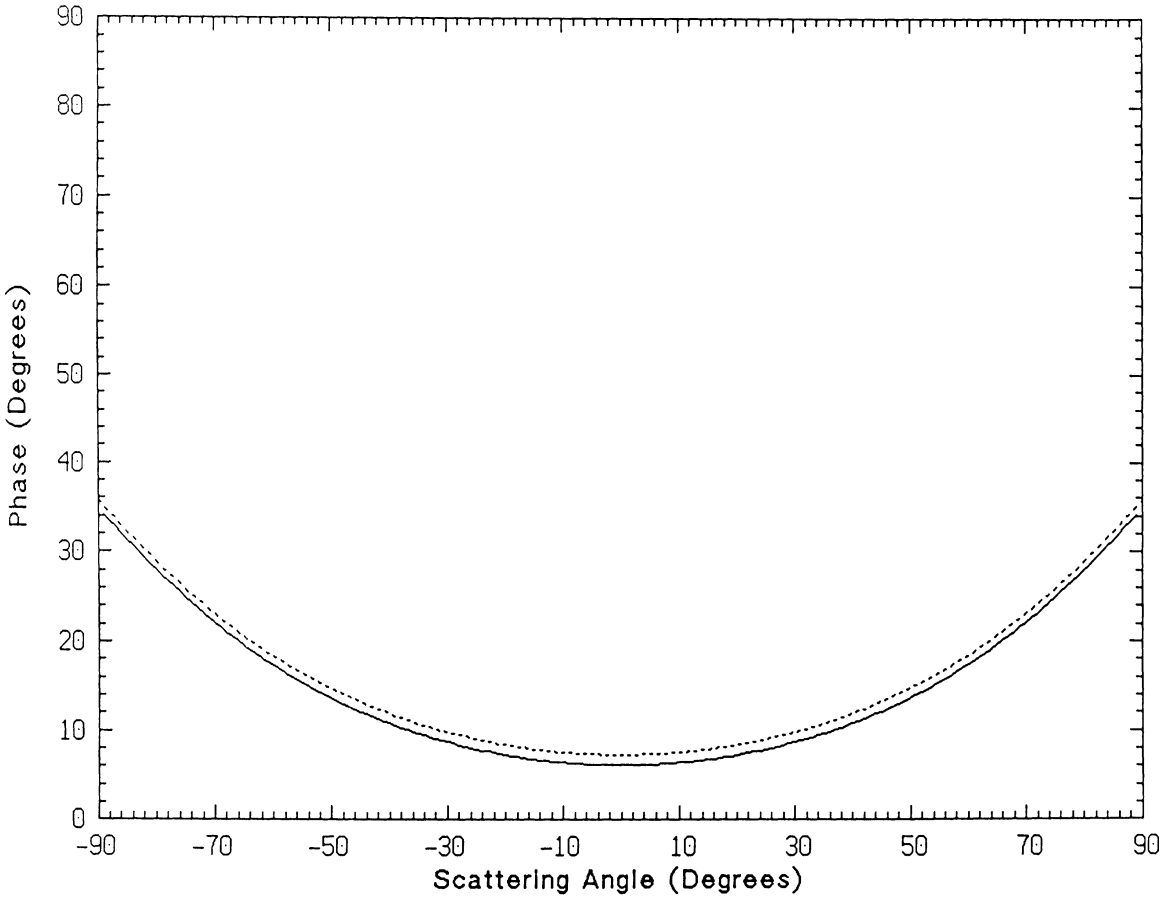

Figure 11: Phase of far field amplitude of a dielectric hump with $\epsilon = 36 + i17$, $\Delta = 0.3$, and $w = \lambda/15$ over a resistive sheet with $R_0 = 180 + i270$ ($\alpha = 112 - i230$) at $f = 10$ GHz and $\phi_0 = 0$ degrees for E polarization: (——) numerical technique, (- - - -) perturbation technique.

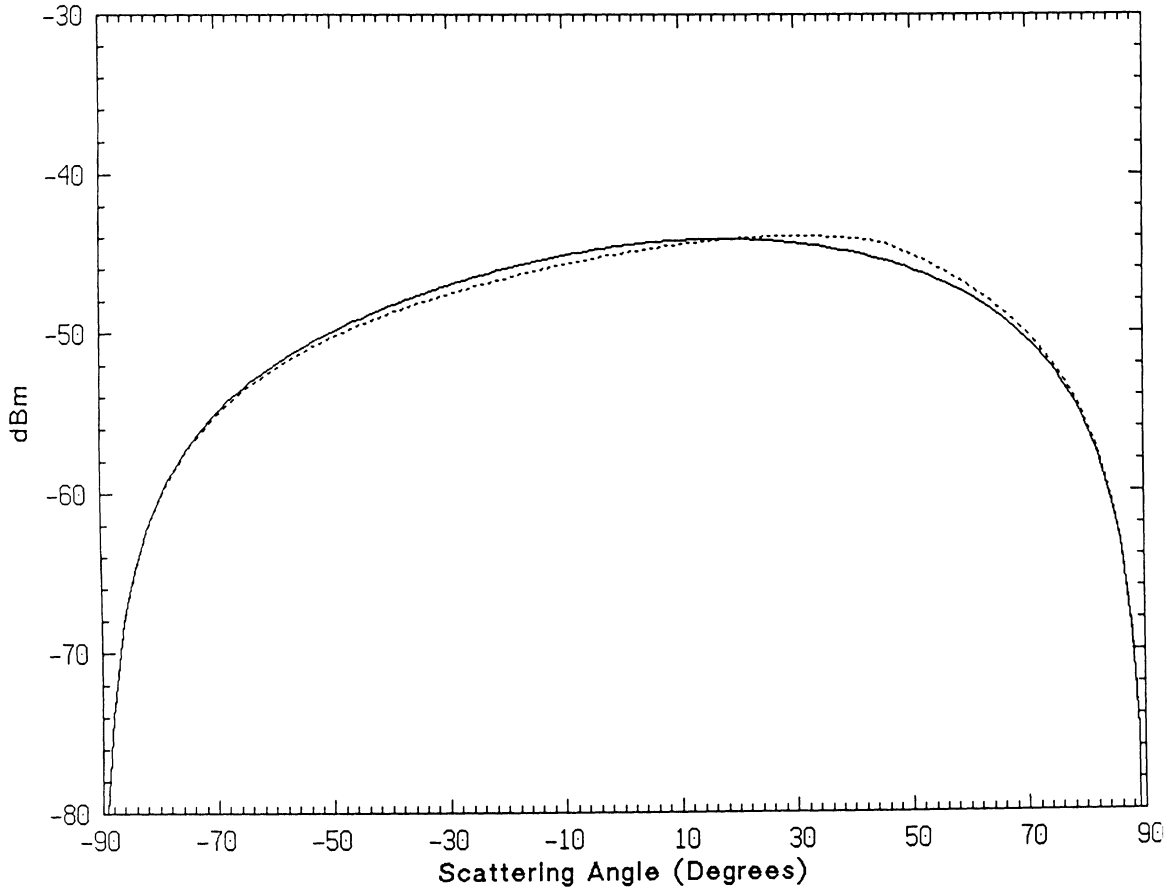

Figure 12: Bistatic echo width of a dielectric hump with $\epsilon = 36 + i17$, $\Delta = 0.3$, and $w = \lambda/15$ over a resistive sheet with $R_0 = 180 + i270$ ($\alpha = 112 - i230$) at $f = 10$ GHz and $\phi_0 = 45$ degrees for E polarization: (——) numerical technique, (- - - - -) perturbation technique.

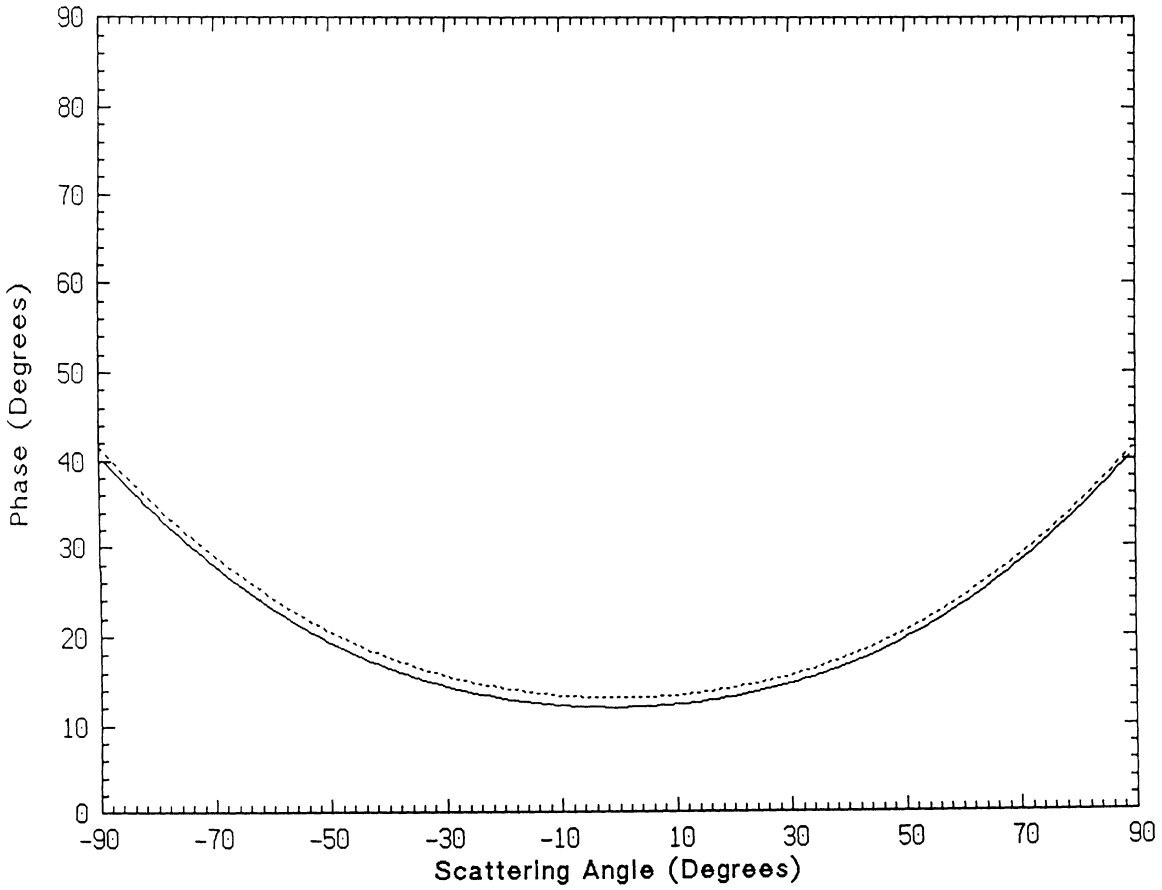

Figure 13: Phase of far field amplitude of a dielectric hump with $\epsilon = 36 + i17$, $\Delta = 0.3$, and $w = \lambda/15$ over a resistive sheet with $R_0 = 180 + i270$ ($\alpha = 112 - i230$) at $f = 10$ GHz and $\phi_0 = 45$ degrees for E polarization: (——) numerical technique, (- - - - -) perturbation technique.

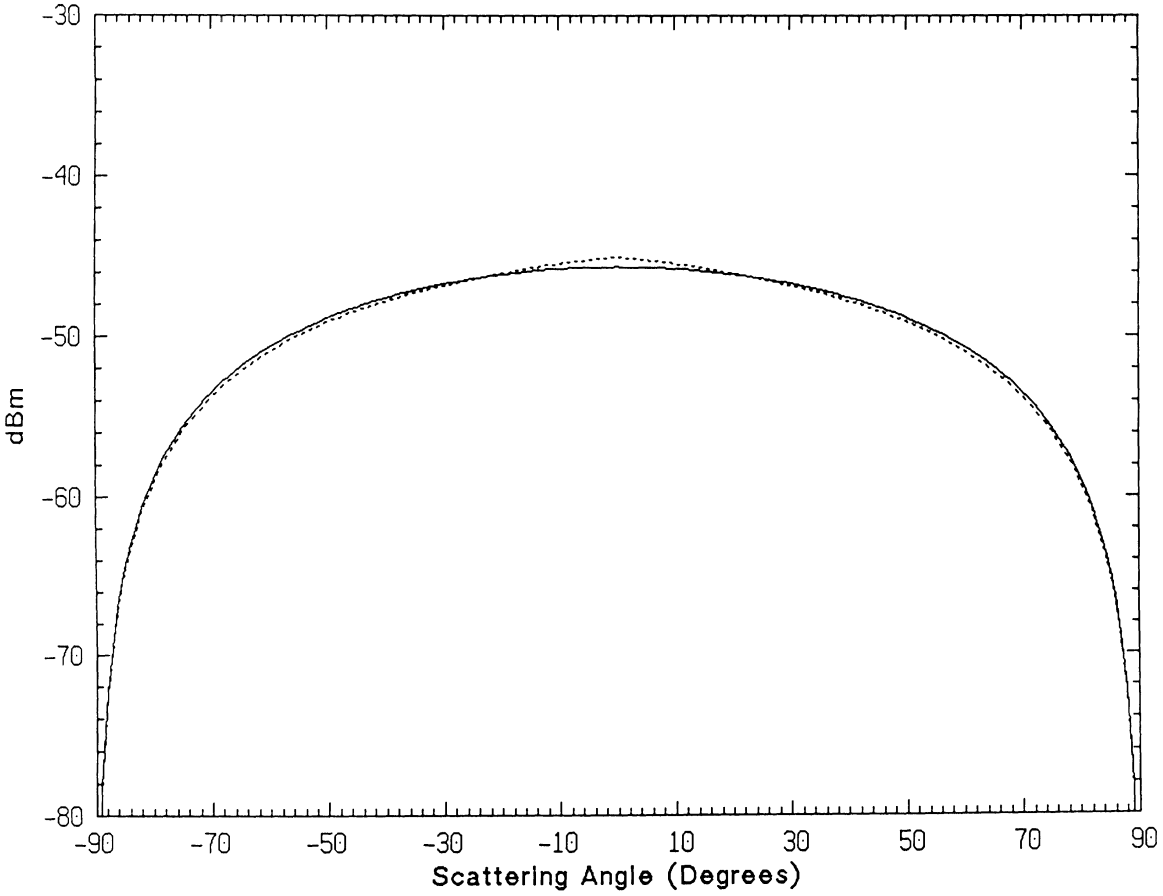

Figure 14: Bistatic echo width of a dielectric hump with $\epsilon = 36 + i17$, $\Delta = 0.3$, and $w = \lambda/25$ over a resistive sheet with $R_0 = 180 + i270$ ($\alpha = 112 - i230$) at $f = 10$ GHz and $\phi_0 = 0$ degrees for E polarization: (——) numerical technique, (- - - -) perturbation technique.

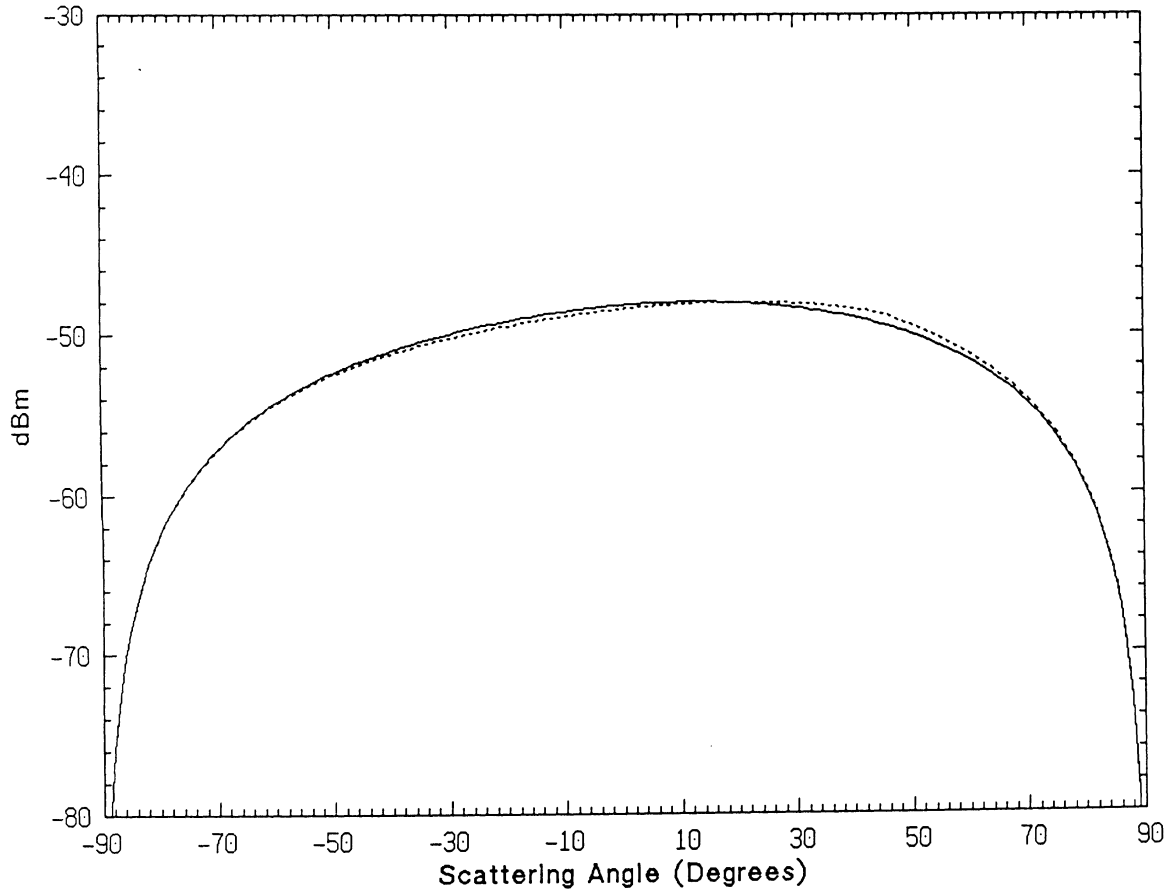

Figure 15: Bistatic echo width of a dielectric hump with $\epsilon = 36 + i17$, $\Delta = 0.3$, and $w = \lambda/25$ over a resistive sheet with $R_0 = 180 + i270$ ($\alpha = 112 - i230$) at $f = 10$ GHz and $\phi_0 = 45$ degrees for E polarization: (——) numerical technique, (- - - - -) perturbation technique.

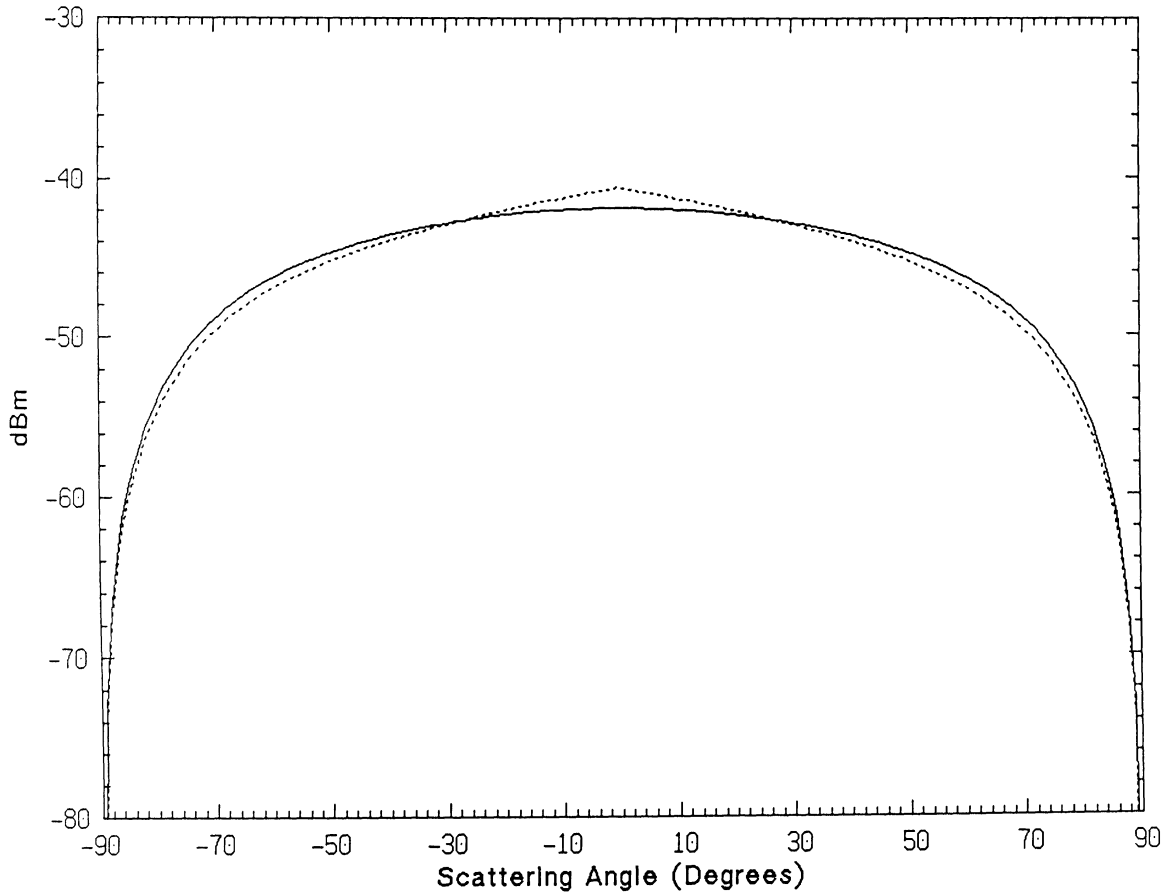

Figure 16: Bistatic echo width of a dielectric hump with $\epsilon = 36 + i17$, $\Delta = 0.3$, and $w = \lambda/15$ over a resistive sheet with $R_0 = 180 + i270$ ($\beta = 75 + i154$) at $f = 10$ GHz and $\phi_0 = 0$ degrees for H polarization: (——) numerical technique, (- - - - -) perturbation technique.

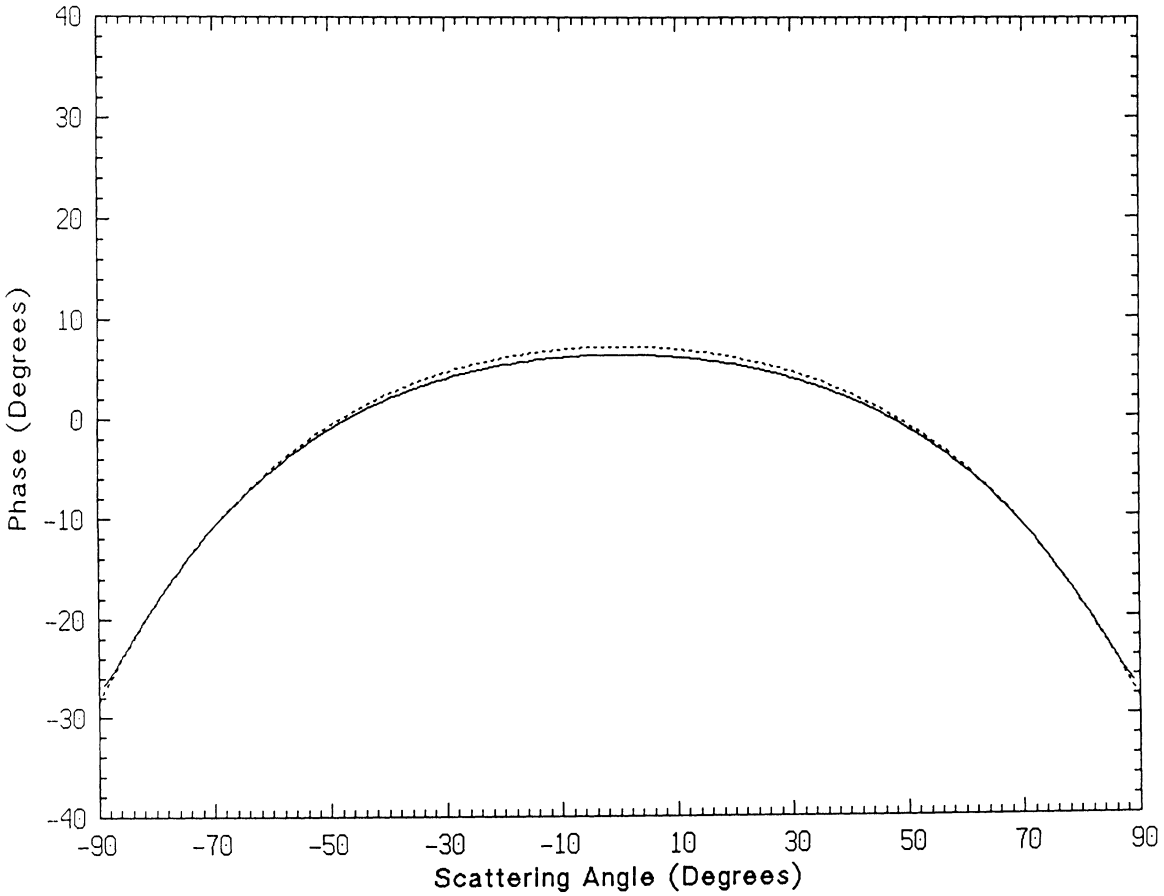

Figure 17: Phase of far field amplitude of a dielectric hump with $\epsilon = 36 + i17$, $\Delta = 0.3$, and $w = \lambda/15$ over a resistive sheet with $R_0 = 180 + i270$ ($\beta = 75 + i154$) at $f = 10$ GHz and $\phi_0 = 0$ degrees for H polarization: (——) numerical technique, (- - - - -) perturbation technique.

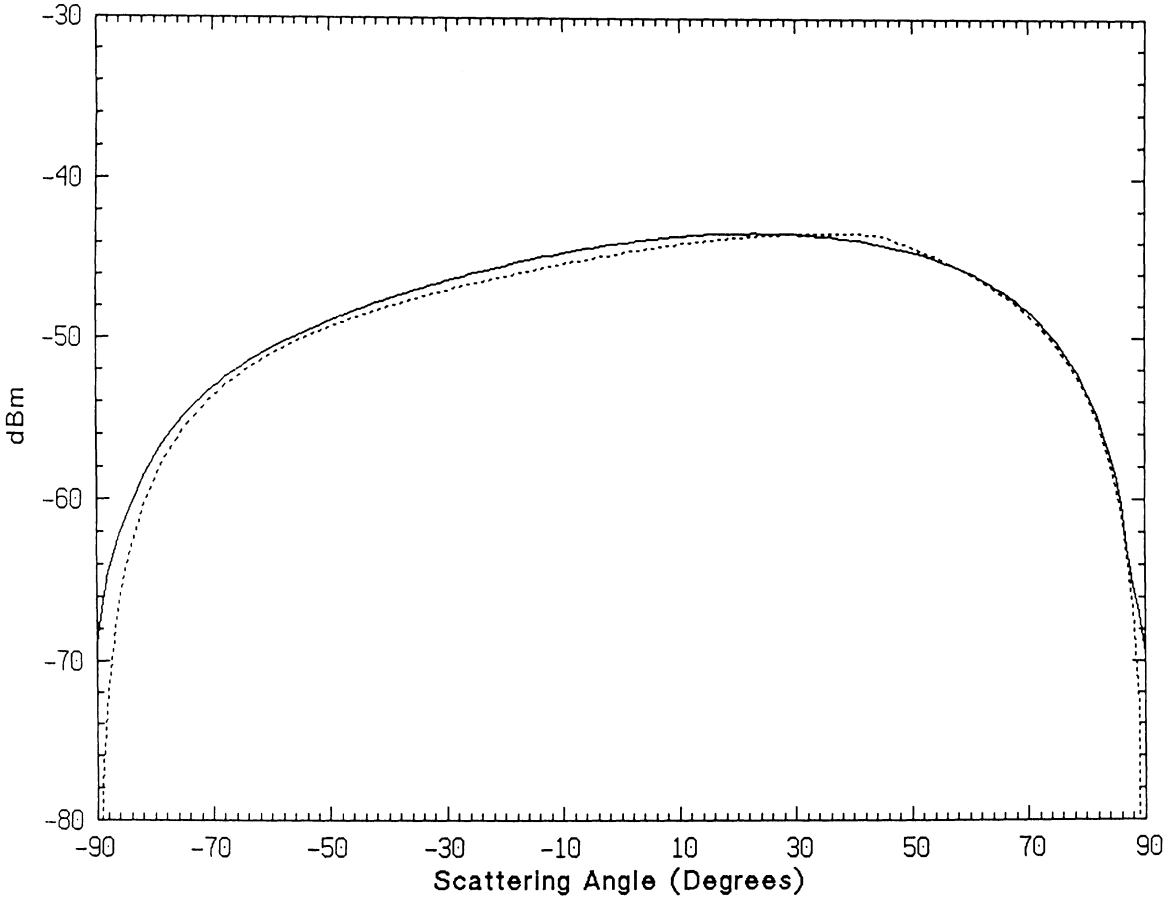

Figure 18: Bistatic echo width of a dielectric hump with $\epsilon = 36 + i17$, $\Delta = 0.3$, and $w = \lambda/15$ over a resistive sheet with $R_0 = 180 + i270$ ($\beta = 75 + i154$) at $f = 10$ GHz and $\phi_0 = 45$ degrees for H polarization: (——) numerical technique, (- - - -) perturbation technique.

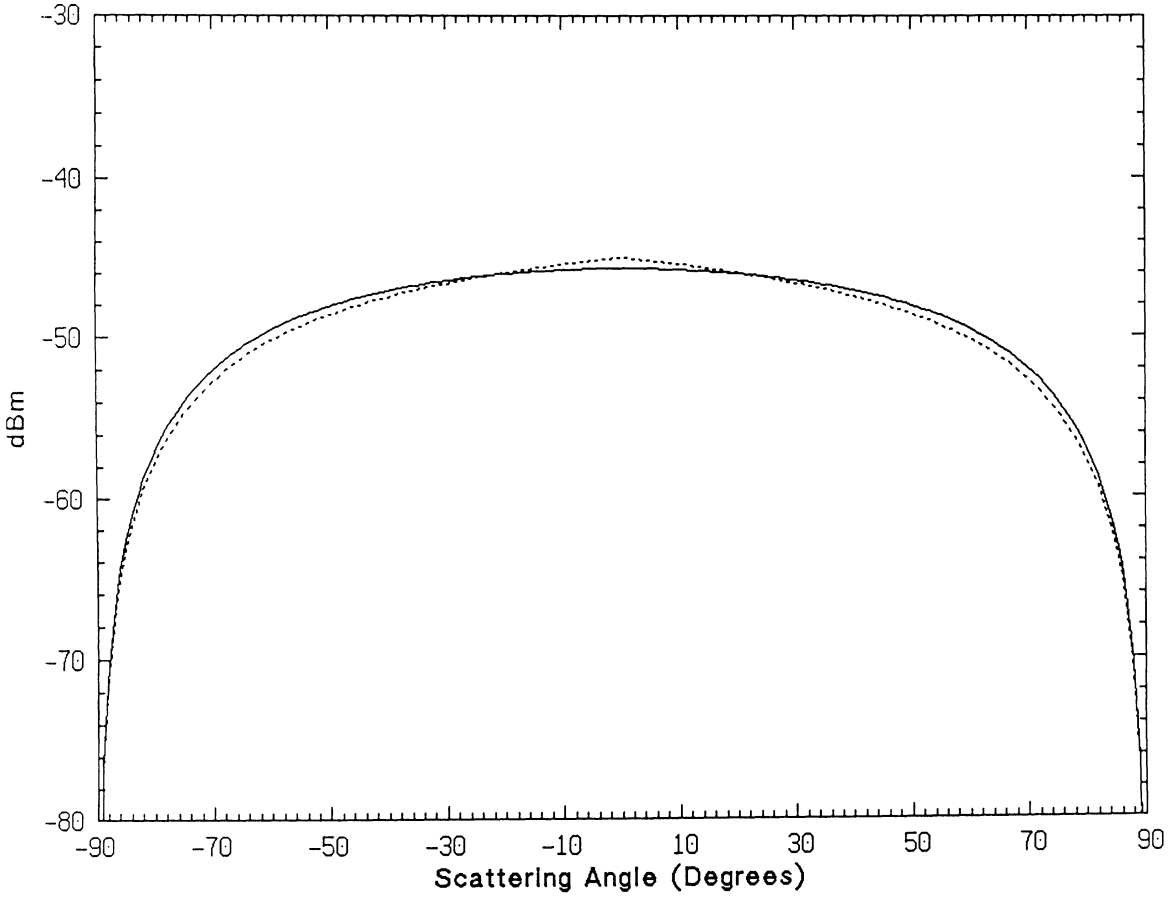

Figure 19: Bistatic echo width of a dielectric hump with $\epsilon = 36 + i17$, $\Delta = 0.3$, and $w = \lambda/25$ over a resistive sheet with $R_0 = 180 + i270$ ($\beta = 75 + i154$) at $f = 10$ GHz and $\phi_0 = 0$ degrees for H polarization: (——) numerical technique, (- - - - -) perturbation technique.

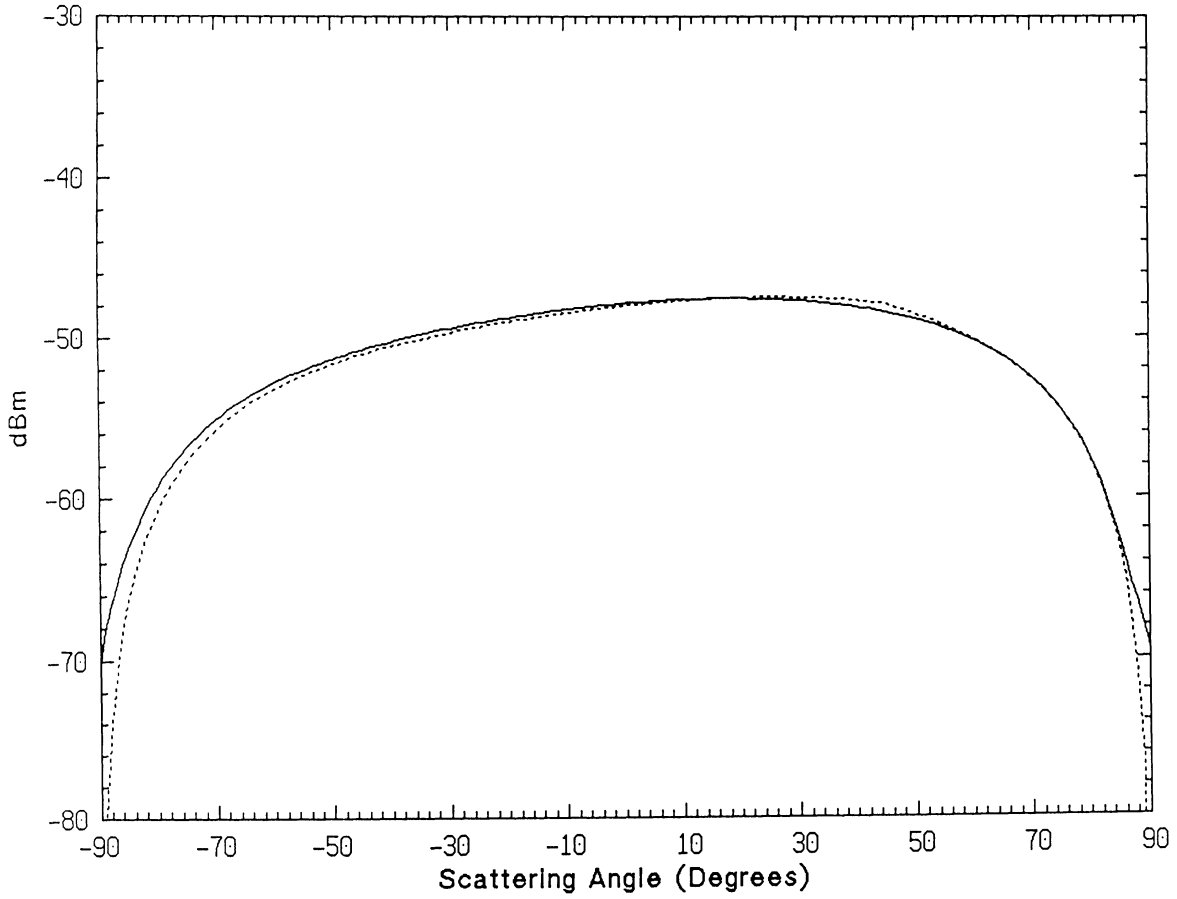

Figure 20: Bistatic echo width of a dielectric hump with $\epsilon = 36 + i17$, $\Delta = 0.3$, and $w = \lambda/25$ over a resistive sheet with $R_0 = 180 + i270$ ($\beta = 75 + i154$) at $f = 10$ GHz and $\phi_0 = 45$ degrees for H polarization: (——) numerical technique, (- - - -) perturbation technique.

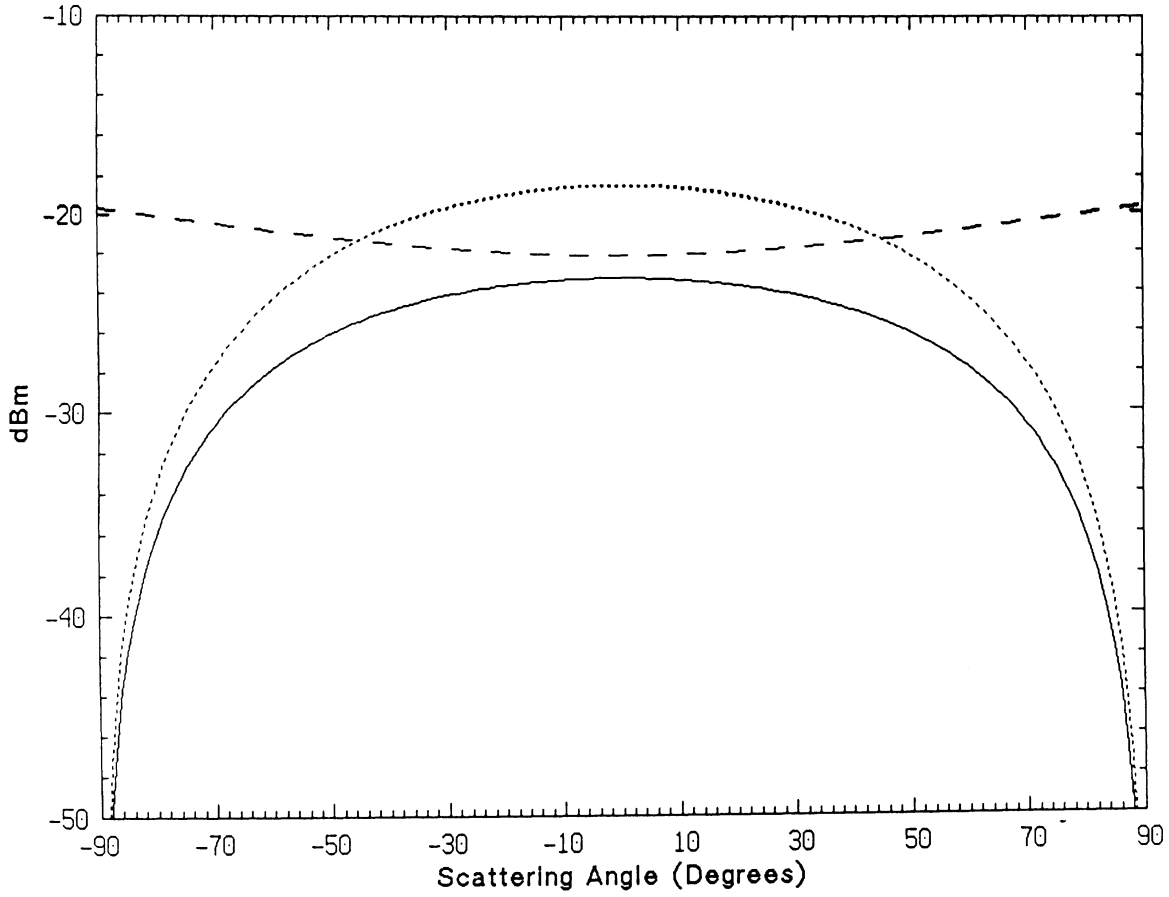

Figure 21: Bistatic echo width of a $\lambda/10 \times \lambda/10$ square dielectric cylinder with $\epsilon = 36 + i17$, at $f = 10$ GHz and $\phi_0 = 0$ degrees for E polarization: (——) cylinder over resistive sheet $R_0 = 180 + i270$, (- - - - -) cylinder over perfect conductor, (— —) cylinder in free space.

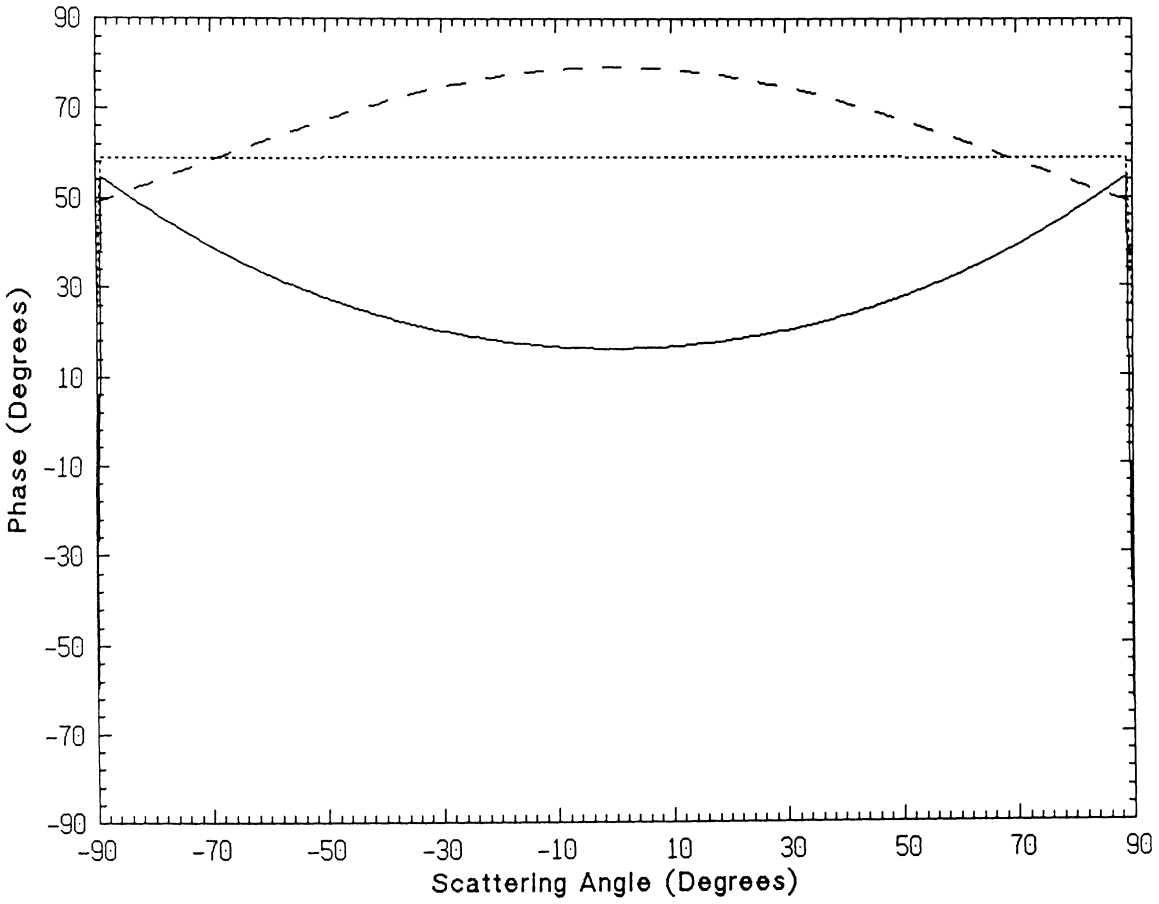

Figure 22: Phase of far field amplitude of a $\lambda/10 \times \lambda/10$ square dielectric cylinder with $\epsilon = 36 + i17$, at $f = 10$ GHz and $\phi_0 = 0$ degrees for E polarization: (— —) cylinder over resistive sheet $R_0 = 180 + i270$, (- - - - -) cylinder over perfect conductor, (— —) cylinder in free space.

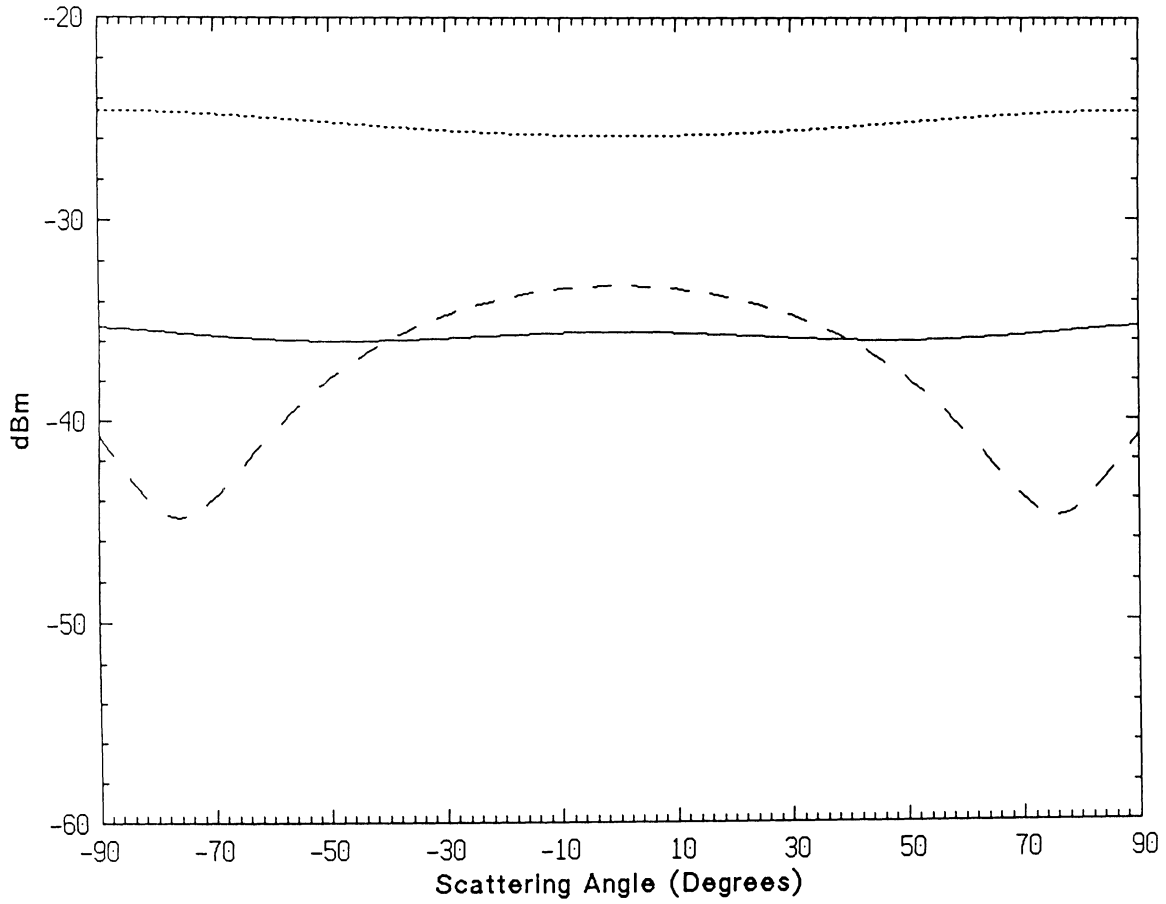

Figure 23: Bistatic echo width of a $\lambda/10 \times \lambda/10$ square dielectric cylinder with $\epsilon = 36 + i17$, at $f = 10$ GHz and $\phi_0 = 0$ degrees for H polarization: (——) cylinder over resistive sheet $R_0 = 180 + i270$, (- - - - -) cylinder over perfect conductor, (— —) cylinder in free space.

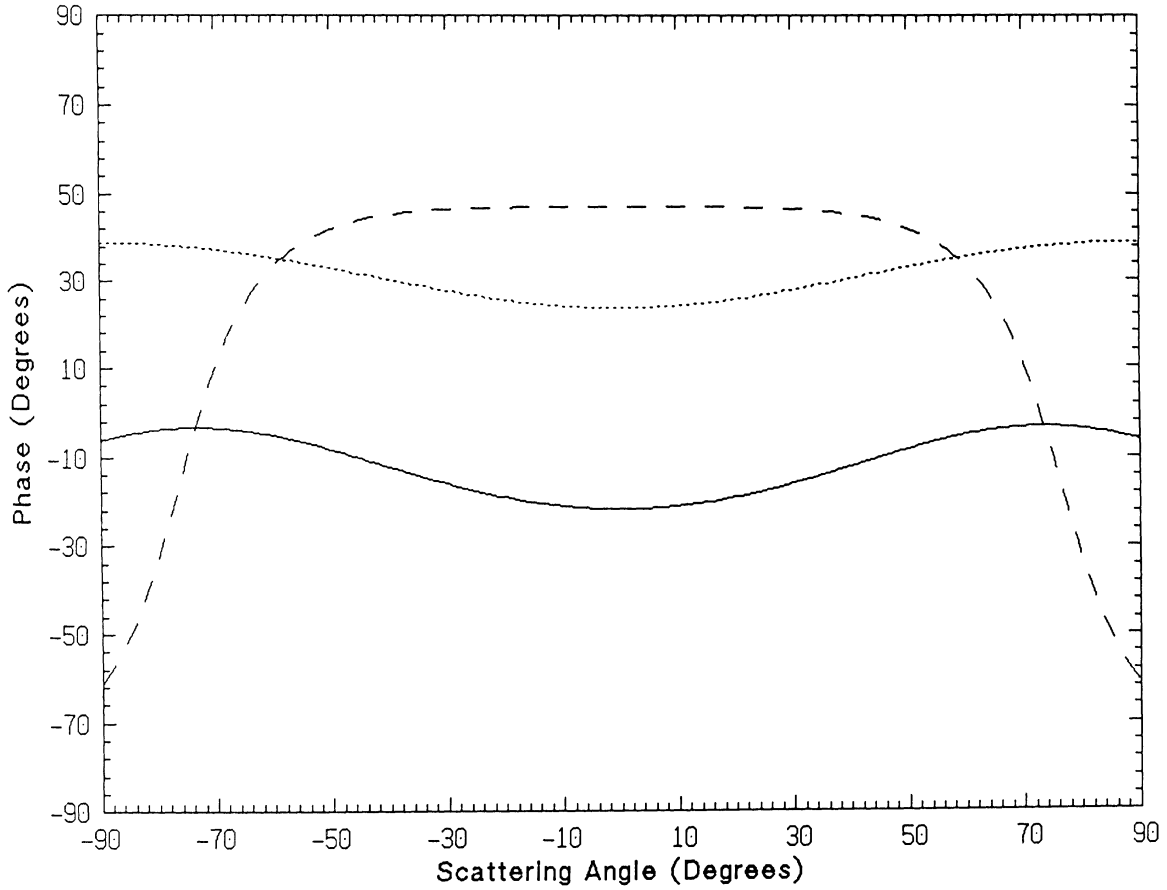

Figure 24: Phase of far field amplitude of a $\lambda/10 \times \lambda/10$ square dielectric cylinder with $\epsilon = 36 + i17$, at $f = 10$ GHz and $\phi_0 = 0$ degrees for H polarization: (— —) cylinder over resistive sheet $R_0 = 180 + i270$, (- - - - -) cylinder over perfect conductor, (— —) cylinder in free space.

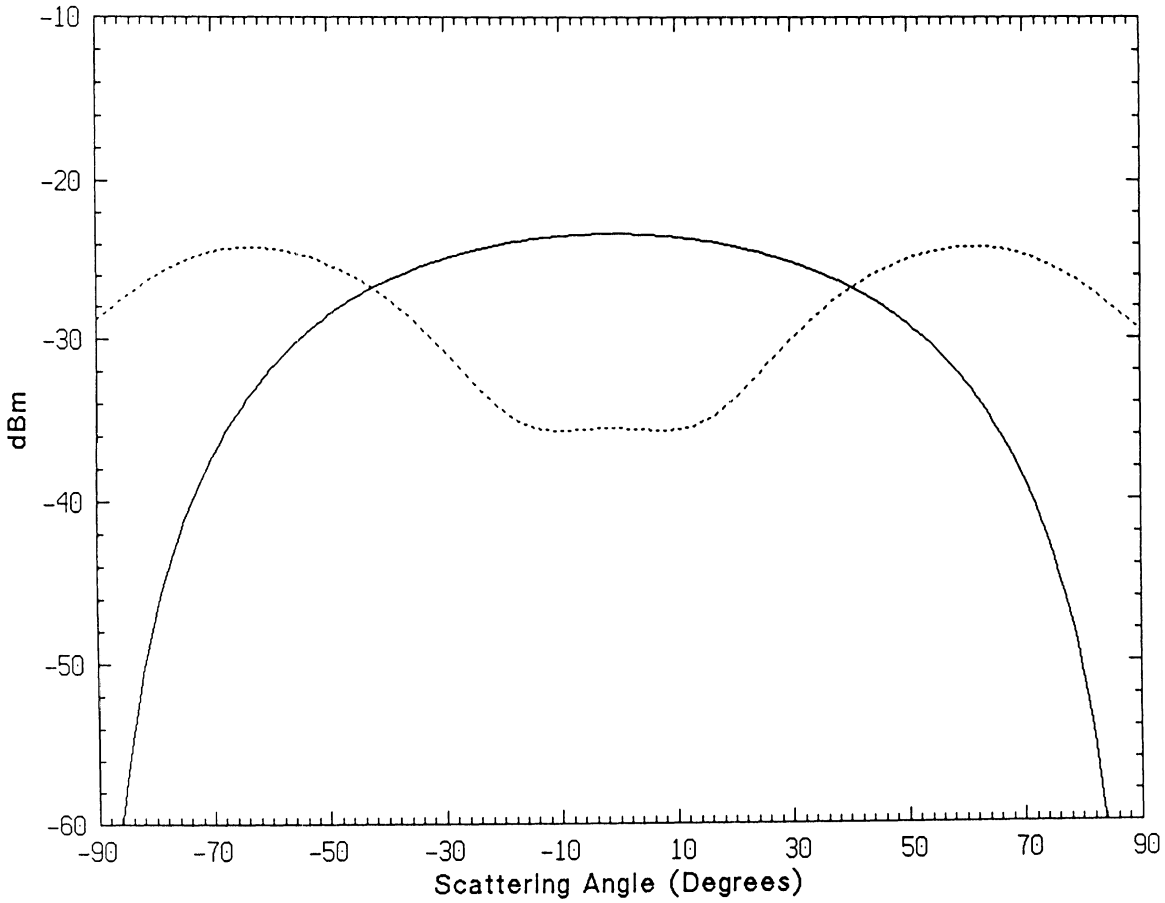

Figure 25: Backscattering echo width of a $\lambda/10 \times \lambda/10$ square dielectric cylinder over resistive sheet $R_0 = 180 + i270$ with $\epsilon = 36 + i17$ at $f = 10$ GHz: (——) E polarization, (- - - - -) H polarization.

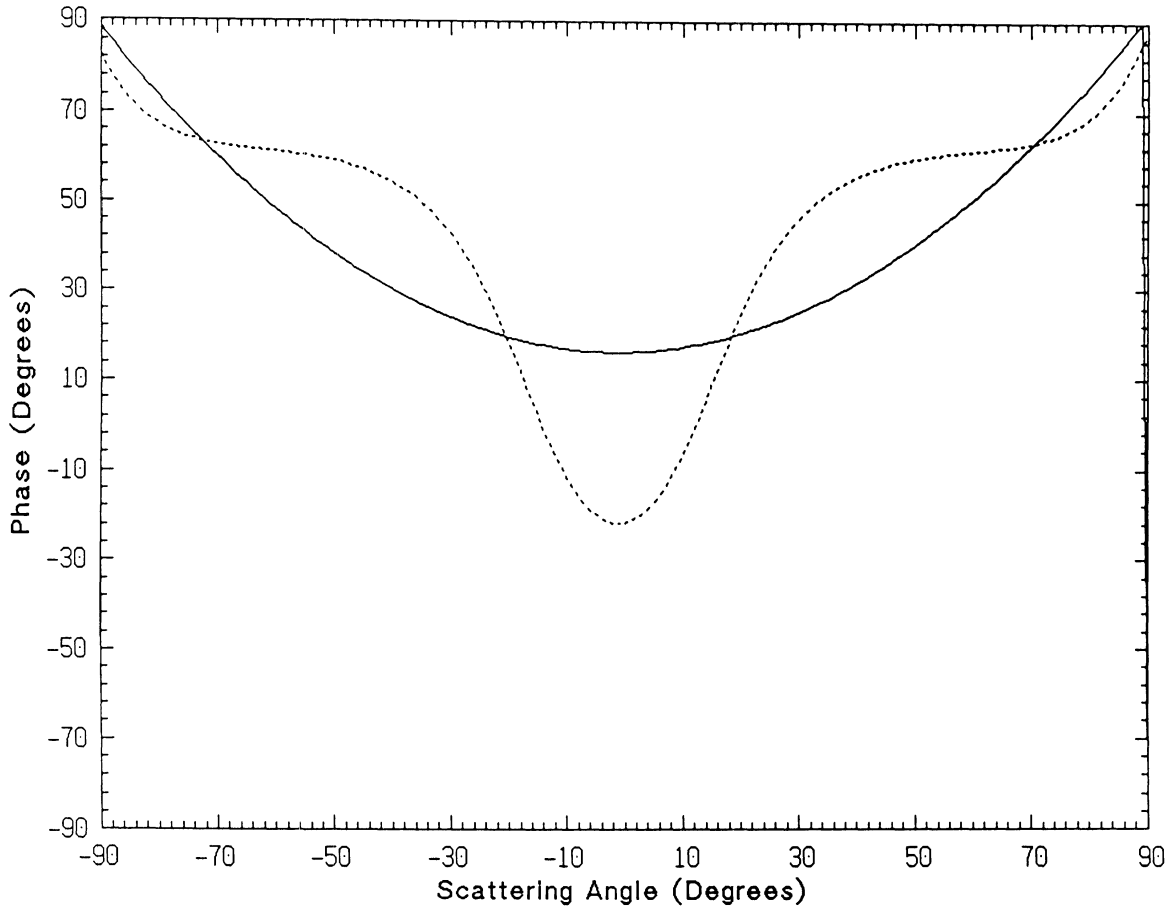

Figure 26: Phase of far field amplitude (backscattering) of a $\lambda/10 \times \lambda/10$ square dielectric cylinder over resistive sheet $R_0 = 180 + i270$ with $\epsilon = 36 + i17$ at $f = 10$ GHz: (——) E polarization, (- - - - -) H polarization.

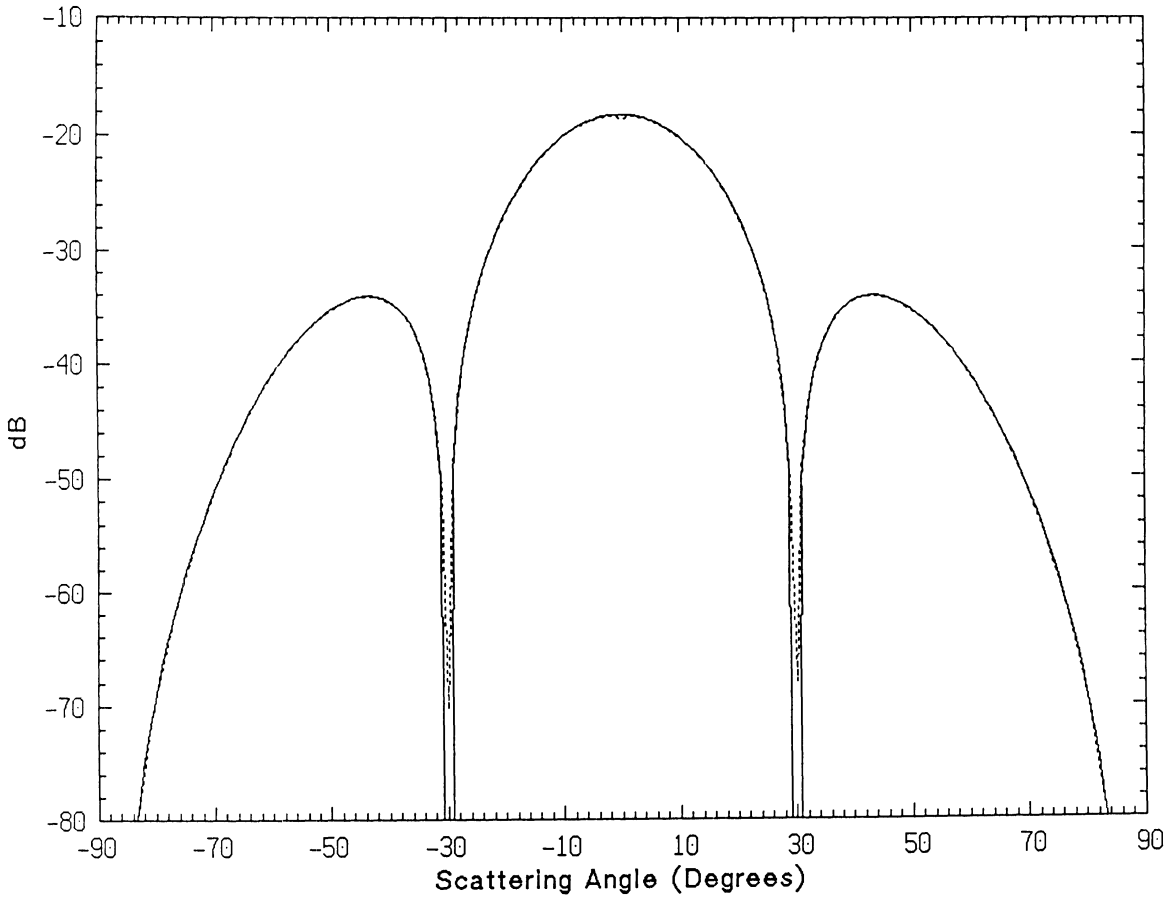

Figure 27: Normalized bistatic echo width (σ/λ) of an impedance insert with $w = 2\lambda$, $\eta_1 = 44 - i44$, $\eta_0 = 40 - i40$ ($\Delta = 0.1$) at $\phi_0 = 0$ degrees for E polarization: (——) perturbation technique, (- - - - -) GTD technique.

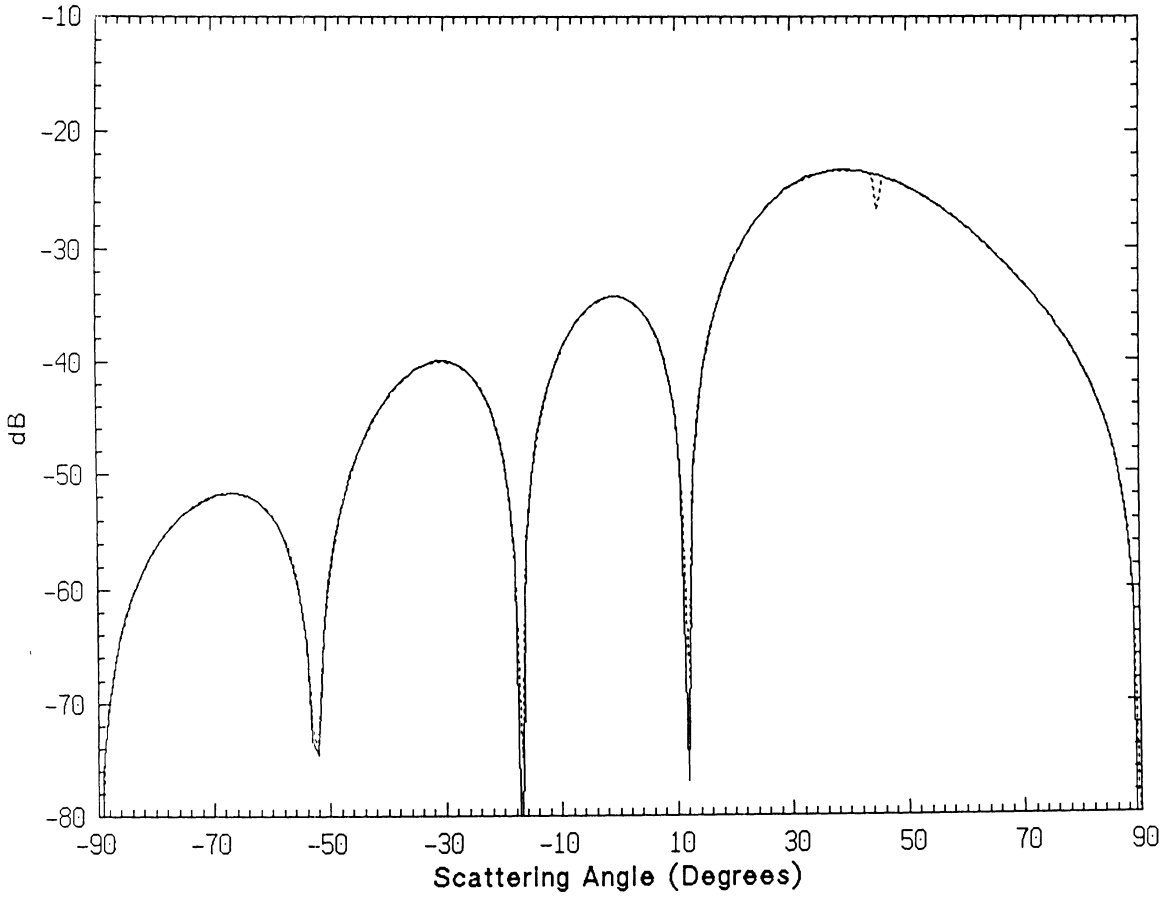

Figure 28: Normalized bistatic echo width (σ/λ) of an impedance insert with $w = 2\lambda$, $\eta_1 = 44 - i44$, $\eta_0 = 40 - i40$ ($\Delta = 0.1$) at $\phi_0 = 45$ degrees for E polarization: (——) perturbation technique, (- - - - -) GTD technique.

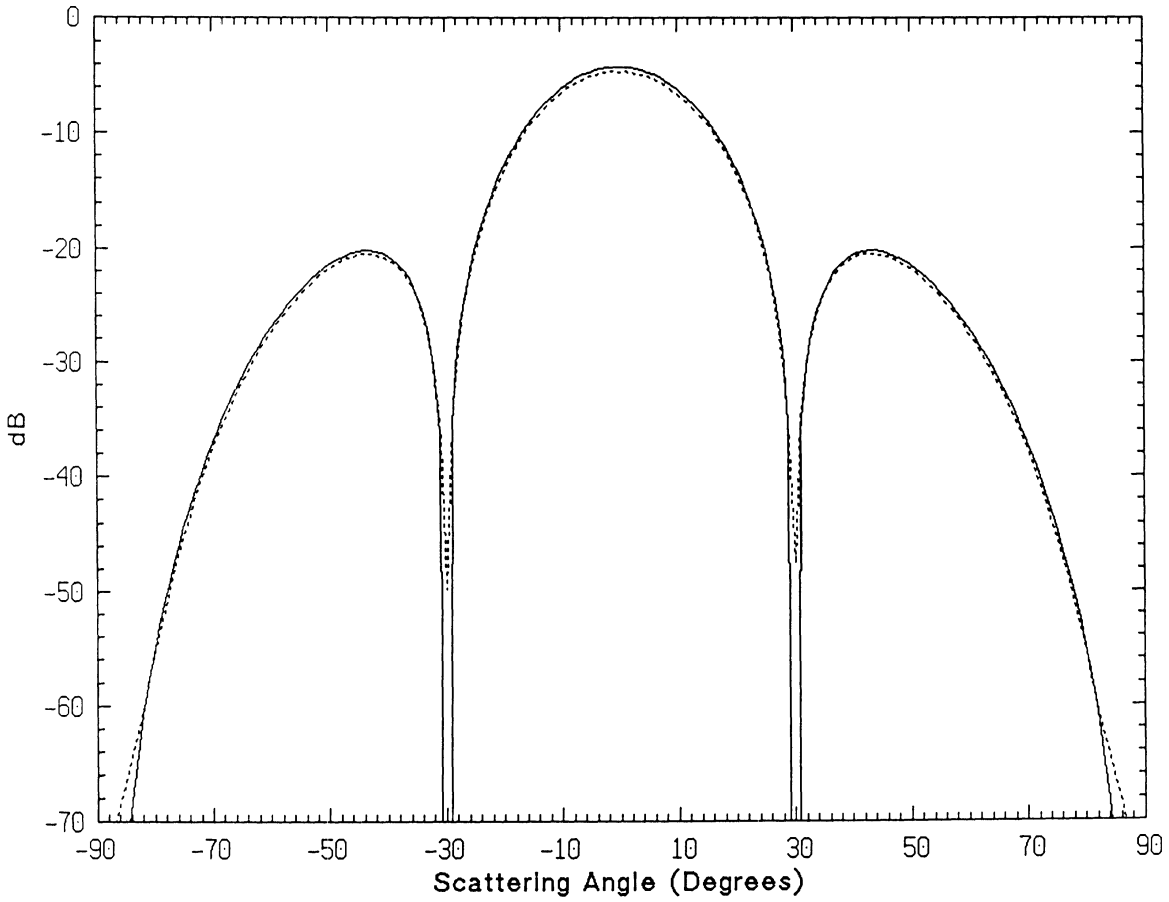

Figure 29: Normalized bistatic echo width (σ/λ) of an impedance insert with $w = 2\lambda$, $\eta_1 = 60 - i60$, $\eta_0 = 40 - i40$ ($\Delta = 0.5$) at $\phi_0 = 0$ degrees for E polarization: (——) perturbation technique, (- - - - -) GTD technique.

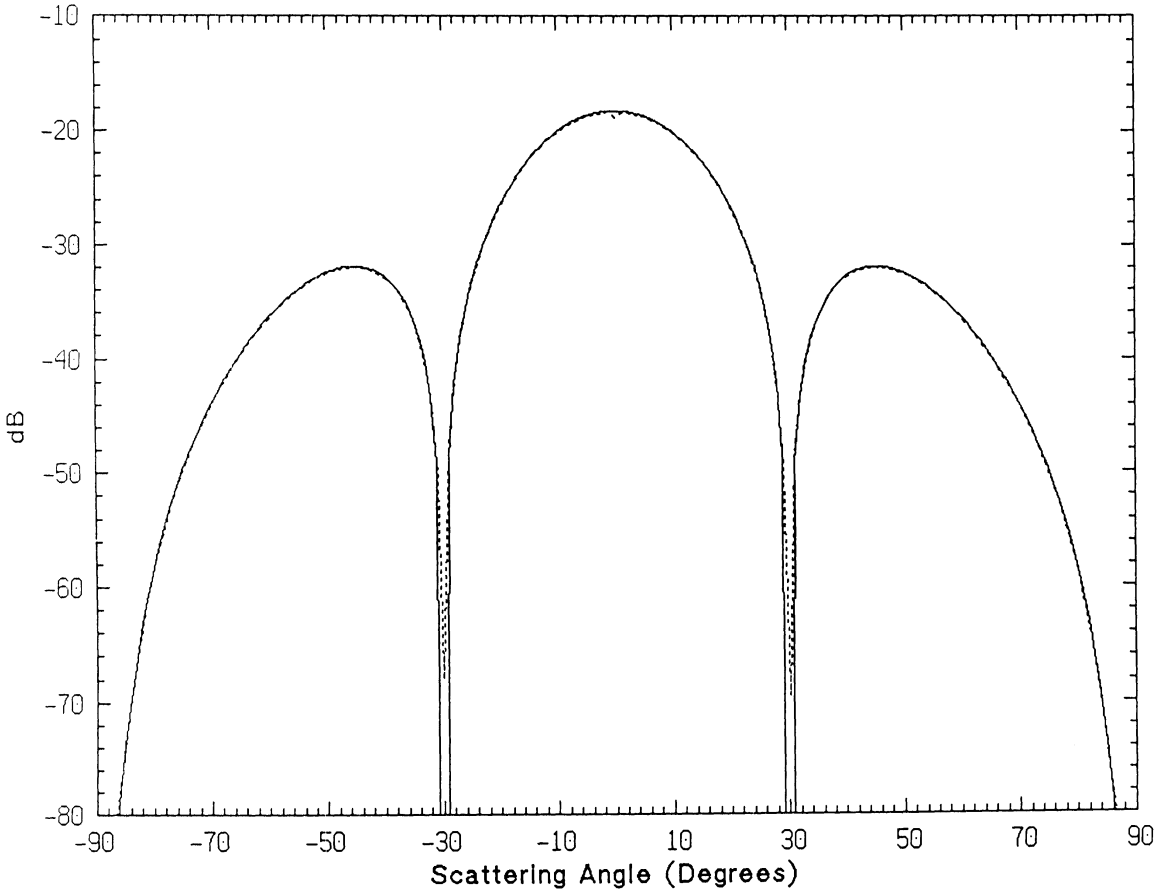

Figure 30: Normalized bistatic echo width (σ/λ) of an impedance insert with $w = 2\lambda$, $\eta_1 = 44 - i44$, $\eta_0 = 40 - i40$ ($\Delta = 0.1$) at $\phi_0 = 0$ degrees for H polarization: (——) perturbation technique, (- - - - -) GTD technique.

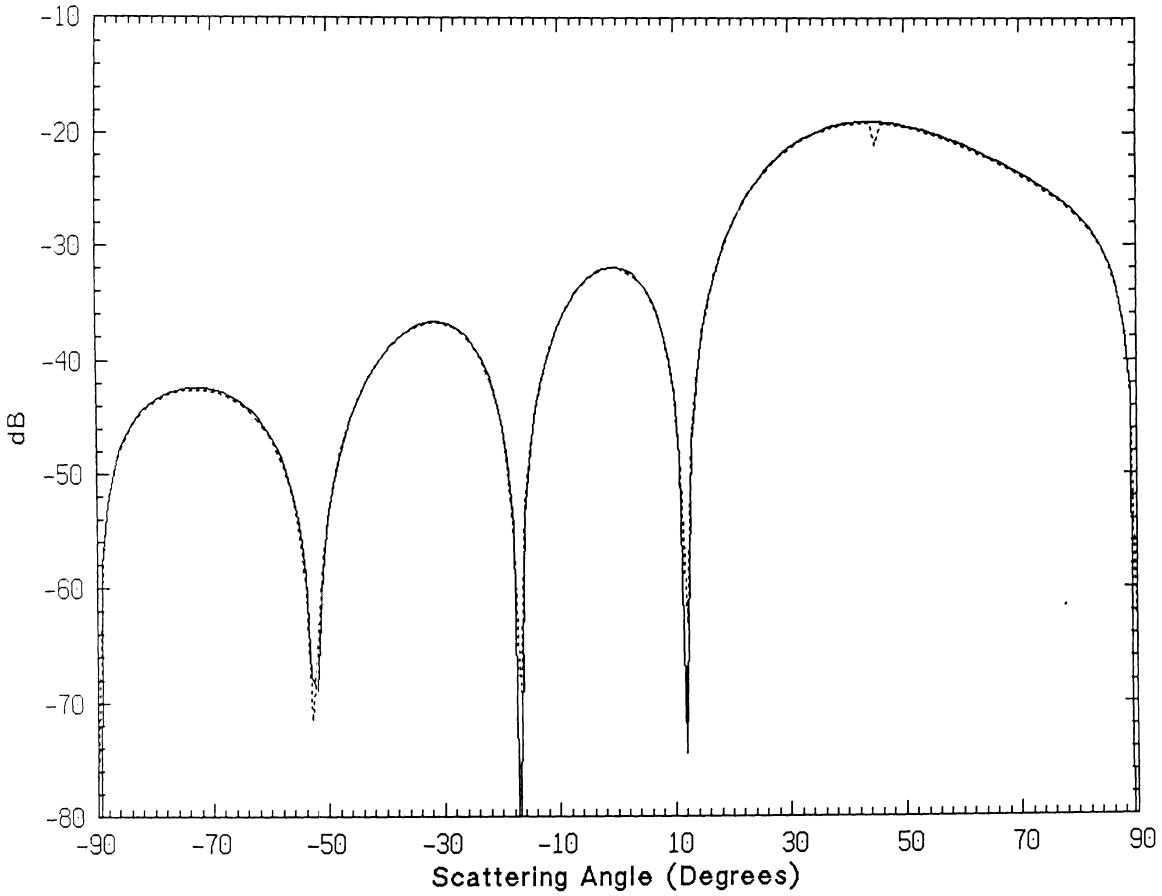

Figure 31: Normalized bistatic echo width (σ/λ) of an impedance insert with $w = 2\lambda$, $\eta_1 = 44 - i44$, $\eta_0 = 40 - i40$ ($\Delta = 0.1$) at $\phi_0 = 45$ degrees for H polarization: (——) perturbation technique, (- - - - -) GTD technique.

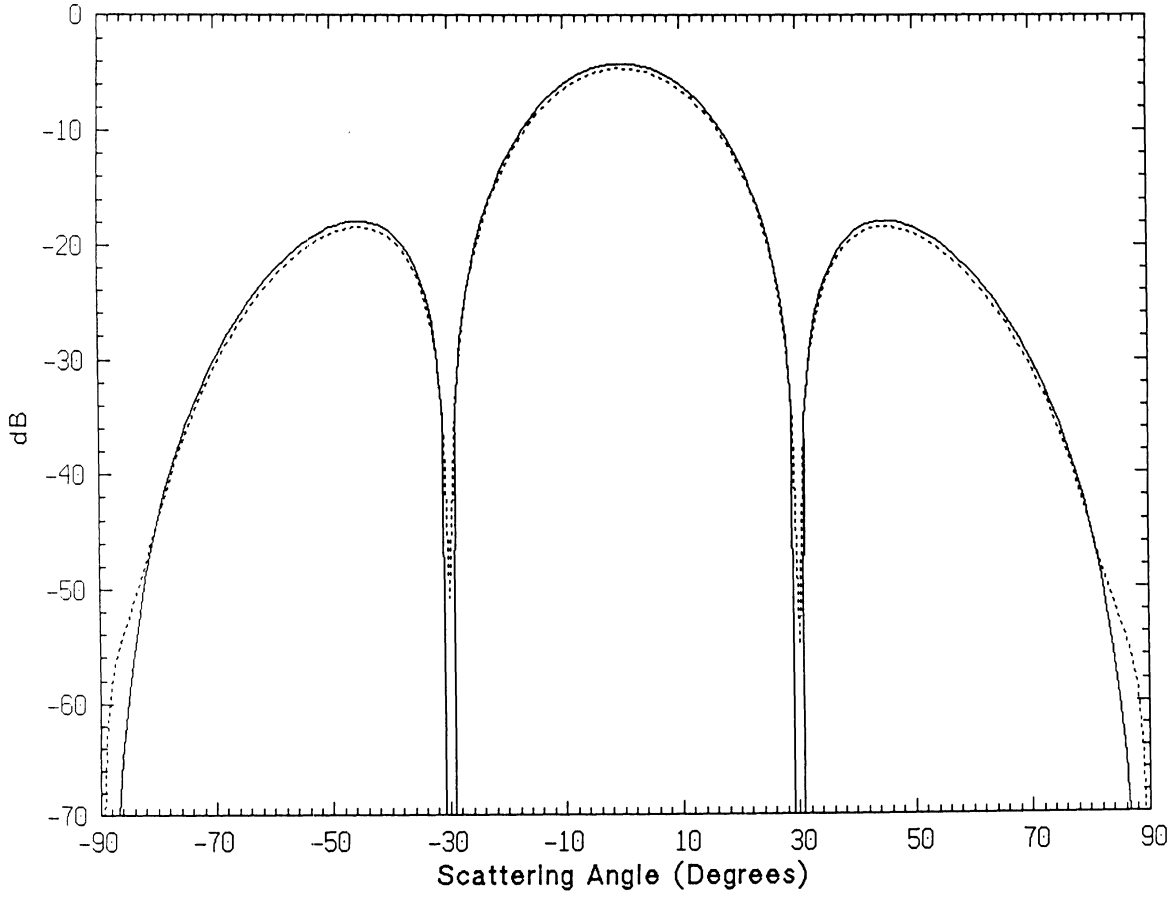

Figure 32: Normalized bistatic echo width (σ/λ) of an impedance insert with $w = 2\lambda$, $\eta_1 = 60 - i60$, $\eta_0 = 40 - i40$ ($\Delta = 0.5$) at $\phi_0 = 0$ degrees for H polarization: (——) perturbation technique, (- - - - -) GTD technique.

APPENDIX A
NUMERICAL ANALYSIS FOR A PERIODIC RESISTIVE SHEET

A1 Derivation of Green's Function

For a resistive sheet which is periodic in one dimension with period L, we have

$$R(x+L) = R(x) \tag{A1}$$

If the resistive sheet is illuminated by a plane wave of the form

$$\mathbf{E}^i = \hat{\mathbf{e}}^i e^{ik_0(\sin\phi_0 x - \cos\phi_0 z)} \tag{A2}$$

where $\hat{\mathbf{e}}^i$ is the polarization unit vector, the induced current on the resistive sheet must satisfy the periodicity requirements imposed by Floquet's theorem, i.e.

$$J(x+nL) = J(x)e^{ik_0 \sin\phi_0 nL} \tag{A3}$$

Let us first consider E polarization case where $\hat{\mathbf{e}}^i = \hat{\mathbf{y}}$. The scattered electric field can derived from (9). By subdividing the integral into multiples of a period, the equation can be written as

$$E_y^s = -\frac{k_0 Z_0}{4} \sum_{n=-\infty}^{+\infty} \int_{x_0+nL}^{x_0+(n+1)L} J_y(x') H_0^{(1)}(k_0\sqrt{(x-x')^2+z^2})\mathrm{d}x' \tag{A4}$$

If the variable x' is now changed to $x' + nL$ and the property (A3) is employed, we get

$$E_y^s = -\frac{k_0 Z_0}{4} \int_{x_0}^{x_0+L} J_y(x') G_e(x, x', z)\mathrm{d}x', \tag{A5}$$

where

$$G_e(x,x',z) \equiv \sum_{n=-\infty}^{+\infty} H_0^{(1)}(k_0\sqrt{(x-x'-nL)^2+z^2})e^{ik_0\sin\phi_0 nL} \tag{A6}$$

is the Green's function of the problem. The series is very slowly converging, specially when L is small compared to the wavelength. To make the problem computationally tractable a better form for Green's function is needed. If the Fourier integral representation of the Hankel function is inserted into (A6) and the order of summation, integration reversed, we have

$$G_e(x,x',z) = \frac{1}{\pi}\int_{-\infty}^{+\infty} \frac{e^{i[\sqrt{k_0^2-\alpha^2}|z|+\alpha(x-x')]}}{\sqrt{k_0^2-\alpha^2}} \sum_{n=-\infty}^{+\infty} e^{-in(\alpha-k_0\sin\phi_0)L}d\alpha. \tag{A7}$$

But

$$\sum_{n=-\infty}^{+\infty} e^{-in(\alpha-k_0\sin\phi_0)L} = 2\pi \sum_{n=-\infty}^{+\infty} \delta[(\alpha-k_0\sin\phi_0)L-2\pi n]. \tag{A8}$$

Applying the above identity to (A7) and changing the order of summation and integration one more time provides the following expression for the Green's function:

$$G_e(x,x',z) = \frac{2}{L}\sum_{n=-\infty}^{+\infty} \frac{e^{i\sqrt{k_0^2-(\frac{2\pi n}{L}+k_0\sin\phi_0)^2}|z|}}{\sqrt{k_0^2-(\frac{2\pi n}{L}+k_0\sin\phi_0)^2}} e^{i(\frac{2\pi n}{L}+k_0\sin\phi_0)(x-x')}. \tag{A9}$$

This series converges very fast specially when z is relatively large, and with the aid of this Green's function, the integral equation for the induced current given in (11) becomes

$$R(x)J_y(x) = e^{ik_0\sin\phi_0 x} - \frac{k_0 Z_0}{4}\int_{x_0}^{x_0+L} J_y(x')G_e(x,x',0^+)dx' \tag{A10}$$

By a similar technique the Green's function for a periodic resistive sheet in the H polarization case can be derived and is given by

$$G_h(x,x',z) = \frac{2}{L}(1+\frac{\partial^2}{\partial x^2})\sum_{n=-\infty}^{+\infty} \frac{e^{i\sqrt{k_0^2-(\frac{2\pi n}{L}+k_0\sin\phi_0)^2}|z|}}{\sqrt{k_0^2-(\frac{2\pi n}{L}+k_0\sin\phi_0)^2}} e^{i(\frac{2\pi n}{L}+k_0\sin\phi_0)(x-x')}, \tag{A11}$$

and the resulting integral equation for the induced current is

$$R(x)J_x(x) = -\cos\phi_0 e^{ik_0 \sin\phi_0 x} - \frac{k_0 Z_0}{4}\int_{x_0}^{x_0+L} J_x(x')G_h(x,x',0^+)\mathrm{d}x'. \qquad \text{(A12)}$$

The form of the Green's functions shows that the scattered field is composed of two types of waves: 1) propagating waves and 2) surface waves. The latter decay exponentially away from the surface and there are an infinite number of them. In contrast, the number of propagating waves is finite, depending upon the period L and the angle of incidence. The n^{th} mode is a propagating mode if n belongs to set $\mathcal{N}$ defined by

$$\mathcal{N} = \{n; -\frac{L}{\lambda}(1+\sin\phi_0) < n < \frac{L}{\lambda}(1-\sin\phi_0)\} \qquad \text{(A13)}$$

Note that even for $L < \lambda$ we get two propagating modes corresponding to $n = 0$ and $n = -1$. In the far zone only the propagating modes are observable and the electric field of the n^{th} mode for E polarization is, for example, given by ($n \in \mathcal{N}$)

$$E_y^n = -[\frac{k_0 Z_0}{2L}\frac{\int_{x_0}^{x_0+L} J_y(x')e^{-i(\frac{2\pi n}{L}+k_0\sin\phi_0)x'}\mathrm{d}x'}{\sqrt{k_0^2-(\frac{2\pi n}{L}+k_0\sin\phi_0)^2}}]e^{i\sqrt{k_0^2-(\frac{2\pi n}{L}+k_0\sin\phi_0)^2}|z|}e^{i(\frac{2\pi n}{L}+k_0\sin\phi_0)x}. \qquad \text{(A14)}$$

For H polarization the scattered magnetic field corresponding to the n^{th} propagating mode can be obtained from

$$H_y^n = \mp[\frac{1}{2L}\int_{x_0}^{x_0+L} J_x(x')e^{-i(\frac{2\pi n}{L}+k_0\sin\phi_0)x'}\mathrm{d}x']e^{i\sqrt{k_0^2-(\frac{2\pi n}{L}+k_0\sin\phi_0)^2}|z|}e^{i(\frac{2\pi n}{L}+k_0\sin\phi_0)x}, \qquad \text{(A15)}$$

where the upper and lower signs apply for an observation point in the upper or lower half-spaces respectively. The direction of propagation of each mode is defined

by the angle ϕ_n^s measured from the normal to the surface and can be obtained from

$$\sin \phi_n^s = \frac{\lambda}{L} n + \sin \phi_0 \tag{A16}$$

Figure (A1) depicts the scattering directions of the propagating waves as indicated by (A16).

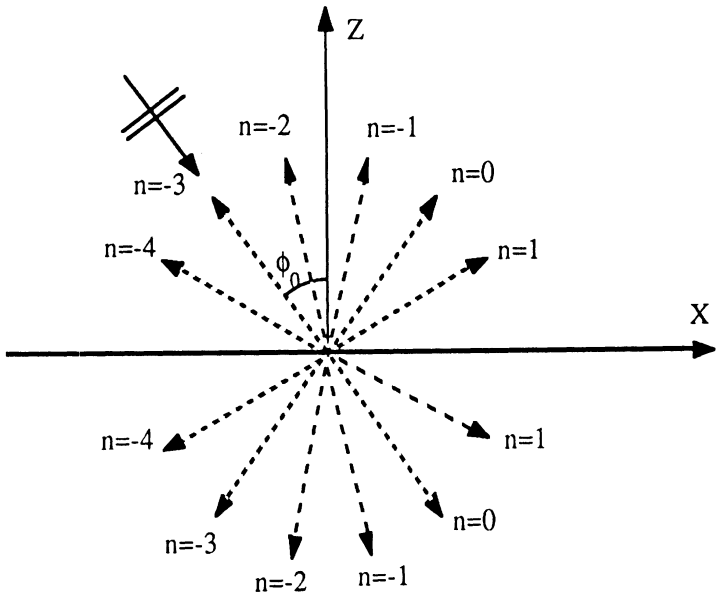

Figure A-1: Scattering directions of propagating waves for a periodic resistive sheet with $L = 3\lambda$ and $\phi_0 = \frac{\pi}{6}$.

A2 Numerical Analysis

Numerical solutions of the integral equations can be obtained by the method of moments. The unknown current is represented approximately by an expansion of pulse basis functions as

$$J(x) = \sum_{m=1}^{M} J_m P(x - x_m) \tag{A17}$$

where J_m are the unknown coefficients to be found, M is the total number of segments, and $P(x)$ is the pulse function defined by

$$P(x) = \begin{cases} 1 & \mid x \mid < \frac{\Delta x}{2} \\ 0 & \text{otherwise} \end{cases} \tag{A18}$$

In the case of E polarization, by substituting (17) into integral equation (A17) and setting $x_0 = -\frac{L}{2}$ we get

$$R(x)J(x) = e^{ik_0 \sin\phi_0 x} - \frac{k_0 Z_0}{4} \sum_{m=1}^{M} J_m \int_{x_m - \frac{\Delta x}{2}}^{x_m + \frac{\Delta x}{2}} G_e(x, x', 0^+) \mathrm{d}x' \tag{A19}$$

After evaluating the integral and setting the observation point at $x = x_k$, the following expression results:

$$\begin{aligned} R(x_k)J(x_k) = \; & e^{ik_0 \sin\phi_0 x_k} \\ & - \frac{k_0 Z_0}{L} \sum_{m=1}^{M} J_m \Big[\sum_{n=-\infty}^{+\infty} \frac{e^{i(\frac{2\pi n}{L} + k_0 \sin\phi_0)(x_k - x_m)} \sin((\frac{2\pi n}{L} + k_0 \sin\phi_0)\frac{\Delta x}{2})}{(\frac{2\pi n}{L} + k_0 \sin\phi_0)\sqrt{k_0^2 - (\frac{2\pi n}{L} + k_0 \sin\phi_0)^2}} \Big] \end{aligned} \tag{A20}$$

This can be cast in matrix form as

$$[\mathcal{Z}][\mathcal{J}] = [\mathcal{V}] \tag{A21}$$

where $[\mathcal{Z}]$ is the impedance matrix and its entries are

$$z_{km} = \frac{k_0 Z_0}{L} \sum_{n=-\infty}^{+\infty} \frac{e^{i(\frac{2\pi n}{L} + k_0 \sin\phi_0)(x_k - x_m)} \sin((\frac{2\pi n}{L} + k_0 \sin\phi_0)\frac{\Delta x}{2})}{(\frac{2\pi n}{L} + k_0 \sin\phi_0)\sqrt{k_0^2 - (\frac{2\pi n}{L} + k_0 \sin\phi_0)^2}} \qquad k \neq m \tag{A22}$$

$$z_{kk} = \frac{k_0 Z_0}{L} \sum_{n=-\infty}^{+\infty} \frac{\sin((\frac{2\pi n}{L} + k_0 \sin\phi_0)\frac{\Delta x}{2})}{(\frac{2\pi n}{L} + k_0 \sin\phi_0)\sqrt{k_0^2 - (\frac{2\pi n}{L} + k_0 \sin\phi_0)^2}} + R(x_k) \qquad k = m \tag{A23}$$

$[\mathcal{J}]$ is a column vector whose components are the unknown J_m's and $[\mathcal{V}]$ is the excitation vector whose components are given by

$$v_k = e^{ik_0 \sin\phi_0 x_k}. \tag{A24}$$

Derivation of the impedance matrix for H polarization is rather difficult because of the higher order singularity of the Green's function. Using the same expansion of the induced current as before and inserting it into the integral equation (A12) we obtain

$$R(x)J(x) = -\cos\phi_0 e^{ik_0 \sin\phi_0 x} - \frac{k_0 Z_0}{4} \sum_{m=1}^{M} J_m \int_{x_m - \frac{\Delta x}{2}}^{x_m + \frac{\Delta x}{2}} (1 + \frac{\partial^2}{\partial x^2}) G_h(x, x', 0^+) \mathrm{d}x' \tag{A25}$$

To find the impedance matrix consider the following integral:

$$\int \frac{\partial^2}{\partial x^2} G_h(x, x', z) \mathrm{d}x' = -G_h'(x, x', z) \tag{A26}$$

where $G_h'(x, x', z)$ is the derivative of $G_h(x, x', z)$ with respect to x and is given by

$$G_h'(x, x', z) = \frac{2}{L} \sum_{n=-\infty}^{+\infty} \frac{e^{i\sqrt{k_0^2 - (\frac{2\pi n}{L} + k_0 \sin\phi_0)^2}|z|}}{\sqrt{k_0^2 - (\frac{2\pi n}{L} + k_0 \sin\phi_0)^2}} \cdot i(\frac{2\pi n}{L} + k_0 \sin\phi_0) e^{i(\frac{2\pi n}{L} + k_0 \sin\phi_0)(x - x')}. \tag{A27}$$

The convergence of the series is very poor when $z \to 0$, but the limit does exist. To achieve a better convergence rate, consider the following geometric series based on the asymptotic behavior of the individual terms in (A.27) for large n, positive and negative:

$$S_1 = \frac{2}{L} \sum_{n=1}^{+\infty} e^{-\frac{2\pi n}{L}|z|} e^{i(\frac{2\pi n}{L} + k_0 \sin\phi_0)(x - x')} = \frac{2}{L} e^{-ik_0 \sin\phi_0 (x - x')} \frac{e^{-\frac{2\pi}{L}(|z| + i(x' - x))}}{1 - e^{-\frac{2\pi}{L}(|z| + i(x' - x))}} \tag{A28}$$

$$S_2 = \frac{2}{L}\sum_{n=-\infty}^{-1} e^{\frac{2\pi n}{L}|z|} e^{i(\frac{2\pi n}{L}+k_0\sin\phi_0)(x-x')} = \frac{2}{L} e^{-ik_0\sin\phi_0(x-x')} \frac{e^{-\frac{2\pi}{L}(|z|-i(x'-x))}}{1-e^{-\frac{2\pi}{L}(|z|-i(x'-x))}} \tag{A29}$$

By adding and subtracting the above series from $G_h'(x,x',z)$ and then letting $z \to 0$ it follows that

$$\begin{aligned} G_h'(x,x',0^+) &= \lim_{z\to 0}[G_h'(x,x',z) - S_1 - S_2] \\ &+ \frac{2}{L} e^{ik_0\sin\phi_0(x-x')}[\frac{e^{-i\frac{2\pi}{L}(x'-x)}}{1-e^{-i\frac{2\pi}{L}(x'-x)}} - \frac{e^{i\frac{2\pi}{L}(x'-x)}}{1-e^{i\frac{2\pi}{L}(x'-x)}}], \end{aligned} \tag{A30}$$

which can be rearranged to give obtain

$$\begin{aligned} G_h'(x,x',0^+) &= \frac{2}{L} e^{-ik_0\sin\phi_0(x-x')}\{\sum_{n=1}^{+\infty}[(\frac{i(\frac{2\pi n}{L}+k_0\sin\phi_0)}{\sqrt{k_0^2-(\frac{2\pi n}{L}+k_0\sin\phi_0)^2}} - 1)e^{-i\frac{2\pi n}{L}(x'-x)} \\ &+ (\frac{i(-\frac{2\pi n}{L}+k_0\sin\phi_0)}{\sqrt{k_0^2-(-\frac{2\pi n}{L}+k_0\sin\phi_0)^2}} + 1)e^{i\frac{2\pi n}{L}(x'-x)}] \\ &+ [i\tan\phi_0 + \frac{e^{-i\frac{2\pi}{L}(x'-x)}}{1-e^{-i\frac{2\pi}{L}(x'-x)}} - \frac{e^{i\frac{2\pi}{L}(x'-x)}}{1-e^{i\frac{2\pi}{L}(x'-x)}}]\} \end{aligned} \tag{A31}$$

The above series is absolutely convergent and its rate of convergence is relatively fast (like $\frac{1}{n^2}$). By defining the following parameters:

$$\begin{aligned} A(x,x_m) = \; & \frac{1}{k_0^2}\int_{x_m-\frac{\Delta x}{2}}^{x_m+\frac{\Delta x}{2}} \frac{\partial^2}{\partial x^2} G_h(x,x',0^+)\mathrm{d}x' = \frac{4i}{Lk_0^2} e^{ik_0\sin\phi_0(x-x_m)} \\ & \cdot\{\sum_{n=1}^{+\infty}[(\frac{i(\frac{2\pi n}{L}+k_0\sin\phi_0)}{\sqrt{k_0^2-(\frac{2\pi n}{L}+k_0\sin\phi_0)^2}} - 1)e^{i\frac{2\pi n}{L}(x-x_m)}\sin((\frac{2\pi n}{L}+k_0\sin\phi_0)\frac{\Delta x}{2}) \\ & + (\frac{i(-\frac{2\pi n}{L}+k_0\sin\phi_0)}{\sqrt{k_0^2-(-\frac{2\pi n}{L}+k_0\sin\phi_0)^2}} + 1)e^{-i\frac{2\pi n}{L}(x-x_m)}\sin((-\frac{2\pi n}{L}+k_0\sin\phi_0)\frac{\Delta x}{2})] \\ & + i\tan\phi_0\sin(k_0\sin\phi_0\frac{\Delta x}{2}) + \frac{1}{2}\cot(\frac{\pi}{L}(x-x_m+\frac{\Delta x}{2}))e^{i(k_0\sin\phi_0\frac{\Delta x}{2})} \\ & - \frac{1}{2}\cot(\frac{\pi}{L}(x-x_m-\frac{\Delta x}{2}))e^{-i(k_0\sin\phi_0\frac{\Delta x}{2})}\}, \end{aligned} \tag{A32}$$

$$\begin{aligned} B(x,x_m) &= \int_{x_m-\frac{\Delta x}{2}}^{x_m+\frac{\Delta x}{2}} G_h(x,x',0^+)\mathrm{d}x' \\ &= \frac{4}{L} e^{ik_0\sin\phi_0(x-x_m)} \sum_{n=-\infty}^{+\infty} \frac{e^{i\frac{2\pi n}{L}(x-x_m)}\sin((\frac{2\pi n}{L}+k_0\sin\phi_0)\frac{\Delta x}{2})}{(\frac{2\pi n}{L}+k_0\sin\phi_0)\sqrt{k_0^2-(\frac{2\pi n}{L}+k_0\sin\phi_0)^2}} \end{aligned} \tag{A33}$$

and setting the observation point $x = x_k$, (A25) can be written as

$$R(x_k)J(x_k) = -\cos\phi_0 e^{ik_0 \sin\phi_0 x} - \frac{k_0 Z_0}{4} \sum_{m=1}^{M} J_m[A(x_k, x_m) + B(x_k, x_m)] \quad \text{(A34)}$$

This can be cast as a matrix equation similar to (A21) with the impedance matrix and excitation vector having entries

$$\begin{aligned} z_{km} &= \tfrac{k_0 Z_0}{4}[A(x_k, x_m) + B(x_k, x_m)] \quad k \neq m \\ z_{kk} &= \tfrac{k_0 Z_0}{4}[A(x_k, x_k) + B(x_k, x_k)] \quad k = m \end{aligned} \quad \text{(A35)}$$

$$v_k = -\cos\phi_0 e^{ik_0 \sin\phi_0 x_k}. \quad \text{(A36)}$$

APPENDIX B
SCATTERING FROM DIELECTRIC STRUCTURES ABOVE RESISTIVE AND IMPEDANCE SHEETS

In this appendix we seek the scattered field of a two dimensional dielectric object with arbitrary cross section above a uniform resistive or impedance sheet when the object is illuminated by a plane wave. The geometry of the problem is depicted in Fig. B-1. First the Green's function is derived by obtaining the the exact image of a line source and then the problem is expressed as an integral equation that can be solved numerically by the method of moments.

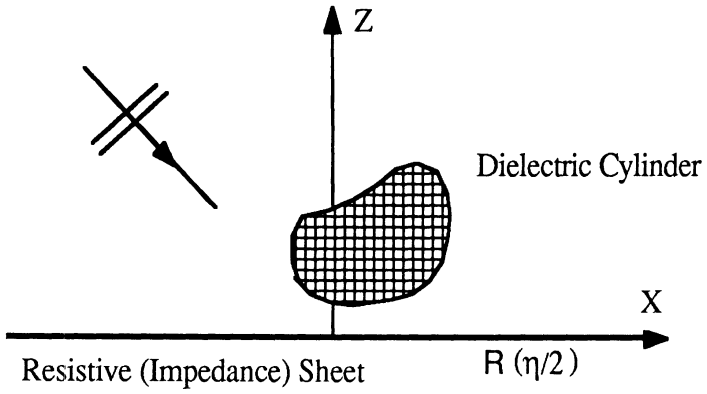

Figure B-1: Geometry for the scattering problem of a dielectric cylinder above a uniform resistive or impedance sheet.

B1 Exact Image of a Current Filament above Resistive Sheets

An integral representation for the image of a source line above a resistive sheet is derived. This representation has an excellent rate of convergence for most practical purposes and can be computed very easily. First, by using the electric vector potential, the exact image is derived for an electric current line source in the y direction. Following the same procedure, the image representation for a line source whose direction is in the transverse plane (xz plane) is obtained next.

B1.1 Line Current in y Direction

Consider a uniform resistive sheet lying in the xy plane of a coordinate system (x, y, z). Assume a constant current is placed above the sheet at $p = (x', z')$ and the current density is given by

$$\mathbf{J} = \hat{\mathbf{y}}\delta(x - x', z - z') \tag{B1}$$

The electric vector potential in this case has only y component and must satisfy the wave equation, i.e.

$$(\nabla^2 + k_0^2)A_y = -\mu_0\delta(x - x')\delta(z - z') \tag{B2}$$

By taking the Fourier transform from both sides of the above equation with respect to x we obtain

$$[\frac{\partial^2}{\partial z^2} + (k_0^2 - k_x^2)]\tilde{a}_y(k_x, z) = -\mu_0\delta(z - z')e^{ik_x x'} \tag{B3}$$

where

$$\tilde{a}_y(k_x, z) = \int_{-\infty}^{+\infty} A_y(x, z) e^{ik_x x} \mathrm{d}x \tag{B4}$$

is the Fourier transform of the electric vector potential. By dividing the space into three regions as shown in Fig. B2 and then imposing the radiation condition, the solution to the differential equation (B3) in each region can be expressed by

$$\tilde{a}_y^1(k_x, z) = c_1 e^{i(k_z z + k_x x')} \tag{B5}$$

$$\tilde{a}_y^2(k_x, z) = c_2 e^{i(k_z z + k_x x')} + c_3 e^{-i(k_z z - k_x x')} \tag{B6}$$

$$\tilde{a}_y^3(k_x, z) = c_4 e^{-i(k_z z - k_x x')} \tag{B7}$$

where $k_z = \sqrt{k_0^2 - k_x^2}$ and branch of the square root is chosen such that $\sqrt{-1} = i$.

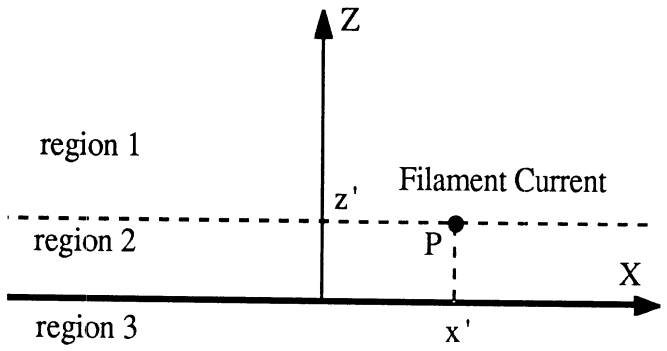

Figure B-2: A constant line source above a uniform resistive sheet.

The field quantities in terms of the vector potential are given by

$$E_y(x, z) = i\omega A_y(x, z) \tag{B8}$$

$$H_x(x,z) = -\frac{1}{\mu_0}\frac{\partial}{\partial z}A_y(x,z) \tag{B9}$$

Continuity of the tangential electric field at $z = z'$ and the resistive sheet boundary conditions as given by (2)-(4) at $z = 0$ together with the equations (B8) and (B9) impose the following conditions on the Fourier transform of the vector potential

$$\tilde{a}_y^1(k_x,z') - \tilde{a}_y^2(k_x,z') = 0 \tag{B10}$$

$$\tilde{a}_y^2(k_x,0) - \tilde{a}_y^3(k_x,0) = 0 \tag{B11}$$

$$\frac{-R}{\mu_0}[\frac{\partial}{\partial z}\tilde{a}_y^2(k_x,0) - \frac{\partial}{\partial z}\tilde{a}_y^3(k_x,0)] = i\omega\tilde{a}_y^2(k_x,0) \tag{B12}$$

and from jump condition we have

$$\frac{\partial}{\partial z}\tilde{a}_y^1(k_x,z') - \frac{\partial}{\partial z}\tilde{a}_y^2(k_x,z') = -\mu_0 \tag{B13}$$

Upon substitution of (B5)-(B7) into (B10)-(B13) and then solving the resultant set of equations simultaneously the unknown coefficients $c_1,\cdots,c_4$ can be obtained and are given by

$$\begin{aligned}
c_1 &= \tfrac{-\mu_0}{2ik_z}[\tfrac{-1}{1+\frac{2RY_0k_z}{k_0}}e^{ik_zz'} + e^{-ik_z'}] \\
c_2 &= \tfrac{\mu_0}{2ik_z}\tfrac{1}{1+\frac{2RY_0k_z}{k_0}}e^{ik_zz'} \\
c_3 &= \tfrac{-\mu_0}{2ik_z}e^{ik_zz'} \\
c_4 &= \tfrac{-\mu_0}{2ik_z}\tfrac{\frac{2RY_0k_z}{k_0}}{1+\frac{2RY_0k_z}{k_0}}e^{ik_zz'}
\end{aligned} \tag{B14}$$

The electric vector potential in each region can be obtained by taking inverse Fourier transform. Let us represent the electric vector potential in the upper and lower half-spaces by $A_y^+(x,z)$ and $A_y^-(x,z)$ respectively and then use the following

identity

$$\int_{-\infty}^{+\infty} \frac{e^{i[k_z|z-z'|-k_x(x-x')]}}{k_z} \mathrm{d}k_x = \pi H_0^{(1)}(k_0\sqrt{(x-x')^2+(z-z')^2}) \tag{B15}$$

we obtain

$$\begin{aligned} A_y^+(x,z) = \; & \tfrac{-\mu_0}{4i} H_0^{(1)}(k_0\sqrt{(x-x')^2+(z-z')^2}) \\ & -\tfrac{\mu_0}{4i\pi}\int_{-\infty}^{+\infty} \tfrac{-1}{(1+\frac{2RY_0k_z}{k_0})k_z} e^{ik_z(z+z')-ik_x(x-x')}\mathrm{d}k_x \end{aligned} \tag{B16}$$

$$\begin{aligned} A_y^-(x,z) = - \; & \tfrac{\mu_0}{4i} H_0^{(1)}(k_0\sqrt{(x-x')^2+(-z+z')^2}) \\ & -\tfrac{\mu_0}{4i\pi}\int_{-\infty}^{+\infty} \tfrac{-1}{(1+\frac{2RY_0k_z}{k_0})k_z} e^{ik_z(-z+z')-ik_x(x-x')}\mathrm{d}k_x \end{aligned} \tag{B17}$$

The first term in the (B16) and (B17) represents the effect of the current filament in absence of the resistive sheet while the second term is due to the image of the current filament. Unfortunately the integral representing the contribution of the image does not have a closed form and its convergence rate is very poor. To achieve the image contribution in an efficient way consider the following transformation

$$\int_0^{+\infty} e^{-\alpha\nu} e^{-k_z\nu}\mathrm{d}\nu = \frac{1}{\alpha+k_z} \qquad \text{provided } Re[\alpha] > -Re[k_z]. \tag{B18}$$

The choice of the branch cut for k_z guarantees that $Re[k_z]$ is nonnegative as k_x takes any real number, therefore the sufficient condition for (B18) is

$$Re[\alpha] > 0. \tag{B19}$$

By defining $\alpha = \frac{k_0}{2RY_0}$ we note that the above condition is satisfied ($Re[\alpha] = \frac{k_0^2\tau\epsilon''}{2} > 0$) and the integral representing the image contribution in the upper half-space can be written as

$$\int_{-\infty}^{+\infty} \frac{-1}{(1+\frac{k_z}{\alpha})k_z} e^{ik_z(z+z')-ik_x(x-x')}\mathrm{d}k_x = \int_0^{+\infty} -\alpha e^{-\alpha\nu}[\int_{-\infty}^{+\infty} \frac{e^{ik_z(z+z'+i\nu)-ik_x(x-x')}}{k_z}\mathrm{d}k_x]\mathrm{d}\nu. \tag{B20}$$

Employing the identity given by (B15), the electric vector potential in the upper half-space is given by

$$\begin{aligned} A_y^+(x,z) = \; & \tfrac{-\mu_0}{4i}[H_0^{(1)}(k_0\sqrt{(x-x')^2+(z-z')^2}) \\ & - \textstyle\int_0^{+\infty} \alpha e^{-\alpha\nu} H_0^{(1)}(k_0\sqrt{(x-x')^2+(z+z'+i\nu)^2}\mathrm{d}\nu]. \end{aligned} \tag{B21}$$

In a same manner the electric vector potential for lower half-space is found to be

$$\begin{aligned} A_y^-(x,z) = \; & \tfrac{-\mu_0}{4i}[H_0^{(1)}(k_0\sqrt{(x-x')^2+(-z+z')^2}) \\ & - \textstyle\int_0^{+\infty} \alpha e^{-\alpha\nu} H_0^{(1)}(k_0\sqrt{(x-x')^2+(-z+z'+i\nu)^2}\mathrm{d}\nu]. \end{aligned} \tag{B22}$$

This integral representation converges very fast because both functions in the inte-

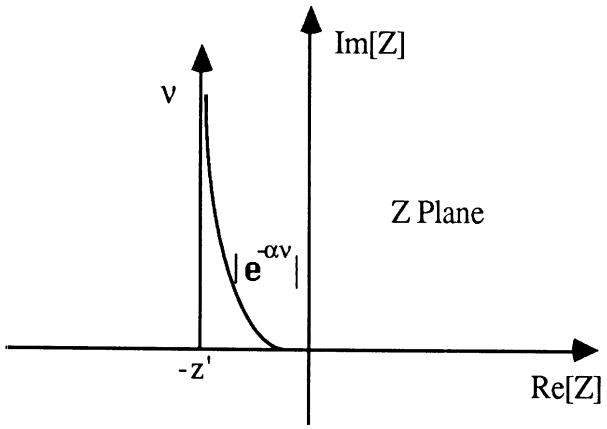

Figure B-3: The location of the image of the line source in the complex z plane.

grand are exponentially decaying. Also from this representation it can be deduced that the image of a line current above a resistive sheet is a half plane current with exponential distribution and is located in the complex z plane occupying region $-z' - i\infty < z < -z'$ (Fig. B-3). The validity of the image representation can be

checked by considering some special limiting cases. Suppose the resistivity is very small (approaching the perfect conductor) which implies that $\mid \alpha \mid \gg 1$. In this case the integral in (B21) can be approximated by

$$\int_0^{+\infty} \alpha e^{-\alpha\nu} H_0^{(1)}(k_0\sqrt{(x-x')^2+(z+z'+i\nu)^2})\mathrm{d}\nu \approx$$
$$H_0^{(1)}(k_0\sqrt{(x-x')^2+(z+z')^2}) \int_0^{+\infty} \alpha e^{-\alpha\nu}\mathrm{d}\nu = H_0^{(1)}(k_0\sqrt{(x-x')^2+(z+z')^2}) \tag{B23}$$

(contribution to the integral comes mostly from point $\nu = 0$) which is the image for the perfectly conducting case. An asymptotic behavior of the integral in terms of a convergent series of inverse power of α can obtained by taking integration by part repeatedly, thus

$$\int_0^{+\infty} \alpha e^{-\alpha\nu} H_0^{(1)}(k_0\sqrt{(x-x')^2+(z+z'+i\nu)^2})\mathrm{d}\nu = \sum_{n=0}^{\infty}(\frac{-1}{\alpha})^n h^{(n)}(0) \tag{B24}$$

where $h^{(n)}(0)$ is the n^{th} derivative of $H_0^{(1)}(k_0\sqrt{(x-x')^2+(z+z'+i\nu)^2})$ with respect to ν evaluated at zero. To the first order of approximation we have

$$\sum_{n=0}^{\infty}(\frac{-1}{\alpha})^n h^{(n)}(0) \approx h(0) - h'(0)\frac{1}{\alpha} \approx h(\frac{-1}{\alpha}) = H_0^{(1)}(k_0\sqrt{(x-x')^2+(z+z'-\frac{i}{\alpha})^2}) \tag{B25}$$

which is a line image located in the complex plane at $z = -z' + \frac{i}{\alpha}$. The other asymptotic behavior of interest is the far field approximation where the point of observation is far from the image point, i.e. $\rho_2 = \sqrt{(x-x')^2+(z+z')^2} \gg \lambda$ (see Fig. B-4). In this condition

$$\sqrt{(x-x')^2+(z+z'+i\nu)^2} \approx \rho_2(1+\frac{i\nu\cos\phi_2}{\rho_2}), \tag{B26}$$

where we have assumed that $\rho_2 \gg \nu$. The validity of this assumption comes from the fact that the integrand of the (B21) is approximately zero if $\nu > \nu_{max}$ for some

finite ν_{max}. Now by using large argument expansion for Hankel function and then substituting for α we get

$$\lim_{\rho_2 \to \infty} \int_0^{+\infty} -\alpha e^{-\alpha\nu} H_0^{(1)}(k_0\sqrt{(x-x')^2+(z+z'+i\nu)^2})d\nu \approx \sqrt{\frac{2}{\pi\rho_2}} e^{i(k_0\rho_2-\frac{\pi}{4})} \frac{-1}{1+2Y_0 R\cos\phi} \quad \text{(B27)}$$

Note that the last term in the above equation is the plane wave reflection coefficient for the E polarization case. This result is identical to the asymptotic value of the integral given in (B16) evaluated by saddle point technique.

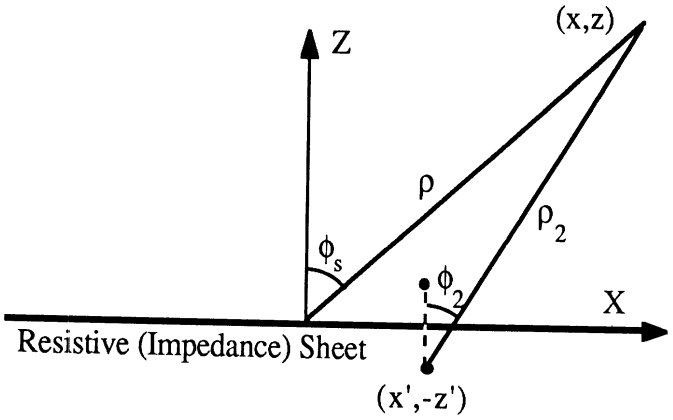

Figure B-4: Geometry of image point for far field approximation.

B1.2 Line Current in the Transverse Plane

Here we separate the problem into two problems: 1) when the current is in x direction and 2) when the current is in the z direction. First consider the situation where the current filament above the resistive sheet is in the x direction and its

current density is given by

$$\mathbf{J} = \hat{\mathbf{x}}\delta(x - x', z - z'). \tag{B28}$$

The electric vector potential has only x component and must satisfy the the wave equation as given in (B2). The analysis of obtaining the electric vector potential $(A_x(x,z))$ is similar to the previous case. The Fourier transform of the vector potential must satisfy an equation similar to (B3), and the solution is identical to those given in (B5)-(B7). The field quantities in terms of the electric vector potential are given by

$$\mathbf{E} = i\omega(A_x(x,z) + \frac{1}{k_0^2}\frac{\partial^2}{\partial x^2}A_x(x,z))\hat{\mathbf{x}} + \frac{i\omega}{k_0^2}\frac{\partial^2}{\partial x \partial z}A_x(x,z)\hat{\mathbf{z}} \tag{B29}$$

$$\mathbf{H} = \frac{1}{\mu_0}\frac{\partial}{\partial z}A_x(x,z)\hat{\mathbf{y}} \tag{B30}$$

The following relations for the Fourier transform of the vector potential can be obtained by using equations (B29) and (B30) and applying the continuity of the tangential electric field at $z = z'$ and the resistive sheet boundary conditions at $z = 0$

$$\frac{-i\omega}{k_0^2}[\frac{\partial^2}{\partial z^2}\tilde{a}_x^1(k_x, z') - \frac{\partial^2}{\partial z^2}\tilde{a}_x^2(k_x, z')] = 0, \tag{B31}$$

$$\frac{-i\omega}{k_0^2}[\frac{\partial^2}{\partial z^2}\tilde{a}_x^2(k_x, 0) - \frac{\partial^2}{\partial z^2}\tilde{a}_x^3(k_x, 0)] = 0 \tag{B32}$$

$$\frac{-R}{\mu_0}[\frac{\partial}{\partial z}\tilde{a}_x^2(k_x, 0) - \frac{\partial}{\partial z}\tilde{a}_x^3(k_x, 0)] = \frac{-i\omega}{k_0^2}\frac{\partial^2}{\partial z^2}\tilde{a}_x^2(k_x, 0) \tag{B33}$$

$$\frac{\partial}{\partial z}\tilde{a}_x^1(k_x, z') - \frac{\partial}{\partial z}\tilde{a}_x^2(k_x, z') = \mu_0 \tag{B34}$$

where the last equation comes from the jump condition. The unknown coefficients $c1, \cdots, c4$ in this case are given by

$$\begin{aligned} c_1 &= \frac{-\mu_0}{2ik_z}\left[\frac{-1}{1+\frac{2RY_0k_0}{k_z}}e^{ik_z z'} + e^{-ik'_z}\right] \\ c_2 &= \frac{\mu_0}{2ik_z}\frac{-1}{1+\frac{2RY_0k_0}{k_z}}e^{ik_z z'} \\ c_3 &= \frac{-\mu_0}{2ik_z}e^{ik_z z'} \\ c_4 &= \frac{-\mu_0}{2ik_z}\left(1+\frac{-1}{1+\frac{2RY_0k_0}{k_z}}\right)e^{ik_z z'} \end{aligned} \tag{B35}$$

The electric vector potential in the upper and lower half-spaces can be obtained by taking the Fourier inverse then using the identity (B15) and respectively are given by

$$\begin{aligned} A_x^+(x,z) &= \frac{-\mu_0}{4i}[H_0^{(1)}(k_0\sqrt{(x-x')^2+(z-z')^2}) - H_0^{(1)}(k_0\sqrt{(x-x')^2+(z+z')^2})] \\ &\quad -\frac{\mu_0}{4i\pi}\int_{-\infty}^{+\infty}\frac{1}{(1+\frac{k_z}{2RY_0k_0})k_z}e^{ik_z(z+z')-ik_x(x-x')}\mathrm{d}k_x \end{aligned} \tag{B36}$$

$$A_x^-(x,z) = -\frac{\mu_0}{4i\pi}\int_{-\infty}^{+\infty}\frac{1}{(1+\frac{k_z}{2RY_0k_0})k_z}e^{ik_z(-z+z')-ik_x(x-x')}\mathrm{d}k_x. \tag{B37}$$

The integral in (B36) represents the contribution of the difference between resistive sheet and perfect conductor images.

Now suppose the current filament is in the z direction and as a result the electric vector potential has only z component. The analysis in this case is very similar to the previous cases. The only difference is that we should use the continuity of the normal component of electric field at $z = z'$ rather than the tangential component. Also note that the field components in terms of the electric vector potential are given by

$$\mathbf{E} = \frac{i\omega}{k_0^2}\frac{\partial^2}{\partial x \partial z}\hat{\mathbf{z}}A_z(x,z)\hat{\mathbf{x}} + i\omega(A_z(x,z) + \frac{1}{k_0^2}\frac{\partial^2}{\partial x^2}A_z(x,z))\hat{\mathbf{z}} \tag{B38}$$

$$\mathbf{H} = -\frac{1}{\mu_0}\frac{\partial}{\partial z}A_z(x,z)\hat{\mathbf{y}} \tag{B39}$$

Following an identical procedure as in the previous case the vector potential can be obtained as

$$\begin{aligned} A_z^+(x,z) &= \frac{-\mu_0}{4i}[H_0^{(1)}(k_0\sqrt{(x-x')^2+(z-z')^2}) + H_0^{(1)}(k_0\sqrt{(x-x')^2+(z+z')^2})] \\ &\quad + \frac{\mu_0}{4i\pi}\int_{-\infty}^{+\infty}\frac{1}{(1+\frac{k_z}{2RY_0k_0})k_z}e^{ik_z(z+z')-ik_x(x-x')}\mathrm{d}k_x \end{aligned} \tag{B40}$$

$$A_z^-(x,z) = -\frac{\mu_0}{4i\pi}\int_{-\infty}^{+\infty}\frac{1}{(1+\frac{k_z}{2RY_0k_0})k_z}e^{ik_z(-z+z')-ik_x(x-x')}\mathrm{d}k_x. \tag{B41}$$

The integral in expressions (B36) and (B40) does not have a closed form and is not appropriate for numerical calculation. A better representation for this integral can be obtained by employing a transformation similar to (B18). By defining $\beta = (2RY_0k_0)$ and noting that $Re[\beta] = \frac{2\epsilon''}{\tau|\epsilon-1|^2} > 0$ then we have

$$\begin{aligned} &\int_{-\infty}^{+\infty}\frac{1}{(1+\frac{k_z}{2RY_0k_0})k_z}e^{ik_z(z+z')-ik_x(x-x')}\mathrm{d}k_x = \\ &\pi\int_0^{+\infty}\beta e^{-\beta\nu}H_0^{(1)}(k_0\sqrt{(x-x')^2+(z+z'+i\nu)^2}\mathrm{d}\nu. \end{aligned} \tag{B42}$$

This representation has a much better rate of convergence when compared to the original form. The rate of convergence depends upon the real part of β and the wavenumber. The asymptotic value of this representation for large value of β can be obtained by the same technique as in the equation (B24) and we have

$$\begin{aligned} &\textstyle\int_0^{+\infty}\beta e^{-\beta\nu}H_0^{(1)}(k_0\sqrt{(x-x')^2+(z+z'+i\nu)^2})\mathrm{d}\nu = \\ &\textstyle\sum_{n=0}^{\infty}(\frac{-1}{\beta})^n h^{(n)}(0) \approx H_0^{(1)}(k_0\sqrt{(x-x')^2+(z+z'-i/\beta)^2}) \end{aligned} \tag{B43}$$

Another asymptotic value of interest is the far field which can be obtained by using the large argument approximation of the Hankel functions and the expression

given in (B26). Therefore the contribution of the image in the far zone can be approximated by

$$\lim_{\rho\to\infty}[H_0^{(1)}(k_0\sqrt{(x-x')^2+(z+z')^2}) - \int_0^{+\infty}\beta e^{-\beta\nu}H_0^{(1)}(k_0\sqrt{(x-x')^2+(z+z'+i\nu)^2})\mathrm{d}\nu] \approx \sqrt{\frac{2}{\pi\rho}}e^{i(k_0\rho-\frac{\pi}{4})}\frac{1}{1+2RY_0\sec\phi} \tag{B44}$$

Employing the new representation into equations (B36)-(B37) and (B40)-(B41) the electric vector potential for x- and z-directed current are given by

$$A_x^+(x,z) = \frac{-\mu_0}{4i}[H_0^{(1)}(k_0\sqrt{(x-x')^2+(z-z')^2}) - H_0^{(1)}(k_0\sqrt{(x-x')^2+(z+z')^2}) + \int_0^{+\infty}\beta e^{-\beta\nu}H_0^{(1)}(k_0\sqrt{(x-x')^2+(z+z'+i\nu)^2})\mathrm{d}\nu], \tag{B45}$$

$$A_x^-(x,z) = -\frac{\mu_0}{4i}\int_0^{+\infty}\beta e^{-\beta\nu}H_0^{(1)}(k_0\sqrt{(x-x')^2+(-z+z'+i\nu)^2}\mathrm{d}\nu, \tag{B46}$$

$$A_z^+(x,z) = \frac{-\mu_0}{4i}[H_0^{(1)}(k_0\sqrt{(x-x')^2+(z-z')^2}) + H_0^{(1)}(k_0\sqrt{(x-x')^2+(z+z')^2}) - \int_0^{+\infty}\beta e^{-\beta\nu}H_0^{(1)}(k_0\sqrt{(x-x')^2+(z+z'+i\nu)^2})\mathrm{d}\nu], \tag{B47}$$

$$A_z^-(x,z) = -\frac{\mu_0}{4i}\int_0^{+\infty}\beta e^{-\beta\nu}H_0^{(1)}(k_0\sqrt{(x-x')^2+(-z+z'+i\nu)^2})\mathrm{d}\nu. \tag{B48}$$

B2 Exact Image of a Current Filament above Impedance Sheets

In Section 2 it was demonstrated that an impedance surface characterized by surface impedance η can be replaced by a perfect magnetic conductor plus an electric current sheet. This fictitious current is identical to the current on the equivalent resistive sheet ($R = \eta/2$). Further it was shown that the scattered field for impedance sheet is twice of the scattered field for the equivalent resistive sheet.

Therefore the image of a current filament over an impedance sheet can be obtained from the expressions derived for resistive sheet by replacing R with $\eta/2$, doubling the expressions, and adding the contribution of image of the current filament above the magnetic wall. By following the above procedure and employing equation (B21), the electric vector potential for a y-directed current filament above the impedance sheet can be obtained from

$$A_y(x,z) = \frac{-\mu_0}{4i}[H_0^{(1)}(k_0\sqrt{(x-x')^2+(z-z')^2}) + H_0^{(1)}(k_0\sqrt{(x-x')^2+(z+z')^2}) \\ -2\int_0^{+\infty}\alpha' e^{-\alpha'\nu}H_0^{(1)}(k_0\sqrt{(x-x')^2+(-z+z'+i\nu)^2}\mathrm{d}\nu]. \tag{B49}$$

where $\alpha' = \frac{k_0}{\eta Y_0}$. By defining $\beta' = \eta Y_0 k_0$ and from equations (B47) and (B48) the electric vector potential for X- and Z-directed current are respectively given by

$$A_x^+(x,z) = \frac{-\mu_0}{4i}[H_0^{(1)}(k_0\sqrt{(x-x')^2+(z-z')^2}) - H_0^{(1)}(k_0\sqrt{(x-x')^2+(z+z')^2}) \\ +2\int_0^{+\infty}\beta' e^{-\beta'\nu}H_0^{(1)}(k_0\sqrt{(x-x')^2+(z+z'+i\nu)^2})\mathrm{d}\nu], \tag{B50}$$

$$A_z^+(x,z) = \frac{-\mu_0}{4i}[H_0^{(1)}(k_0\sqrt{(x-x')^2+(z-z')^2}) + H_0^{(1)}(k_0\sqrt{(x-x')^2+(z+z')^2}) \\ -2\int_0^{+\infty}\beta' e^{-\beta'\nu}H_0^{(1)}(k_0\sqrt{(x-x')^2+(z+z'+i\nu)^2})\mathrm{d}\nu], \tag{B51}$$

B3 Derivation of Integral Equations

Suppose the dielectric object above the resistive sheet is illuminated by a plane wave whose direction of propagation is denoted by angle ϕ_0 measured from normal to the resistive sheet. The incident field induces conduction and displacement current in the dielectric object which are known as polarization current and is

given by

$$\mathbf{J} = -ik_0 Y_0(\epsilon(x,z) - 1)\mathbf{E}^t \tag{B52}$$

where $\epsilon(x,z)$ is the relative dielectric constant of the object and $\mathbf{E}^t$ is the total electric field inside the dielectric body. If the incident, reflected, and scattered field respectively are denoted by $\mathbf{E}^i$, $\mathbf{E}^r$, and $\mathbf{E}^s$, then

$$\mathbf{E}^t = \mathbf{E}^i + \mathbf{E}^r + \mathbf{E}^s \tag{B53}$$

Let us first consider the E polarization case where the electric field is perpendicular to the plane of incidence. The incident and reflected fields are given by

$$\mathbf{E}^i = \hat{\mathbf{y}} e^{ik_0(\sin\phi_0 x - \cos\phi_0 z)}, \tag{B54}$$

$$\mathbf{E}^r = \hat{\mathbf{y}} \frac{-1}{1 + 2RY_0 \cos\phi_0} e^{ik_0(\sin\phi_0 x - \cos\phi_0 z)}. \tag{B55}$$

In this case the incident field excites y-directed polarization current therefore the scattered field is in the y direction and can be obtained using equations (B8) and (B21) as follows

$$E_y^s = \frac{-k_0 Z_0}{4} \iint_s J_y(x',z') G_y(x,z;x',z') \mathrm{d}x' \mathrm{d}z' \tag{B56}$$

where

$$\begin{aligned} G_y(x,z;x',z') = \; & H_0^{(1)}(k_0\sqrt{(x-x')^2 + (z-z')^2}) \\ & - \textstyle\int_0^{+\infty} \alpha e^{-\alpha\nu} H_0^{(1)}(k_0\sqrt{(x-x')^2 + (z+z'+i\nu)^2}) \mathrm{d}\nu. \end{aligned} \tag{B57}$$

Now an integral equation for the polarization current can be obtained by substituting (B54),(B55), and (B56) into (B52) therefore

$$\begin{aligned} J_y(x,z) = \; & -ik_0 Y_0(\epsilon(x,z)-1)e^{ik_0 \sin\phi_0 x}(e^{-ik_0\cos\phi_0 z} - \tfrac{1}{1+2RY_0\cos\phi_0}e^{ik_0\cos\phi_0 z}) \\ & \tfrac{ik_0^2}{4}(\epsilon(x,z)-1)\iint_s J_y(x',z')G_y(x,z;x',z')\mathrm{d}x'\mathrm{d}z'. \end{aligned} \tag{B58}$$

In the H polarization case where the incident electric field is parallel to the plane of incidence assume

$$\mathbf{E}^i = -(\cos\phi_0\hat{\mathbf{x}} + \sin\phi_0\hat{\mathbf{z}})e^{ik_0(\sin\phi_0 x - \cos\phi_0 z)}. \tag{B59}$$

The reflected field in the absence of the dielectric structure above the sheet is of the form

$$\mathbf{E}^r = \frac{1}{1+2RY_0\sec\phi_0}(\cos\phi_0\hat{\mathbf{x}} - \sin\phi_0\hat{\mathbf{z}})e^{ik_0(\sin\phi_0 x + \cos\phi_0 z)}. \tag{B60}$$

The induced polarization current has both x and z components which are denoted by $J_x(x,z)$ and $J_z(x,z)$ respectively. The scattered field can be evaluated using the expressions for the electric vector potential as given in (B29) and (B38) and are of the following form

$$\begin{aligned} E_x^s = \; & \tfrac{-k_0 Z_0}{4}(1+\tfrac{1}{k_0^2}\tfrac{\partial^2}{\partial x^2})\iint_s J_x(x',z')G_x(x,z;x',z')\mathrm{d}x'\mathrm{d}z' \\ & -\tfrac{Z_0}{4k_0}\tfrac{\partial^2}{\partial x\partial z}\iint_s J_z(x',z')G_z(x,z;x',z')\mathrm{d}x'\mathrm{d}z', \end{aligned} \tag{B61}$$

$$\begin{aligned} E_z^s = \; & \tfrac{-Z_0}{4k_0}\tfrac{\partial^2}{\partial x\partial z}\iint_s J_x(x',z')G_x(x,z;x',z')\mathrm{d}x'\mathrm{d}z' \\ & -\tfrac{k_0 Z_0}{4}(1+\tfrac{1}{k_0^2}\tfrac{\partial^2}{\partial z^2})\iint_s J_z(x',z')G_z(x,z;x',z')\mathrm{d}x'\mathrm{d}z', \end{aligned} \tag{B62}$$

where

$$
\begin{aligned}
G_x(x,z;x',z') = \; & H_0^{(1)}(k_0\sqrt{(x-x')^2+(z-z')^2}) - H_0^{(1)}(k_0\sqrt{(x-x')^2+(z+z')^2}) \\
& + \int_0^{+\infty} \beta e^{-\beta\nu} H_0^{(1)}(k_0\sqrt{(x-x')^2+(z+z'+i\nu)^2})\mathrm{d}\nu, \\
G_z(x,z;x',z') = \; & H_0^{(1)}(k_0\sqrt{(x-x')^2+(z-z')^2}) + H_0^{(1)}(k_0\sqrt{(x-x')^2+(z+z')^2}) \\
& - \int_0^{+\infty} \beta e^{-\beta\nu} H_0^{(1)}(k_0\sqrt{(x-x')^2+(z+z'+i\nu)^2})\mathrm{d}\nu.
\end{aligned}
\tag{B63}
$$

Upon substitution of the incident, reflected, and scattered field as given in equations (B59), (B60), and (B61), (B62) respectively into (B52) the following coupled integral equations for the induced current can be derived

$$
\begin{aligned}
J_x(x,z) = \; & -ik_0 Y_0(\epsilon(x,z)-1)\cos\phi_0 e^{ik_0\sin\phi_0 x}(-e^{-ik_0\cos\phi_0 z} + \tfrac{1}{1+2RY_0\sec\phi_0} e^{ik_0\cos\phi_0 z}) \\
& + \tfrac{i}{4}(\epsilon(x,z)-1)(1+\tfrac{1}{k_0^2}\tfrac{\partial^2}{\partial x^2}) \iint_s J_x(x',z')G_x(x,z;x',z')\mathrm{d}x'\mathrm{d}z' \\
& + \tfrac{i}{4}(\epsilon(x,z)-1)\tfrac{\partial^2}{\partial x\partial z} \iint_s J_z(x',z')G_z(x,z;x',z')\mathrm{d}x'\mathrm{d}z',
\end{aligned}
\tag{B64}
$$

$$
\begin{aligned}
J_z(x,z) = \; & ik_0 Y_0(\epsilon(x,z)-1)\sin\phi_0 e^{ik_0\sin\phi_0 x}(e^{-ik_0\cos\phi_0 z} + \tfrac{1}{1+2RY_0\sec\phi_0} e^{ik_0\cos\phi_0 z}) \\
& + \tfrac{i}{4}(\epsilon(x,z)-1)\tfrac{\partial^2}{\partial x\partial z} \iint_s J_x(x',z')G_x(x,z;x',z')\mathrm{d}x'\mathrm{d}z' \\
& + \tfrac{i}{4}(\epsilon(x,z)-1)(1+\tfrac{1}{k_0^2}\tfrac{\partial^2}{\partial z^2}) \iint_s J_z(x',z')G_z(x,z;x',z')\mathrm{d}x'\mathrm{d}z'.
\end{aligned}
\tag{B65}
$$

B4 The Method of Moment Solution

There is no known exact solution for the integral equations which were developed in the previous Section. In this section approximate numerical solution of these equations is obtained by employing the moment method technique.

Let us divide the cross section of the dielectric structure into N sufficiently small

rectangular cells such that the dielectric constant and the polarization current can be approximated by a constant over each cell.

B4.1 E Polarization

First consider the integral equation (B58) which correspond to the E polarization case. Using point matching technique the integral equation can be cast into a matrix equation of the following form

$$[\mathcal{Z}][\mathcal{J}] = [\mathcal{V}] \tag{B66}$$

where $[\mathcal{Z}]$ is the impedance matrix, $[\mathcal{J}]$ is the unknown vector whose entries are the value of polarization current at the center of each cell, i.e. (x_n, z_n), and finally $[\mathcal{V}]$ is the excitation vector whose entries are given by

$$v_n = ik_0 Y_0(\epsilon(x_n, z_n)-1)e^{ik_0 \sin\phi_0 x_n}(e^{-ik_0 \cos\phi_0 z_n} - \frac{1}{1+2RY_0\cos\phi_0} e^{ik_0 \cos\phi_0 z_n}) \tag{B67}$$

The off-diagonal elements of the impedance matrix can be obtained by approximating the Green's function via its Taylor series expansion around the midpoint of each cell and then performing the integration analytically. This technique allows us to choose very small cell sizes without incurring too much error because of the adjacent cells . For diagonal elements the free space Green's function is approximated by its small argument expansion and then integration is performed analytically over the cell area. This allows us to choose rectangular shape cells instead of squares that are approximated by circle of equal area in the traditional method [Richmond 1965]. In order to give the expressions for elements of the

impedance matrix, let us define the following functions

$$U(r^q_{mn},\theta^q_{mn}) = -H_0^{(1)}(k_0 r^q_{mn})\cos^2\theta^q_{mn} + \frac{H_1^{(1)}(k_0 r^q_{mn})}{k_0 r^q_{mn}}(\cos^2\theta^q_{mn} - \sin^2\theta^q_{mn}) \quad \text{(B68)}$$

$$V(r^q_{mn},\theta^q_{mn}) = -H_0^{(1)}(k_0 r^q_{mn})\sin^2\theta^q_{mn} + \frac{H_1^{(1)}(k_0 r^q_{mn})}{k_0 r^q_{mn}}(\sin^2\theta^q_{mn} - \cos^2\theta^q_{mn}) \quad \text{(B69)}$$

where r^q_{mn} and θ^q_{mn} are defined as

$$r^q_{mn} = \begin{cases} \sqrt{(x_m - x_n)^2 + (z_m - z_n)^2} & \text{if } q = s \\ \sqrt{(x_m - x_n)^2 + (z_m + z_n)^2} & \text{if } q = i \\ \sqrt{(x_m - x_n)^2 + (z_m + z_n + i\nu)^2} & \text{if } q = c \end{cases} \quad \text{(B70)}$$

$$\theta^q_{mn} = \begin{cases} \arctan(\frac{z_m - z_n}{x_m - x_n}) & \text{if } q = s \\ \arctan(\frac{z_m + z_n}{x_m - x_n}) & \text{if } q = i \\ \arctan(\frac{z_m + z_n + i\nu}{x_m - x_n}) & \text{if } q = c \end{cases} \quad \text{(B71)}$$

The diagonal entries are given by

$$\begin{aligned} z_{nn} = \; & -1 - \tfrac{1}{\pi}(\epsilon(x_n, z_n) - 1)\{\tfrac{k_0^2 \Delta x_n \Delta z_n}{2}[\ln(\tfrac{k_0}{4}\sqrt{\Delta x_n^2 + \Delta z_n^2}) + \gamma - \tfrac{i\pi}{2} - \tfrac{3}{2}] \\ & + (\tfrac{k_0 \Delta x_n}{2})^2 \arctan(\tfrac{\Delta z_n}{\Delta x_n}) + (\tfrac{k_0 \Delta z_n}{2})^2(\tfrac{\pi}{2} - \arctan(\tfrac{\Delta z_n}{\Delta x_n}))\} \\ & - \tfrac{i k_0^2 \Delta x_n \Delta z_n}{4}(\epsilon(x_n, z_n) - 1)\alpha \int_0^\infty e^{-\alpha\nu} H_0^{(1)}(k_0 r^c_{mn})\mathrm{d}\nu, \end{aligned} \quad \text{(B72)}$$

and the non-diagonal entries are expressed by

$$\begin{aligned} z_{mn} = \; & \tfrac{i k_0^2 \Delta x_n \Delta z_n}{4}(\epsilon(x_m, z_m) - 1)\{H_0^{(1)}(k_0 r^s_{mn}) + \tfrac{(k_0 \Delta x_n)^2}{24} U(r^s_{mn}, \theta^s_{mn}) \\ & + \tfrac{(k_0 \Delta z_n)^2}{24} V(r^s_{mn}, \theta^s_{mn}) - \alpha \int_0^\infty e^{-\alpha\nu} H_0^{(1)}(k_0 r^c_{mn})\mathrm{d}\nu\}, \end{aligned} \quad \text{(B73)}$$

Here, Δx_n and Δz_n are the dimension of the n^{th} rectangular cell and $\gamma = 0.57721$ is the Euler's constant.

The integrals in the (B72) and (B73) are evaluated numerically using Gauss-legendre quadrature technique. It should be mentioned here that when the observation and source points are both close to the surface ($k_0(z_m + z_n) \ll 1$) for some value of $\nu = \nu_0$ the distance function $r_0 = \sqrt{(x_m - x_n)^2 + (z_m + z_n + i\nu_0)^2}$ becomes very small. Consequently the integrand of the integral representing the image contribution varies very sharply around this point. In order to evaluate the integral accurately the contribution of the integrand around ν_0 should be evaluated analytically. The integrand achieves its maximum when the absolute value of the distance function is minimum. This minimum occurs at

$$\nu_0 = \sqrt{(x_m - x_n)^2 - (z_m + z_n)^2} \tag{B74}$$

If the argument of the square root in (B74) is negative then the distance function takes its minimum at $\nu_0 = 0$. Figure B-5 shows the integrand function in (B72) when both observation and source points are very close to the surface. The analytical evaluation of the integral around the point ν_0 can be performed by using small argument expansion of Hankel function, i.e.

$$e^{-\alpha\nu} H_0^{(1)}(k_0 r_{mn}^c) \approx e^{-\alpha\nu_0}[1 + \frac{2i\gamma}{\pi} + \frac{2i}{\pi}\ln(\frac{k_0 r_{mn}^c}{2})] \qquad \nu_0 - \Delta\nu \le \nu \le \nu_0 + \Delta\nu$$

and

$$\int_{\nu_0-\Delta\nu}^{\nu_0+\Delta\nu} e^{-\alpha\nu} H_0^{(1)}(k_0 r_{mn}^c)\mathrm{d}\nu = e^{-\alpha\nu_0}[2\Delta\nu(1 + \frac{i2\gamma}{\pi}) + \frac{i2}{\pi} I_1]$$

where

$$\begin{aligned} I_1 = \; & \tfrac{i}{2}(z_m + z_n + i\nu_0)\ln\tfrac{r_0^2 - \Delta\nu^2 - i2\Delta\nu(z_m+z_n+i\nu_0)}{r_0^2 - \Delta\nu^2 + i2\Delta\nu(z_m+z_n+i\nu_0)} + \tfrac{x_m - x_n}{2}\ln\tfrac{r_0^2 + \Delta\nu^2 + 2\Delta\nu(x_m - x_n)}{r_0^2 + \Delta\nu^2 - 2\Delta\nu(x_m - x_n)} \\ & -\Delta\nu[2 - \ln\tfrac{k_0^2}{4}\sqrt{(r_0^2 - \Delta\nu^2)^2 + 4\Delta\nu^2(z_m + z_n + i\nu_0)^2}]. \end{aligned}$$

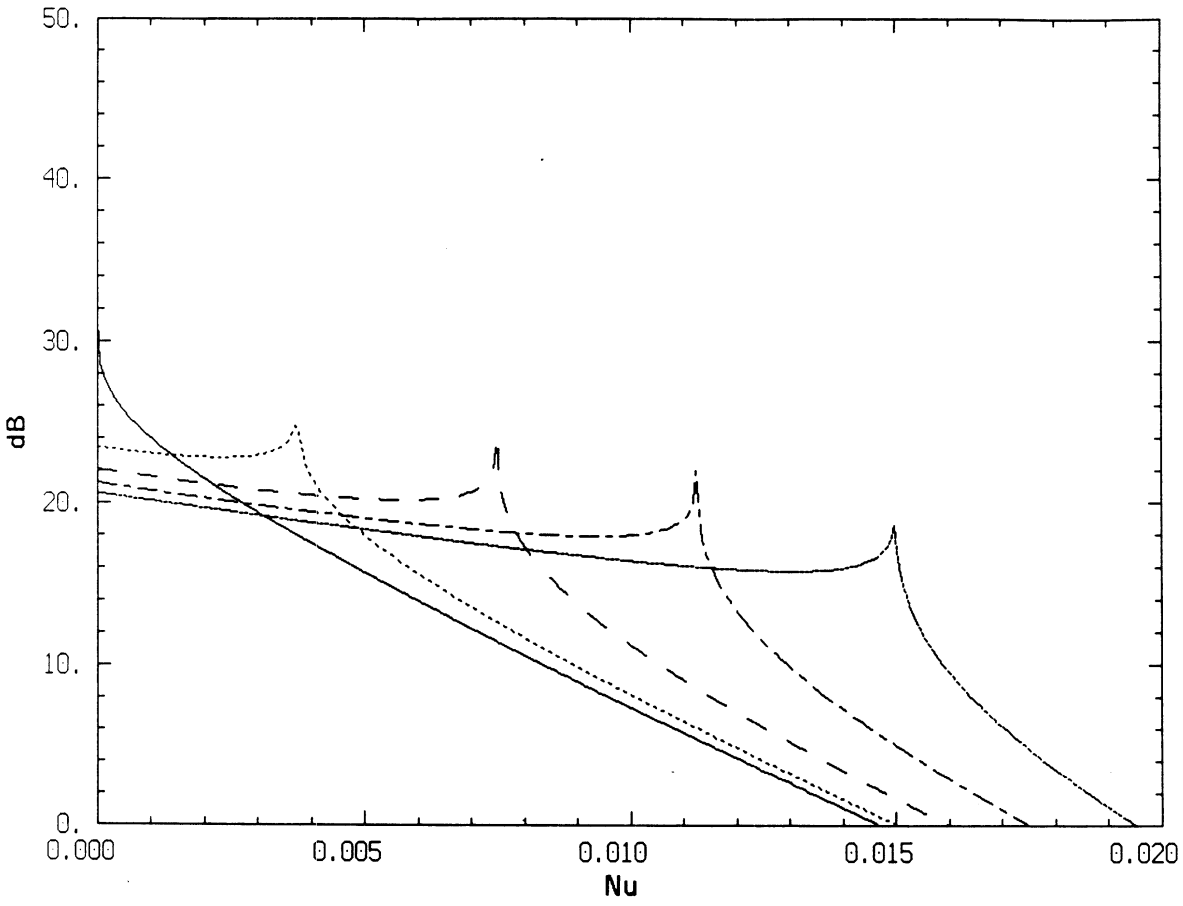

Figure B-5: The absolute value of the integrand function in (B73) for $\alpha = 112 - i230$ at 10 GHz, $z_m + z_n = 6 \times 10^{-5}\lambda$, and five values of $x_m - x_n$: (——) 0, (- - - - -) $\lambda/8$, (— —) $\lambda/4$, (— - —) $3\lambda/8$, (— - - - —) $\lambda/2$.

For self-image calculation we note that $x_m = x_n$ which renders $\nu_0 = 0$ and

$$\int_0^{\Delta\nu} e^{-\alpha\nu} H_0^{(1)}(k_0 r_{mn}^c)\mathrm{d}\nu = [\Delta\nu(1 + \frac{i2\gamma}{\pi}) + \frac{2}{\pi} I_1']$$

where

$$I_1' = (z_m + z_n)\ln\frac{z_m + z_n + i\Delta\nu}{z_m + z_n} + i\Delta\nu[\ln\frac{k_0(z_m + z_n + i\Delta\nu)}{2} - 1]$$

B4.2 H Polarization

In the H polarization case using the same partitioning of the cross section of the dielectric body the coupled integral equations (B64) and (B65) can be cast into the following coupled matrix equation

$$\begin{aligned} \mathcal{Z}_1\mathcal{J}_x + \mathcal{Z}_2\mathcal{J}_z &= \mathcal{V}_x \\ \mathcal{Z}_3\mathcal{J}_x + \mathcal{Z}_4\mathcal{J}_z &= \mathcal{V}_z \end{aligned} \tag{B75}$$

where as before $\mathcal{Z}_1, \cdots, \mathcal{Z}_4$ are $N \times N$ impedance matrices and $\mathcal{V}_x$ and $\mathcal{V}_z$ are the excitation vectors. The above coupled matrix equation can be represented by a $2N \times 2N$ matrix equation similar to (B66) with

$$[\mathcal{J}] = \begin{bmatrix} \mathcal{J}_x \\ \mathcal{J}_z \end{bmatrix}, \quad [\mathcal{Z}] = \begin{bmatrix} \mathcal{Z}_1 & \mathcal{Z}_2 \\ \mathcal{Z}_3 & \mathcal{Z}_4 \end{bmatrix}, \text{and} \quad [\mathcal{V}] = \begin{bmatrix} \mathcal{V}_x \\ \mathcal{V}_z \end{bmatrix}. \tag{B76}$$

The elements of excitation vector are given by $(m = 1, \cdots, N)$

$$\begin{aligned} v_m = \quad & ik_0 Y_0(\epsilon(x_m, z_m) - 1)\cos\phi_0 e^{ik_0 \sin\phi_0 x_m}(-e^{-ik_0\cos\phi_0 z_m} + \frac{1}{1+2RY_0\sec\phi_0} e^{ik_0\cos\phi_0 z_m}) \\ v_{m+N} = \quad & -ik_0 Y_0(\epsilon(x_m, z_m) - 1)\sin\phi_0 e^{ik_0\sin\phi_0 x_m} \\ & \cdot(e^{-ik_0\cos\phi_0 z_m} + \frac{1}{1+2RY_0\sec\phi_0} e^{ik_0\cos\phi_0 z_m}) \end{aligned} \tag{B77}$$

Here again the entries of the impedance matrix are obtained by expansion of the Green's function over each cell as explained in the E polarization case. Because of higher degree of singularity of the Green's function in this case using these expansions are even more important to avoid anomalous errors. The following derivative of the functions defined by (B68) and (B69) are needed to obtain the entries of the impedance matrix

$$\begin{aligned}\frac{\partial^2}{\partial x^2}U(r^q_{mn},\theta^q_{mn}) = \; & k_0^2\{H_0^{(1)}(k_0r^q_{mn})[\cos^2\theta^q_{mn}(\tfrac{3}{8}\cos^2\theta^q_{mn}+\tfrac{1}{8}\sin^2\theta^q_{mn}) \\ & +\tfrac{2\sin^2\theta^q_{mn}}{(k_0r^q_{mn})^2}(3\cos^2\theta^q_{mn}-\sin^2\theta^q_{mn})] \\ & +H_1^{(1)}(k_0r^q_{mn})[\tfrac{5}{k_0r^q_{mn}}\cos^2\theta^q_{mn}\sin^2\theta^q_{mn}-\tfrac{4\sin^2\theta^q_{mn}}{(k_0r^q_{mn})^3}(3\cos^2\theta^q_{mn}-\sin^2\theta^q_{mn})] \\ & +H_2^{(1)}(k_0r^q_{mn})[-\tfrac{1}{2}\cos^4\theta^q_{mn}+\tfrac{\sin^2\theta^q_{mn}}{(k_0r^q_{mn})^2}(-9\cos^2\theta^q_{mn}+\sin^2\theta^q_{mn})] \\ & +H_4^{(1)}(k_0r^q_{mn})[\tfrac{1}{8}\cos^2\theta^q_{mn}(\cos^2\theta^q_{mn}-\sin^2\theta^q_{mn})]\}\end{aligned} \tag{B78}$$

$$\begin{aligned}\frac{\partial^2}{\partial z^2}U(r^q_{mn},\theta^q_{mn}) = \; & k_0^2\{H_0^{(1)}(k_0r^q_{mn})[\sin^2\theta^q_{mn}(\tfrac{3}{8}\cos^2\theta^q_{mn}+\tfrac{1}{8}\sin^2\theta^q_{mn}) \\ & +\tfrac{2\cos^2\theta^q_{mn}}{(k_0r^q_{mn})^2}(\cos^2\theta^q_{mn}-3\sin^2\theta^q_{mn})] \\ & +H_1^{(1)}(k_0r^q_{mn})[-\tfrac{4}{k_0r^q_{mn}}\cos^2\theta^q_{mn}\sin^2\theta^q_{mn}+\tfrac{4\cos^2\theta^q_{mn}}{(k_0r^q_{mn})^3}(3\sin^2\theta^q_{mn}-\cos^2\theta^q_{mn})] \\ & +H_2^{(1)}(k_0r^q_{mn})[-\tfrac{1}{2}\sin^2\theta^q_{mn}\cos^2\theta^q_{mn}+\tfrac{\cos^2\theta^q_{mn}}{(k_0r^q_{mn})^2}(9\sin^2\theta^q_{mn}-\cos^2\theta^q_{mn})] \\ & +H_4^{(1)}(k_0r^q_{mn})[\tfrac{1}{8}\sin^2\theta^q_{mn}(\cos^2\theta^q_{mn}-\sin^2\theta^q_{mn})]\}\end{aligned} \tag{B79}$$

$$\frac{\partial^2}{\partial x \partial z} U(r^q_{mn}, \theta^q_{mn}) = k_0^2 \sin\theta^q_{mn} \cos\theta^q_{mn} \{ H_0^{(1)}(k_0 r^q_{mn}) [\tfrac{3}{8}\cos^2\theta^q_{mn} + \tfrac{1}{8}\sin^2\theta^q_{mn}$$
$$+ \tfrac{4}{(k_0 r^q_{mn})^2}(\sin^2\theta^q_{mn} - \cos^2\theta^q_{mn})]$$
$$+ H_1^{(1)}(k_0 r^q_{mn}) [\tfrac{1}{k_0 r^q_{mn}}(2\sin^2\theta^q_{mn} - 3\cos^2\theta^q_{mn}) + \tfrac{8}{(k_0 r^q_{mn})^3}(\cos^2\theta^q_{mn} - \sin^2\theta^q_{mn})]$$
$$+ H_2^{(1)}(k_0 r^q_{mn}) [-\tfrac{1}{2}\cos^2\theta^q_{mn} + \tfrac{5}{(k_0 r^q_{mn})^2}(\cos^2\theta^q_{mn} - \sin^2\theta^q_{mn})]$$
$$+ H_4^{(1)}(k_0 r^q_{mn}) [\tfrac{1}{8}(\cos^2\theta^q_{mn} - \sin^2\theta^q_{mn})]\} \tag{B80}$$

$$\frac{\partial^2}{\partial x^2} V(r^q_{mn}, \theta^q_{mn}) = k_0^2 \{ H_0^{(1)}(k_0 r^q_{mn}) [\cos^2\theta^q_{mn} (\tfrac{3}{8}\sin^2\theta^q_{mn} + \tfrac{1}{8}\cos^2\theta^q_{mn})$$
$$+ \tfrac{2\sin^2\theta^q_{mn}}{(k_0 r^q_{mn})^2}(\sin^2\theta^q_{mn} - 3\cos^2\theta^q_{mn})]$$
$$+ H_1^{(1)}(k_0 r^q_{mn}) [\tfrac{\sin^2\theta^q_{mn}}{k_0 r^q_{mn}}(-4\cos^2\theta^q_{mn} + \sin^2\theta^q_{mn}) + \tfrac{4\sin^2\theta^q_{mn}}{(k_0 r^q_{mn})^3}(3\cos^2\theta^q_{mn} - \sin^2\theta^q_{mn})]$$
$$+ H_2^{(1)}(k_0 r^q_{mn}) [-\tfrac{1}{2}\sin^2\theta^q_{mn}\cos^2\theta^q_{mn} + \tfrac{\sin^2\theta^q_{mn}}{(k_0 r^q_{mn})^2}(9\cos^2\theta^q_{mn} - \sin^2\theta^q_{mn})]$$
$$+ H_4^{(1)}(k_0 r^q_{mn}) [\tfrac{1}{8}\cos^2\theta^q_{mn}(\sin^2\theta^q_{mn} - \cos^2\theta^q_{mn})]\} \tag{B81}$$

$$\frac{\partial^2}{\partial z^2} V(r^q_{mn}, \theta^q_{mn}) = k_0^2 \{ H_0^{(1)}(k_0 r^q_{mn}) [\sin^2\theta^q_{mn} (\tfrac{3}{8}\sin^2\theta^q_{mn} + \tfrac{1}{8}\cos^2\theta^q_{mn})$$
$$+ \tfrac{2\cos^2\theta^q_{mn}}{(k_0 r^q_{mn})^2}(3\sin^2\theta^q_{mn} - \cos^2\theta^q_{mn})]$$
$$+ H_1^{(1)}(k_0 r^q_{mn}) [\tfrac{5}{k_0 r^q_{mn}}\sin^2\theta^q_{mn}\cos^2\theta^q_{mn} - \tfrac{4\cos^2\theta^q_{mn}}{(k_0 r^q_{mn})^3}(3\sin^2\theta^q_{mn} - \cos^2\theta^q_{mn})]$$
$$+ H_2^{(1)}(k_0 r^q_{mn}) [-\tfrac{1}{2}\sin^4\theta^q_{mn} - \tfrac{\cos^2\theta^q_{mn}}{(k_0 r^q_{mn})^2}(9\sin^2\theta^q_{mn} - \cos^2\theta^q_{mn})]$$
$$+ H_4^{(1)}(k_0 r^q_{mn}) [\tfrac{1}{8}\sin^2\theta^q_{mn}(\sin^2\theta^q_{mn} - \cos^2\theta^q_{mn})]\} \tag{B82}$$

$$\frac{\partial^2}{\partial x \partial z} V(r^q_{mn}, \theta^q_{mn}) = k_0^2 \sin\theta^q_{mn} \cos\theta^q_{mn} \{ H_0^{(1)}(k_0 r^q_{mn}) [\tfrac{3}{8}\sin^2\theta^q_{mn} + \tfrac{1}{8}\cos^2\theta^q_{mn}$$
$$+ \tfrac{4}{(k_0 r^q_{mn})^2}(\cos^2\theta^q_{mn} - \sin^2\theta^q_{mn})]$$
$$+ H_1^{(1)}(k_0 r^q_{mn}) [\tfrac{1}{k_0 r^q_{mn}}(2\cos^2\theta^q_{mn} - 3\sin^2\theta^q_{mn}) + \tfrac{8}{(k_0 r^q_{mn})^3}(\sin^2\theta^q_{mn} - \cos^2\theta^q_{mn})]$$
$$+ H_2^{(1)}(k_0 r^q_{mn}) [-\tfrac{1}{2}\sin^2\theta^q_{mn} + \tfrac{5}{(k_0 r^q_{mn})^2}(\sin^2\theta^q_{mn} - \cos^2\theta^q_{mn})]$$
$$+ H_4^{(1)}(k_0 r^q_{mn}) [\tfrac{1}{8}(\sin^2\theta^q_{mn} - \cos^2\theta^q_{mn})]\} \tag{B83}$$

The non-diagonal elements of the impedance matrix are given by

$$
\begin{aligned}
z_{1mn} = \; & \tfrac{ik_0^2\Delta x_n\Delta z_n}{4}(\epsilon(x_m,z_m)-1)\{H_0^{(1)}(k_0r_{mn}^s)\sin^2\theta_{mn}^s + \tfrac{H_1^{(1)}(k_0r_{mn}^s)}{(k_0r_{mn}^s)}(\cos^2\theta_{mn}^s - \sin^2\theta_{mn}^s) \\
& + \tfrac{(\Delta x_n)^2}{24}(\tfrac{\partial^2}{\partial x^2}+k_0^2)U(r_{mn}^s,\theta_{mn}^s) + \tfrac{(\Delta z_n)^2}{24}(\tfrac{\partial^2}{\partial x^2}+k_0^2)V(r_{mn}^s,\theta_{mn}^s) \\
& - H_0^{(1)}(k_0r_{mn}^i)\sin^2\theta_{mn}^i - \tfrac{H_1^{(1)}(k_0r_{mn}^i)}{(k_0r_{mn}^i)}(\cos^2\theta_{mn}^i - \sin^2\theta_{mn}^i) \\
& - \tfrac{(\Delta x_n)^2}{24}(\tfrac{\partial^2}{\partial x^2}+k_0^2)U(r_{mn}^i,\theta_{mn}^i) - \tfrac{(\Delta z_n)^2}{24}(\tfrac{\partial^2}{\partial x^2}+k_0^2)V(r_{mn}^i,\theta_{mn}^i) \\
& + \beta\textstyle\int_0^\infty e^{-\beta\nu}[H_0^{(1)}(k_0r_{mn}^c)\sin^2\theta_{mn}^c + \tfrac{H_1^{(1)}(k_0r_{mn}^c)}{(k_0r_{mn}^c)}(\cos^2\theta_{mn}^c - \sin^2\theta_{mn}^c)]\mathrm{d}\nu\},
\end{aligned}
\tag{B84}
$$

$$
\begin{aligned}
z_{2mn} = \; & \tfrac{ik_0^2\Delta x_n\Delta z_n}{4}(\epsilon(x_m,z_m)-1)\{[-H_0^{(1)}(k_0r_{mn}^s) + \tfrac{2H_1^{(1)}(k_0r_{mn}^s)}{(k_0r_{mn}^s)}]\cos\theta_{mn}^s\sin\theta_{mn}^s \\
& + \tfrac{(\Delta x_n)^2}{24}\tfrac{\partial^2}{\partial x\partial z}U(r_{mn}^s,\theta_{mn}^s) + \tfrac{(\Delta z_n)^2}{24}\tfrac{\partial^2}{\partial x\partial z}V(r_{mn}^s,\theta_{mn}^s) \\
& + [-H_0^{(1)}(k_0r_{mn}^i) + \tfrac{2H_1^{(1)}(k_0r_{mn}^i)}{(k_0r_{mn}^i)}]\cos\theta_{mn}^i\sin\theta_{mn}^i \\
& + \tfrac{(\Delta x_n)^2}{24}\tfrac{\partial^2}{\partial x\partial z}U(r_{mn}^i,\theta_{mn}^i) + \tfrac{(\Delta z_n)^2}{24}\tfrac{\partial^2}{\partial x\partial z}V(r_{mn}^i,\theta_{mn}^i) \\
& - \beta\textstyle\int_0^\infty e^{-\beta\nu}[(-H_0^{(1)}(k_0r_{mn}^c) + \tfrac{2H_1^{(1)}(k_0r_{mn}^c)}{(k_0r_{mn}^c)})\cos\theta_{mn}^c\sin\theta_{mn}^c]\mathrm{d}\nu\},
\end{aligned}
\tag{B85}
$$

$$
\begin{aligned}
z_{3mn} = \; & \tfrac{ik_0^2\Delta x_n\Delta z_n}{4}(\epsilon(x_m,z_m)-1)\{[-H_0^{(1)}(k_0r_{mn}^s) + \tfrac{2H_1^{(1)}(k_0r_{mn}^s)}{(k_0r_{mn}^s)}]\cos\theta_{mn}^s\sin\theta_{mn}^s \\
& + \tfrac{(\Delta x_n)^2}{24}\tfrac{\partial^2}{\partial x\partial z}U(r_{mn}^s,\theta_{mn}^s) + \tfrac{(\Delta z_n)^2}{24}\tfrac{\partial^2}{\partial x\partial z}V(r_{mn}^s,\theta_{mn}^s) \\
& - [-H_0^{(1)}(k_0r_{mn}^i) + \tfrac{2H_1^{(1)}(k_0r_{mn}^i)}{(k_0r_{mn}^i)}]\cos\theta_{mn}^i\sin\theta_{mn}^i \\
& - \tfrac{(\Delta x_n)^2}{24}\tfrac{\partial^2}{\partial x\partial z}U(r_{mn}^i,\theta_{mn}^i) - \tfrac{(\Delta z_n)^2}{24}\tfrac{\partial^2}{\partial x\partial z}V(r_{mn}^i,\theta_{mn}^i) \\
& + \beta\textstyle\int_0^\infty e^{-\beta\nu}[(-H_0^{(1)}(k_0r_{mn}^c) + \tfrac{2H_1^{(1)}(k_0r_{mn}^c)}{(k_0r_{mn}^c)})\cos\theta_{mn}^c\sin\theta_{mn}^c]\mathrm{d}\nu\},
\end{aligned}
\tag{B86}
$$

$$
\begin{aligned}
z_{4mn} = \; & \tfrac{ik_0^2\Delta x_n\Delta z_n}{4}(\epsilon(x_m,z_m)-1)\{H_0^{(1)}(k_0r_{mn}^s)\cos^2\theta_{mn}^s+\tfrac{H_1^{(1)}(k_0r_{mn}^s)}{(k_0r_{mn}^s)}(\sin^2\theta_{mn}^s-\cos^2\theta_{mn}^s) \\
& +\tfrac{(\Delta x_n)^2}{24}(\tfrac{\partial^2}{\partial z^2}+k_0^2)U(r_{mn}^s,\theta_{mn}^s)+\tfrac{(\Delta z_n)^2}{24}(\tfrac{\partial^2}{\partial z^2}+k_0^2)V(r_{mn}^s,\theta_{mn}^s) \\
& +H_0^{(1)}(k_0r_{mn}^i)\cos^2\theta_{mn}^i+\tfrac{H_1^{(1)}(k_0r_{mn}^i)}{(k_0r_{mn}^i)}(\sin^2\theta_{mn}^i-\cos^2\theta_{mn}^i) \\
& +\tfrac{(\Delta x_n)^2}{24}(\tfrac{\partial^2}{\partial z^2}+k_0^2)U(r_{mn}^i,\theta_{mn}^i)+\tfrac{(\Delta z_n)^2}{24}(\tfrac{\partial^2}{\partial z^2}+k_0^2)V(r_{mn}^i,\theta_{mn}^i) \\
& -\beta\textstyle\int_0^\infty e^{-\beta\nu}[H_0^{(1)}(k_0r_{mn}^c)\cos^2\theta_{mn}^c+\tfrac{H_1^{(1)}(k_0r_{mn}^c)}{(k_0r_{mn}^c)}(\sin^2\theta_{mn}^c-\cos^2\theta_{mn}^c)]\mathrm{d}\nu\}.
\end{aligned}
\tag{B87}
$$

Noting that $\cos\theta_{nn}^i = \cos\theta_{nn}^c = 0$ and $\sin\theta_{nn}^i = \sin\theta_{nn}^c = 1$, the diagonal elements are of the following form

$$
\begin{aligned}
z_{1nn} = \; & -1-\tfrac{1}{\pi}(\epsilon(x_n,z_n)-1)\{\tfrac{k_0^2\Delta x_n\Delta z_n}{4}[\ln(\tfrac{k_0}{4}\sqrt{\Delta x_n^2+\Delta z_n^2})+\gamma-\tfrac{i\pi}{2}-\tfrac{3}{2}] \\
& +2\arctan(\tfrac{\Delta z_n}{\Delta x_n})+(\tfrac{k_0\Delta z_n}{2})^2(\tfrac{\pi}{2}-\arctan(\tfrac{\Delta z_n}{\Delta x_n}))\} \\
& \tfrac{ik_0^2\Delta x_n\Delta z_n}{4}(\epsilon(x_m,z_m)-1)\{-H_0^{(1)}(k_0r_{nn}^i)+\tfrac{H_1^{(1)}(k_0r_{nn}^i)}{(k_0r_{nn}^i)} \\
& -\tfrac{(\Delta x_n)^2}{24}(\tfrac{\partial^2}{\partial x^2}+k_0^2)U(r_{nn}^i,\theta_{nn}^i)-\tfrac{(\Delta z_n)^2}{24}(\tfrac{\partial^2}{\partial x^2}+k_0^2)V(r_{nn}^i,\theta_{nn}^i) \\
& +\beta\textstyle\int_0^\infty e^{-\beta\nu}[H_0^{(1)}(k_0r_{nn}^c)-\tfrac{H_1^{(1)}(k_0r_{nn}^c)}{(k_0r_{nn}^c)}]\mathrm{d}\nu\},
\end{aligned}
\tag{B88}
$$

$$
z_{2nn} = \; z_{3nn} = 0 \tag{B89}
$$

$$
\begin{aligned}
z_{4nn} = \; & -1-\tfrac{1}{\pi}(\epsilon(x_n,z_n)-1)\{\tfrac{k_0^2\Delta x_n\Delta z_n}{4}[\ln(\tfrac{k_0}{4}\sqrt{\Delta x_n^2+\Delta z_n^2})+\gamma-\tfrac{i\pi}{2}-\tfrac{3}{2}] \\
& +2(\tfrac{\pi}{2}-\arctan(\tfrac{\Delta z_n}{\Delta x_n}))+(\tfrac{k_0\Delta x_n}{2})^2\arctan(\tfrac{\Delta z_n}{\Delta x_n}))\} \\
& \tfrac{ik_0^2\Delta x_n\Delta z_n}{4}(\epsilon(x_m,z_m)-1)\{\tfrac{H_1^{(1)}(k_0r_{nn}^i)}{(k_0r_{nn}^i)} \\
& +\tfrac{(\Delta x_n)^2}{24}(\tfrac{\partial^2}{\partial z^2}+k_0^2)U(r_{nn}^i,\theta_{nn}^i)+\tfrac{(\Delta z_n)^2}{24}(\tfrac{\partial^2}{\partial z^2}+k_0^2)V(r_{nn}^i,\theta_{nn}^i) \\
& -\beta\textstyle\int_0^\infty e^{-\beta\nu}\tfrac{H_1^{(1)}(k_0r_{nn}^c)}{(k_0r_{nn}^c)}\mathrm{d}\nu\}.
\end{aligned}
\tag{B90}
$$

The distance function in the integrand of all the integrals in (B84)-(B87) assumes a very small number when the observation and source points are both close to

the surface of the resistive sheet. Since the singularity of the integrands in this case are much higher than the E polarization case analytical evaluation of the integrals around the point ν_0 is even more important. For example the integrand in equation (B83) can be approximated by

$$e^{-\beta\nu}[H_0^{(1)}(k_0 r_{mn}^c)\sin^2\theta_{mn}^c + \frac{H_1^{(1)}(k_0 r_{mn}^c)}{(k_0 r_{mn}^c)}(\cos^2\theta_{mn}^c - \sin^2\theta_{mn}^c)] \approx e^{-\beta\nu_0}\{H_0^{(1)}(k_0 r_0)$$
$$\cdot\frac{(z_m+z_n+i\nu_0)^2}{(r_{mn}^c)^2} - [\frac{i2}{\pi}\frac{1}{(k_0 r_{mn}^c)^2} + (\frac{i}{2\pi} - \frac{i\gamma}{\pi} - \frac{1}{2}) - \frac{i}{\pi}\ln\frac{k_0 r_0}{2}]\frac{(x_m-x_n)^2-(z_m+z_n+i\nu_0)^2}{(r_{mn}^c)^2}\} \tag{B91}$$

where small argument expansion of $H_1^{(1)}(k_0 r_{mn}^c)$ is used and ν is set to ν_0 everywhere except in the denominators. Figure B-6 shows the variation of integrand as a function of ν for some typical values of source and observation points and Fig. B-7 compares the integrand with its approximation. It should be noted here that the phase of integrand varies very rapidly around ν_0 resulting in faster variation of the integrand than what is shown in Fig. B6. If the integrand in (B83) around the $\Delta\nu$ neighborhood of ν_0 is denoted by S_1 then

$$\begin{aligned} S_1 = \; & e^{-\beta\nu_0}\{H_0^{(1)}(k_0 r_0)(z_m+z_n+i\nu_0)^2 - [(\frac{i}{2\pi} - \frac{i\gamma}{\pi} - \frac{1}{2}) - \frac{i}{\pi}\ln\frac{k_0 r_0}{2}] \\ & \cdot[(x_m-x_n)^2 - (z_m+z_n+i\nu_0)^2]\}I_2 \\ & - e^{-\beta\nu_0}\frac{2i}{\pi k_0^2}[(x_m-x_n)^2 - (z_m+z_n+i\nu_0)^2]I_3 \end{aligned}$$

where

$$I_2 = \frac{1}{2(x_m-x_n)}\ln\frac{r_0^2+\Delta\nu^2+2(x_m-x_n)\Delta\nu}{r_0^2+\Delta\nu^2-2(x_m-x_n)\Delta\nu},$$
$$I_3 = \frac{\Delta\nu}{(x_m-x_n)^2}\frac{r_0^2-\Delta\nu^2-2(z_m+z_n+i\nu_0)^2}{(r_0^2-\Delta\nu^2)^2+4\Delta\nu^2(z_m+z_n+i\Delta\nu_0)^2} + \frac{1}{4(x_m-x_n)^3}\ln\frac{r_0^2+\Delta\nu^2+2(x_m-x_n)\Delta\nu}{r_0^2+\Delta\nu^2-2(x_m-x_n)\Delta\nu}.$$

In evaluation of diagonal elements when $x_m = x_n$ then $\nu_0 = 0$ and the integral in

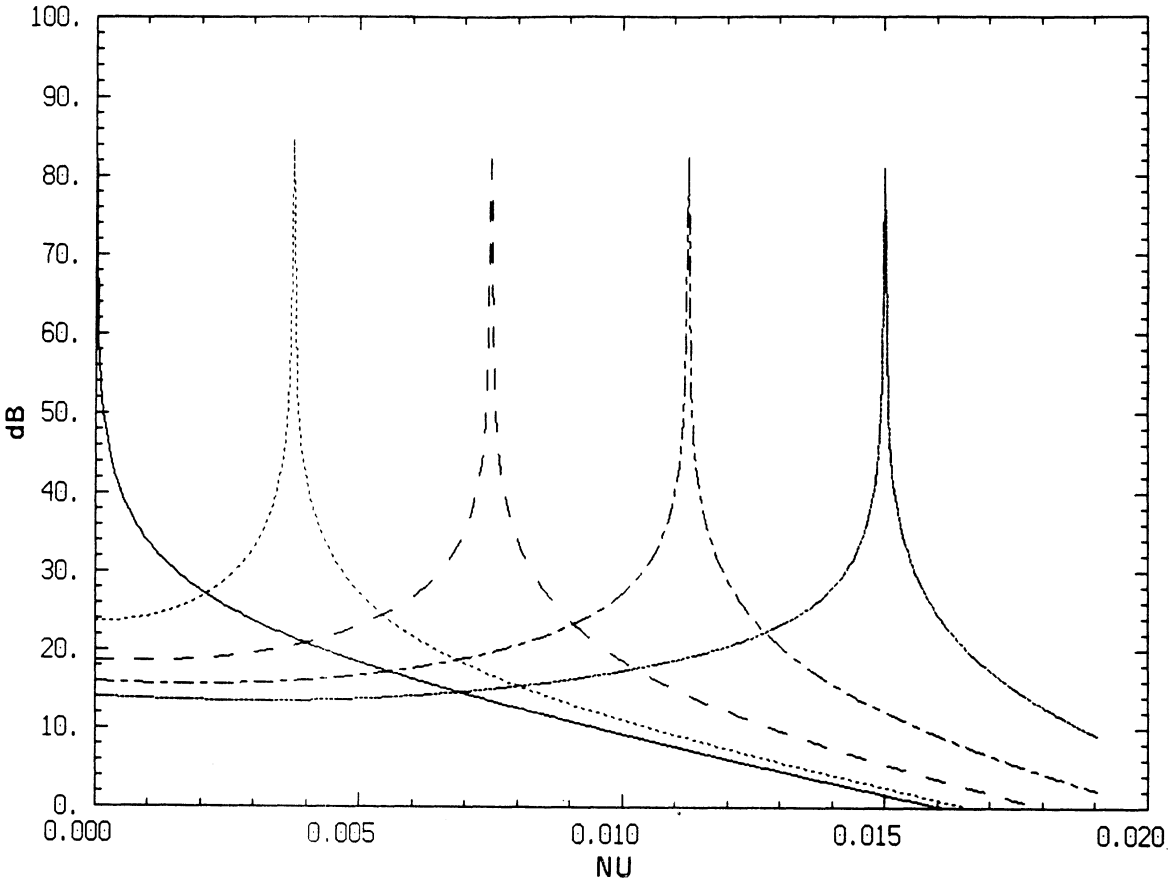

Figure B-6: The absolute value of the integrand function in (B) for $\beta = 75 + i154$ at 10 GHz, $z_m + z_n = 6 \times 10^{-5}\lambda$, and five values of $x_m - x_n$: (——) 0, (- - - - -) $\lambda/8$, (— —) $\lambda/4$, (— —) $3\lambda/8$, (— - - - —) $\lambda/2$.

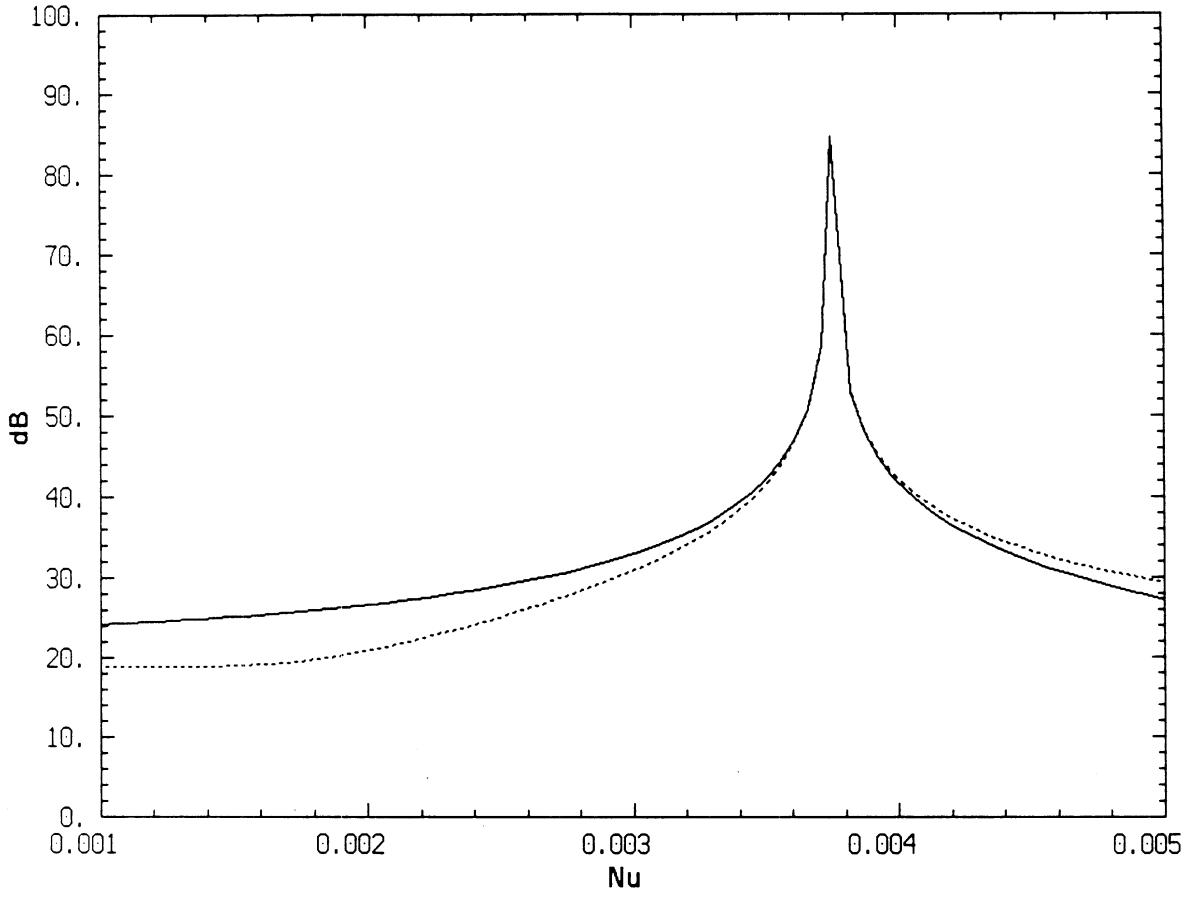

Figure B-7: The absolute value of the integrand function in (B) and its approximation for $\beta = 75 + i154$ at 10 GHz, $z_m + z_n = 6 \times 10^{-5}\lambda$, and $x_m - x_n = \lambda/8$: (——) integrand, (- - - - -) approximation of integrand.

(B88) is approximated by

$$\text{Integrand} \approx (\frac{i}{2\pi} - \frac{i\gamma}{\pi} - \frac{1}{2}) + \frac{i}{\pi} \ln \frac{k_0(z_m + z_n + i\nu)}{2} + \frac{i2}{\pi} \frac{1}{K_0^2(z_m + z_n + i\nu)^2}$$

If S_1' is the integral between 0 and $\Delta\nu$, then

$$S_1' = \frac{i2}{\pi k_0^2} I_3' + \frac{i}{\pi} I_2' + (\frac{i}{2\pi} - \frac{i\gamma}{\pi} - \frac{1}{2})\Delta\nu,$$

where

$$\begin{aligned} I_2' = & -i[(z_m + z_n) \ln \tfrac{z_m+z_n+i\Delta\nu}{z_m+z_n} + i\Delta\nu \ln \tfrac{k_0(z_m+z_n+i\Delta\nu)}{2} - i\Delta\nu] \\ I_3' = & \tfrac{\Delta\nu}{(z_m+z_n)(z_m+z_n+i\Delta\nu)} \end{aligned}$$

To extract the contribution of the integrand in (B85) around ν_0 we use similar approximations as in (B84). If this integral is denoted by S_2, then

$$S_2 = e^{-\beta\nu_0}(x_m - x_n)(z_m + z_n + i\nu_0)\{[H_0^{(1)}(k_0 r_0) + (\frac{i}{\pi} - \frac{i2\gamma}{\pi} - 1) - \frac{i2}{\pi} \ln \frac{k_0 r_0}{2}]I_2 \frac{4i}{\pi k_0^2} I_3\}.$$

The integral in (B86) around the point ν_0 is approximated by S_3 where

$$S_3 = S_2$$

and similarly for the integral in (B87) if S_4 represents the integral around ν_0 then

$$\begin{aligned} S_4 = & \; e^{-\beta\nu_0}\{H_0^{(1)}(k_0 r_0)(x_m - x_n)^2 + [(\tfrac{i}{2\pi} - \tfrac{i\gamma}{\pi} - \tfrac{1}{2}) - \tfrac{i}{\pi} \ln \tfrac{k_0 r_0}{2}] \\ & \cdot[(x_m - x_n)^2 - (z_m + z_n + i\nu_0)^2]\}I_2 \\ & - e^{-\beta\nu_0} \tfrac{2i}{\pi k_0^2}[(x_m - x_n)^2 - (z_m + z_n + i\nu_0)^2]I_3 \end{aligned}$$

When $x_m = x_n$ then $\nu_0 = 0$ and this integral is represented by

$$S_4' = \frac{i2}{\pi k_0^2} I_3' - \frac{i}{\pi} I_2' + (\frac{i}{2\pi} - \frac{i\gamma}{\pi} - \frac{1}{2})\Delta\nu,$$

B4.3 Far Field Evaluation

Once the system of linear equation (B66) for the polarization current has been solved the scattered field due to dielectric structure at any point in the upper half-space can be obtained by means of (B56) and (B61) and (B62) for E and H polarization respectively. Here again it is convenient to approximate the integral representing the scattered field by summation of integrals over each cell. For E polarization we get

$$\begin{aligned} E_y^s(x,z) = \; & \tfrac{-k_0 Z_0}{4} \textstyle\sum_{n=1}^{N} J_y(x_n,z_n)\Delta x_n \Delta z_n \\ & \{H_0^{(1)}(k_0 r_n^s) + \tfrac{(k_0\Delta x_n)^2}{24} U(r_n^s,\theta_n^s) + \tfrac{(k_0\Delta z_n)^2}{24} V(r_n^s,\theta_n^s) \\ & -\alpha \textstyle\int_0^\infty e^{-\alpha\nu} H_0^{(1)}(k_0 r_n^c)\mathrm{d}\nu\}, \end{aligned} \tag{B92}$$

where r_n^q and θ_n^q ($q = s$ or c) are similar to those defined in equations (B70) and (B71) with x_m and z_m replaced by x and z respectively. The far zone radiation pattern may be obtained by employing expression (B92) and the large argument expansion of Hankel function (keeping the terms up to the order $\rho^{\frac{1}{2}}$). If the angle between the direction of observation and normal to the sheet is denoted by ϕ_s as shown in Fig. B4, then

$$r_n^s \approx \rho - x_n \sin\phi_s - z_n \cos\phi_s \tag{B93}$$

Finally employing the definition of far field amplitude as given by (70) in the upper half-space ($|\,\phi_s\,| < \frac{\pi}{2}$) we have

$$\begin{aligned} \mathbf{P}_e^+(\phi_0,\phi_s) = \; & \hat{\mathbf{y}} \tfrac{-k_0 Z_0}{4} \textstyle\sum_{n=1}^{N} J_y(x_n,z_n)\Delta x_n \Delta z_n \{[1 - \tfrac{(k_0\Delta x_n)^2}{24}\sin^2\phi_s - \tfrac{(k_0\Delta z_n)^2}{24}\cos^2\phi_s] \\ & \cdot e^{-ik_0 \sin\phi_s x_n}\big(e^{-ik_0\cos\phi_s z_n} - \tfrac{1}{1+2RY_0\cos\phi_s} e^{ik_0\cos\phi_s z_n}\big)\}. \end{aligned} \tag{B94}$$

The far field amplitude in the lower half-space also can be found if we use the Green's function for lower half-space as given by equation (B22). Again employing distant approximations the far field amplitude in the lower half-space ($\mid \phi_s \mid > \frac{\pi}{2}$) can be obtained from

$$\begin{aligned}\mathbf{P}_e^-(\phi_0,\phi_s) = \; & \hat{\mathbf{y}}\tfrac{-k_0 Z_0}{4}\textstyle\sum_{n=1}^{N} J_y(x_n,z_n)\Delta x_n \Delta z_n[1-\tfrac{(k_0\Delta x_n)^2}{24}\sin^2\phi_s - \tfrac{(k_0\Delta z_n)^2}{24}\cos^2\phi_s] \\ & \cdot e^{-ik_0(\sin\phi_s x_n+\cos\phi_s z_n)}\cdot\tfrac{-2RY_0\cos\phi_s}{1-2RY_0\cos\phi_s}.\end{aligned} \tag{B95}$$

The scattered field in the H polarization can be obtained from equations (B61) and (B62) which can basically be expressed similar to (B92). In far zone such expression can be simplified by noting that

$$\begin{aligned}\tfrac{1}{k_0^2}\tfrac{\partial^2}{\partial x^2}H_0^{(1)}(r_n^q,\theta_n^q) \approx \; & -H_0^{(1)}(r_n^q,\theta_n^q)\sin^2\theta_n^q \\ \tfrac{1}{k_0^2}\tfrac{\partial^2}{\partial z^2}H_0^{(1)}(r_n^q,\theta_n^q) \approx \; & -H_0^{(1)}(r_n^q,\theta_n^q)\cos^2\theta_n^q \\ \tfrac{1}{k_0^2}\tfrac{\partial^2}{\partial x\partial z}H_0^{(1)}(r_n^q,\theta_n^q) \approx \; & H_0^{(1)}(r_n^q,\theta_n^q)\cos\theta_n^q\sin\theta_n^q\end{aligned} \tag{B96}$$

and further as distance from origin to the observation point (ρ) approaches to infinity then $\theta_n^q \to \phi_s$. Under the mentioned conditions we notice that the scattered field in the polar coordinate system has only $\hat{\phi}$ component. Using large argument expansion of Hankel functions and expression (B44) the far field amplitude in the upper half-space is of the following form

$$\begin{aligned}\mathbf{P}_h^+(\phi_0,\phi_s) = \; & \hat{\phi}\tfrac{-k_0 Z_0}{4}\textstyle\sum_{n=1}^{N}\Delta x_n\Delta z_n[1-\tfrac{(k_0\Delta x_n)^2}{24}\sin^2\phi_s - \tfrac{(k_0\Delta z_n)^2}{24}\cos^2\phi_s] \\ & \cdot e^{-ik_0\sin\phi_s x_n}\{J_z(x_n,z_n)\sin\phi_s(e^{-ik_0\cos\phi_s z_n}+\tfrac{e^{ik_0\cos\phi_s z_n}}{1+2RY_0\sec\phi_s}) \\ & -J_x(x_n,z_n)\cos\phi_s(e^{-ik_0\cos\phi_s z_n}-\tfrac{e^{ik_0\cos\phi_s z_n}}{1+2RY_0\sec\phi_s})\},\end{aligned} \tag{B97}$$

and in the lower half-space ($| \phi_s | > \frac{\pi}{2}$) we get

$$\begin{aligned}\mathbf{P}_h^-(\phi_0, \phi_s) = \quad & \hat{\phi} \frac{-k_0 Z_0}{4} \sum_{n=1}^{N} \Delta x_n \Delta z_n [1 - \frac{(k_0 \Delta x_n)^2}{24} \sin^2 \phi_s - \frac{(k_0 \Delta z_n)^2}{24} \cos^2 \phi_s] \\ & \cdot e^{-ik_0 (\sin \phi_s x_n + \cos \phi_s z_n)} \cdot [J_z(x_n, z_n) \sin \phi_s - J_x(x_n, z_n) \cos \phi_s] \\ & \cdot (\frac{-2RY_0 \sec \phi_s}{1 - 2RY_0 \sec \phi_s}).\end{aligned} \tag{B98}$$